


12-2011

## NOVEL AMINO ACID TRANSPORTER-TARGETED RADIOTRACERS FOR BREAST CANCER IMAGING

FanLin Kong

Follow this and additional works at: [https://digitalcommons.library.tmc.edu/utgsbs\\_dissertations](https://digitalcommons.library.tmc.edu/utgsbs_dissertations)

 Part of the [Diagnosis Commons](#), [Medical Pharmacology Commons](#), [Medicinal and Pharmaceutical Chemistry Commons](#), [Oncology Commons](#), and the [Radiology Commons](#)

---

### Recommended Citation

Kong, FanLin, "NOVEL AMINO ACID TRANSPORTER-TARGETED RADIOTRACERS FOR BREAST CANCER IMAGING" (2011). *The University of Texas MD Anderson Cancer Center UTHealth Graduate School of Biomedical Sciences Dissertations and Theses (Open Access)*. 194.  
[https://digitalcommons.library.tmc.edu/utgsbs\\_dissertations/194](https://digitalcommons.library.tmc.edu/utgsbs_dissertations/194)

This Dissertation (PhD) is brought to you for free and open access by the The University of Texas MD Anderson Cancer Center UTHealth Graduate School of Biomedical Sciences at DigitalCommons@TMC. It has been accepted for inclusion in The University of Texas MD Anderson Cancer Center UTHealth Graduate School of Biomedical Sciences Dissertations and Theses (Open Access) by an authorized administrator of DigitalCommons@TMC. For more information, please contact [digitalcommons@library.tmc.edu](mailto:digitalcommons@library.tmc.edu).

# **NOVEL AMINO ACID TRANSPORTER-TARGETED RADIOTRACERS FOR BREAST CANCER IMAGING**

by

FanLin Kong, B.S.

APPROVED:

---

David J Yang, Ph.D.

---

Wei Hu, M.D., Ph.D.

---

Euishin Edmund Kim, M.D.

---

Osama R Mawlawi, Ph.D.

---

Firas Mourtada, M.S.E., Ph.D., DABR

---

APPROVED:

---

Dean, The University of Texas  
Graduate School of Biomedical Sciences at Houston

# **NOVEL AMINO ACID TRANSPORTER-TARGETED RADIOTRACERS FOR BREAST CANCER IMAGING**

A  
DISSERTATION

Presented to the Faculty of  
The University of Texas  
Health Science Center at Houston  
and  
The University of Texas  
M. D. Anderson Cancer Center  
Graduate School of Biomedical Sciences  
in Partial Fulfillment  
of the Requirements  
for the Degree of  
DOCTOR OF PHILOSOPHY

BY

FanLin Kong, B.S.

Houston, Texas

December 2011

## **ACKNOWLEDGEMENTS**

This work would not have been accomplished without the help of a lot of people. First and foremost, I would like to thank my mentor Dr. David J. Yang for his continuous support and extraordinary guidance over the past few years. I am very fortunate and honored to be one of his graduate students and his mentorship paved my way for becoming an independent scientist. I would also like to thank my advisory, examination and supervisory committee members, Drs. Wei Hu, Euishin Edmund Kim, Osama R Mawlawi, Firas Mourtada, David L Schwartz, and Zahid Siddik for their invaluable time and scientific input to my research project. I would like to extend my sincere thanks to everyone in Dr. Yang's lab and in our department. Particularly, Drs. Yinhan Zhang and Mohammad S Ali, who taught me the chemical synthesis of my compounds; Dr. Daniel P Young, who coached me the immunohistochemical staining; Drs. Andrei Volgin and Lucia Le Roux, who trained me during my rotation; Dong-Fang Yu, who always helped me with my animal studies.

Furthermore, I am greatly appreciative of all the faculty and staff at the University Of Texas Graduate School Of Biomedical Sciences. They are always available and helpful when I need their help. Also, I would like to thank all the members in the Student Intercouncil of UT Health Science Center at Houston. I had a great time to serve on the council and attend all kinds of volunteer activities.

Last but not least, I am truly thankful to all my dear friends and wonderful family members for always supporting, encouraging, and believing in me. I could not have done this without you.

## **ABSTRACT**

### **NOVEL AMINO ACID TRANSPORTER-TARGETED RADIOTRACERS FOR BREAST CANCER IMAGING**

Publication No. \_\_\_\_\_

FanLin Kong, Ph.D.

Supervisory Professor: David J. Yang, Ph.D.

Breast cancer is the most common malignancy among women in the world. Its 5-year survival rate ranges from 23.4% in patients with stage IV to 98% in stage I disease, highlighting the importance of early detection and diagnosis.  $^{18}\text{F}$ -2-Fluoro-2-deoxy-glucose ( $^{18}\text{F}$ -FDG), using positron emission tomography (PET), is the most common functional imaging tool for breast cancer diagnosis currently. Unfortunately,  $^{18}\text{F}$ -FDG-PET has several limitations such as poorly differentiating tumor tissues from inflammatory and normal brain tissues. Therefore,  $^{18}\text{F}$ -labeled amino acid-based radiotracers have been reported as an alternative, which is based on the fact that tumor cells uptake and consume more amino acids to sustain their uncontrolled growth. Among those radiotracers,  $^{18}\text{F}$ -labeled tyrosine and its derivatives have shown high tumor uptake and great ability to differentiate tumor tissue from inflammatory sites in brain tumors and squamous cell carcinoma. They enter the tumor cells via L-type amino acid transporters (LAT), which were reported to be highly expressed in many cancer cell lines and correlate positively with tumor

growth. Nevertheless, the low radiosynthesis yield and demand of an on-site cyclotron limit the use of  $^{18}\text{F}$ -labeled tyrosine analogues.

In this study, four Technetium-99m ( $^{99\text{m}}\text{Tc}$ ) labeled tyrosine/ AMT ( $\alpha$ -methyl tyrosine)-based radiotracers were successfully synthesized and evaluated for their potentials in breast cancer imaging. In order to radiolabel tyrosine and AMT, the chelators N,N'-ethylene-di-L-cysteine (EC) and 1,4,8,11-tetra-azacyclotetradecane (N4 cyclam) were selected to coordinate  $^{99\text{m}}\text{Tc}$ . These chelators have been reported to provide stable chelation ability with  $^{99\text{m}}\text{Tc}$ . By using the chelator technology, the same target ligand could be labeled with different radioisotopes for various imaging modalities for tumor diagnosis, or for internal radionuclide therapy in future.

Based on the *in vitro* and *in vivo* evaluation using the rat mammary tumor models,  $^{99\text{m}}\text{Tc}$ -EC-AMT is considered as the most suitable radiotracer for breast cancer imaging overall, however,  $^{99\text{m}}\text{Tc}$ -EC-Tyrosine will be more preferred for differential diagnosis of tumor from inflammation.

## TABLE OF CONTENTS

<b>Approval Sheet</b> .....	i
<b>Title Page</b> .....	ii
<b>Acknowledgements</b> .....	iii
<b>Abstract</b> .....	v
<b>Table of Contents</b> .....	vii
<b>List of Figures</b> .....	ix
<b>List of Tables</b> .....	xiv
<b>Abbreviations</b> .....	xvii
<b>Chapter 1 Introduction</b> .....	1
I.    Breast cancer and its diagnosis.....	1
II.   Amino acid transporter systems.....	13
III.  Tyrosine-based radiotracers for tumor imaging.....	18
IV.   Technetium-99m and its coordination with chelators.....	27
V.    Scope of the dissertation.....	28
<b>Chapter 2 Development of <sup>99m</sup>Tc-EC-Tyrosine for breast cancer imaging</b> .....	31
I.    Introduction.....	31
II.   Materials and methods.....	33
III.  Results.....	39
IV.   Discussion.....	51
<b>Chapter 3 Development of <sup>99m</sup>Tc-EC-AMT for breast cancer imaging</b> .....	55
I.    Introduction.....	55



II.	Materials and methods.....	57
III.	Results.....	64
IV.	Discussion.....	78
<b>Chapter 4 Development of <math>^{99m}\text{Tc}</math>-N4-Tyrosine for breast cancer imaging.....</b>		<b>82</b>
I.	Introduction.....	82
II.	Materials and methods.....	84
III.	Results.....	91
IV.	Discussion.....	103
<b>Chapter 5 Development of <math>^{99m}\text{Tc}</math>-N4-AMT for breast cancer imaging.....</b>		<b>106</b>
I.	Introduction.....	106
II.	Materials and methods.....	107
III.	Results.....	117
IV.	Discussion.....	129
<b>Chapter 6 Overview: comparison of <math>^{99m}\text{Tc}</math>-labeled Tyrosine-based radiotracers in breast cancer imaging.....</b>		<b>132</b>
I.	Specific aim 1.....	134
II.	Specific aim 2.....	137
III.	Specific aim 3.....	140
IV.	Conclusions and future directions.....	144
<b>Bibliography.....</b>		<b>146</b>
<b>Vita.....</b>		<b>167</b>

## LIST OF FIGURES

<b>Figure 1.1</b> Predicted structure of L-type amino acid transporter LAT-1 and its transport mechanism.....	17
<b>Figure 1.2</b> Synthetic scheme of L-[2- <sup>18</sup> F]Fluorotyrosine.....	21
<b>Figure 1.3</b> Synthetic scheme of O-2-[ <sup>18</sup> F]fluoroethyl-L-tyrosine ( <sup>18</sup> F-FET).....	26
<b>Figure 1.4</b> Proposed structures of four tyrosine-based precursors.....	30
<b>Figure 2.1</b> Synthetic scheme of precursor EC-Tyrosine.....	40
<b>Figure 2.2</b> Time course of <sup>99m</sup> Tc-EC-Tyrosine, <sup>99m</sup> Tc-EC and <sup>18</sup> F-FDG uptake in rat breast tumor cell line 13762 (0– 240 min). Data are expressed in mean ± S.D. percentage of cellular uptake (%Uptake).....	41
<b>Figure 2.3</b> Competitive inhibition uptake of <sup>99m</sup> Tc-EC-Tyrosine by L-tyrosine in rat breast tumor cell line 13762 up to 1 h. A set of concentrations of L-tyrosine [10X– 100X; of EC-Tyrpsine concentration (8 mg/well)] were used. Data are expressed in mean ± S.D. percentage of cellular uptake (%Uptake). *P<0.05 compared with the control group.....	42
<b>Figure 2.4</b> Blood clearance (%ID/g) of <sup>99m</sup> Tc-EC-Tyrosine in normal female Fischer 344 rats (n=3). The data represent the mean radioactivity expressed as a percentage of the injected dose per gram of blood ± S.D.....	43
<b>Figure 2.5</b> Planar scintigraphy of <sup>99m</sup> Tc-EC-Tyrosine at 30 – 240 min in rat breast tumor-bearing rats (T: tumor).....	46
<b>Figure 2.6</b> Planar scintigraphic images of <sup>99m</sup> Tc-EC-Tyrosine at 30 – 240 min in rat breast tumor and inflammation-bearing rats (T: tumor, I: inflammation). The tumor-	

to-muscle ratios (T/Ms), inflammation-to-muscle ratios (I/Ms), and tumor-to-inflammation ratios (T/Is) are listed below the figure.....	49
<b>Figure 2.7</b> microPET images of $^{18}\text{F}$ -FDG at 30 – 90 min in rat breast tumor and inflammation-bearing rats (T: tumor, I: inflammation). The tumor-to-muscle ratios (T/Ms), inflammation-to-muscle ratios (I/Ms), and tumor-to-inflammation ratios (T/Is) are listed below the figure.....	50
<b>Figure 3.1</b> Synthetic scheme of precursor EC-AMT and cold standard reference compound rhenium (Re) EC-AMT.....	66
<b>Figure 3.2</b> High performance liquid chromatography analysis of $^{99\text{m}}\text{Tc}$ -EC-AMT and Re-EC-AMT at a flow rate of 0.5 mL/min using a C-18 reverse column under UV absorbance of 274 nm.....	67
<b>Figure 3.3</b> Time course of $^{99\text{m}}\text{Tc}$ -EC-AMT, $^{99\text{m}}\text{Tc}$ -EC and $^{18}\text{F}$ -FDG uptake in rat breast tumor cell line 13762 (0–240 min). Data are expressed in mean $\pm$ SD percentage of cellular uptake (%Uptake).....	68
<b>Figure 3.4</b> Competitive inhibition uptake of $^{99\text{m}}\text{Tc}$ -EC-AMT by L-tyrosine in rat breast tumor cell line 13762 up to 1 h. A set of concentrations of L-tyrosine [10X–100X; of EC-AMT concentration (8 mg/well)] were used. Data are expressed in mean $\pm$ S.D. percentage of cellular uptake (%Uptake). *P<0.05 compared with the control group.....	69
<b>Figure 3.5</b> Blood clearance (%ID/g) of $^{99\text{m}}\text{Tc}$ -EC-AMT in normal female Fischer 344 rats (n=3). The data represent the mean radioactivity expressed as a percentage of the injected dose per gram of blood $\pm$ S.D.....	70

<b>Figure 3.6</b> Planar scintigraphy of $^{99m}\text{Tc}$ -EC-AMT at 30 – 240 min in rat breast tumor-bearing rats (T: tumor).....	73
<b>Figure 3.7</b> Planar scintigraphic images of $^{99m}\text{Tc}$ -EC-AMT at 30 – 240 min in rat breast tumor and inflammation-bearing rats (T: tumor, I: inflammation). The tumor-to-muscle ratios (T/Ms), inflammation-to-muscle ratios (I/Ms), and tumor-to-inflammation ratios (T/Is) are listed below the figure.....	76
<b>Figure 3.8</b> microPET images of $^{18}\text{F}$ -FDG at 30 – 90 min in rat breast tumor and inflammation-bearing rats (T: tumor, I: inflammation). The tumor-to-muscle ratios (T/Ms), inflammation-to-muscle ratios (I/Ms), and tumor-to-inflammation ratios (T/Is) are listed below the figure.....	77
<b>Figure 4.1</b> Synthetic scheme of precursor N4-Tyrosine.....	92
<b>Figure 4.2</b> Time course of $^{99m}\text{Tc}$ -N4-Tyrosine, $^{99m}\text{Tc}$ -N4 and $^{18}\text{F}$ -FDG uptake in rat breast tumor cell line 13762 (0– 240 min). Data are expressed in mean $\pm$ S.D. percentage of cellular uptake (%Uptake).....	93
<b>Figure 4.3</b> Competitive inhibition uptake of $^{99m}\text{Tc}$ -N4-Tyrosine by L-tyrosine in rat breast tumor cell line 13762 up to 1 h. A set of concentrations of L-tyrosine [150-300X of N4-Tyrosine concentration (8 mg/well)] were used. Data are expressed in mean $\pm$ S.D. percentage of cellular uptake (%Uptake).....	94
<b>Figure 4.4</b> Blood clearance (%ID/g) of $^{99m}\text{Tc}$ -N4-Tyrosine in normal female Fischer 344 rats (n=3). The data represent the mean radioactivity expressed as a percentage of the injected dose per gram of blood $\pm$ S.D.....	95
<b>Figure 4.5</b> Planar scintigraphy of $^{99m}\text{Tc}$ -N4-Tyrosine at 30 – 240 min in rat breast tumor-bearing rats (T: tumor).....	98

<b>Figure 4.6</b> Planar scintigraphic images of $^{99m}\text{Tc}$ -N4-Tyrosine at 30 – 240 min in rat breast tumor and inflammation-bearing rats (T: tumor, I: inflammation). The tumor-to-muscle ratios (T/Ms), inflammation-to-muscle ratios (I/Ms), and tumor-to-inflammation ratios (T/Is) are listed below the figure.....	101
<b>Figure 4.7</b> microPET images of $^{18}\text{F}$ -FDG at 30 – 90 min in rat breast tumor and inflammation-bearing rats (T: tumor, I: inflammation). The tumor-to-muscle ratios (T/Ms), inflammation-to-muscle ratios (I/Ms), and tumor-to-inflammation ratios (T/Is) are listed below the figure.....	102
<b>Figure 5.1</b> Synthetic scheme of manufacturing of the precursor N4-AMT.....	118
<b>Figure 5.2</b> Time course of $^{99m}\text{Tc}$ -N4-AMT, $^{99m}\text{Tc}$ -N4 and $^{18}\text{F}$ -FDG uptake in rat breast tumor cell line 13762 (0– 240 min). Data are expressed in mean $\pm$ S.D. percentage of cellular uptake (%Uptake).....	119
<b>Figure 5.3</b> Competitive inhibition uptake of $^{99m}\text{Tc}$ -N4-AMT by L-tyrosine in rat breast tumor cell line 13762 up to 1 h. A set of concentrations of L-tyrosine [150X and 200X; of N4-AMT concentration (8 mg/well)] were used. Data are expressed in mean $\pm$ S.D. percentage of cellular uptake (%Uptake). *P<0.05 compared with the control group.....	120
<b>Figure 5.4</b> Blood clearance (%ID/g) of $^{99m}\text{Tc}$ -N4-AMT in normal female Fischer 344 rats (n=3). The data represent the mean radioactivity expressed as a percentage of the injected dose per gram of blood $\pm$ S.D.....	121
<b>Figure 5.5</b> Planar scintigraphy of $^{99m}\text{Tc}$ -N4-AMT at 30 – 240 min in rat breast tumor-bearing rats (T: tumor).....	124

<b>Figure 5.6</b> Planar scintigraphic images of $^{99m}\text{Tc}$ -N4-AMT at 30 – 240 min in rat breast tumor and inflammation-bearing rats (T: tumor, I: inflammation). The tumor-to-muscle ratios (T/Ms), inflammation-to-muscle ratios (I/Ms), and tumor-to-inflammation ratios (T/Is) are listed below the figure.....	127
<b>Figure 5.7</b> microPET images of $^{18}\text{F}$ -FDG at 30 – 90 min in rat breast tumor and inflammation-bearing rats (T: tumor, I: inflammation). The tumor-to-muscle ratios (T/Ms), inflammation-to-muscle ratios (I/Ms), and tumor-to-inflammation ratios (T/Is) are listed below the figure.....	128
<b>Figure 6.1</b> Proposed structures of four tyrosine-based precursors.....	132
<b>Figure 6.2</b> Time course of $^{99m}\text{Tc}$ -labeled four radiotracers and $^{18}\text{F}$ -FDG uptake in rat breast tumor cell line 13762 (0– 240 min). Data are expressed in mean $\pm$ S.D. percentage of cellular uptake (%Uptake).....	138
<b>Figure 6.3</b> Blood clearance (%ID/g) of four $^{99m}\text{Tc}$ -labeled radiotracers in normal female Fischer 344 rats up to 240 min (n=3). The data represent the mean radioactivity expressed as a percentage of the injected dose per gram of blood $\pm$ S.D.....	141

## LIST OF TABLES

<b>Table 1.1</b> Radionuclides commonly used in PET imaging.....	6
<b>Table 1.2</b> PET-based radiotracers used to detect breast cancer in humans, by tumor-specific target.....	7
<b>Table 1.3</b> Radionuclides commonly used in SPECT imaging.....	8
<b>Table 1.4</b> Planar and SPECT-based radiotracers used to detect breast cancer in humans, by tumor-specific target.....	12
<b>Table 1.5</b> Major amino acid transporter systems in mammalian.....	14
<b>Table 2.1</b> Biodistribution of $^{99m}\text{Tc}$ -EC-Tyrosine in normal Fischer 344 female rats.....	44
<b>Table 2.2</b> Biodistribution of $^{18}\text{F}$ -FDG in normal Fischer 344 female rats.....	45
<b>Table 2.3</b> Percentage of injected dose (%ID) of selected organs before and after <i>in vivo</i> blocking of $^{99m}\text{Tc}$ -EC-Tyrosine by unlabeled L-Tyrosine in mammary tumor-bearing rats. Red font indicates the decreased %ID when compared to the corresponding control group. Blue shading indicates $P < 0.05$ when compared to the corresponding control group (n=3/group/time interval).....	47
<b>Table 2.4</b> Selected organ to muscle ratios before and after <i>in vivo</i> blocking of $^{99m}\text{Tc}$ -EC-Tyrosine by unlabeled L-Tyrosine in mammary tumor-bearing rats. Red font indicates the decreased %ID when compared to the corresponding control group. Blue shading indicates $P < 0.05$ when compared to the corresponding control group (n=3/group/time interval).....	48
<b>Table 3.1</b> Biodistribution of $^{99m}\text{Tc}$ -EC-AMT in normal Fischer 344 female rats.....	71
<b>Table 3.2</b> Biodistribution of $^{18}\text{F}$ -FDG in normal Fischer 344 female rats.....	72

<b>Table 3.3</b> Percentage of injected dose (%ID) of selected organs before and after <i>in vivo</i> blocking of $^{99m}\text{Tc}$ -EC-AMT by unlabeled L-Tyrosine in mammary tumor-bearing rats. Red font indicates the decreased %ID when compared to the corresponding control group. Blue shading indicates $P < 0.05$ when compared to the corresponding control group (n=3/group/time interval).....	74
<b>Table 3.4</b> Selected organ to muscle ratios before and after <i>in vivo</i> blocking of $^{99m}\text{Tc}$ -EC-AMT by unlabeled L-Tyrosine in mammary tumor-bearing rats. Red font indicates the decreased %ID when compared to the corresponding control group. Blue shading indicates $P < 0.05$ when compared to the corresponding control group (n=3/group/time interval).....	75
<b>Table 4.1</b> Biodistribution of $^{99m}\text{Tc}$ -N4-Tyrosine in normal Fischer 344 female rats.	96
<b>Table 4.2</b> Biodistribution of $^{18}\text{F}$ -FDG in normal Fischer 344 female rats.....	97
<b>Table 4.3</b> Percentage of injected dose (%ID) of selected organs before and after <i>in vivo</i> blocking of $^{99m}\text{Tc}$ -N4-Tyrosine by unlabeled L-Tyrosine in mammary tumor-bearing rats. Red font indicates the decreased %ID when compared to the corresponding control group. Blue shading indicates $P < 0.05$ when compared to the corresponding control group (n=3/group/time interval).....	99
<b>Table 4.4</b> Selected organ to muscle ratios before and after <i>in vivo</i> blocking of $^{99m}\text{Tc}$ -N4-Tyrosine by unlabeled L-Tyrosine in mammary tumor-bearing rats. Red font indicates the decreased %ID when compared to the corresponding control group. Blue shading indicates $P < 0.05$ when compared to the corresponding control group (n=3/group/time interval).....	100
<b>Table 5.1</b> Biodistribution of $^{99m}\text{Tc}$ -N4-AMT in normal Fischer 344 female rats.....	122



<b>Table 5.2</b> Biodistribution of $^{18}\text{F}$ -FDG in normal Fischer 344 female rats.....	123
<b>Table 5.3</b> Percentage of injected dose (%ID) of selected organs before and after <i>in vivo</i> blocking of $^{99\text{m}}\text{Tc}$ -N4-AMT by unlabeled L-Tyrosine in mammary tumor-bearing rats. Red font indicates the decreased %ID when compared to the corresponding control group. Blue shading indicates $P < 0.05$ when compared to the corresponding control group (n=3/group/time interval).....	125
<b>Table 5.4</b> Selected organ to muscle ratios before and after <i>in vivo</i> blocking of $^{99\text{m}}\text{Tc}$ -N4-AMT by unlabeled L-Tyrosine in mammary tumor-bearing rats. Red font indicates the decreased %ID when compared to the corresponding control group. Blue shading indicates $P < 0.05$ when compared to the corresponding control group (n=3/group/time interval).....	126
<b>Table 6.1</b> The studies designed to synthesize and evaluate four radiotracers.....	133
<b>Table 6.2</b> Summary of the chemical synthesis of four precursors.....	135
<b>Table 6.3</b> The partition coefficient value (logP) of four radiotracers at pH=5-6 (n=6).....	136
<b>Table 6.4</b> Conclusion of Specific Aim 1. Score 1 indicates the best compound, and score 4 indicates the worst compound.....	136
<b>Table 6.5</b> Conclusion of Specific Aim 2. Score 1 indicates the best compound, and score 4 indicates the worst compound.....	139
<b>Table 6.6</b> Conclusion of Specific Aim 3. Score 1 indicates the best compound, and score 4 indicates the worst compound.....	143
<b>Table 6.7</b> Final conclusions of the dissertation. Score 1 indicates the best compound, and score 4 indicates the worst compound.....	145

## ABBREVIATIONS

%ID/g	percentage of the injected dose per gram
%Uptake	percent of cellular uptake
$^{11}\text{C}$	carbon-11
$^{11}\text{C}$ -Tyr	L-[1- $^{11}\text{C}$ ]-tyrosine
$^{123}\text{I}$ -AMT	L-3-[ $^{123}\text{I}$ ]iodo- $\alpha$ -methyltyrosine
$^{123}\text{I}$ -IMT	3-[ $^{123}\text{I}$ ]iodo- $\alpha$ -methyl-L-tyrosine
$^{13}\text{N}$	nitrogen-13
$^{15}\text{O}$	oxygen-15
$^{188}\text{Re}$	rhenium-188
$^{18}\text{F}$	fluorine-18
$^{18}\text{F}$ -FAMT	[ $^{18}\text{F}$ ]fluoro- $\alpha$ -methyl tyrosine
$^{18}\text{F}$ -FDG	$^{18}\text{F}$ -2-fluoro-2-deoxy-glucose
$^{18}\text{F}$ -FES	$^{18}\text{F}$ -fluoroestradiol
$^{18}\text{F}$ -FET	O-(2- $^{18}\text{F}$ -Fluoroethyl)-L-Tyrosine
$^{18}\text{F}$ -FLT	$^{18}\text{F}$ -fluorothymidine
$^{18}\text{F}$ -FMT	L-[3- $^{18}\text{F}$ ]- $\alpha$ -methyl tyrosine
$^{18}\text{F}$ -galacto-RGD	$^{18}\text{F}$ -galacto-arginine-glycine-aspartic acid
$^{18}\text{F}$ -Tyr	L-2-[ $^{18}\text{F}$ ]fluorotyrosine
$^{64}\text{Cu}$	copper-64
$^{68}\text{Ga}$	gallium-68

$^{82}\text{Rb}$	rubidium-82
$^{89}\text{Zr}$	zirconium-89
$^{99}\text{Mo}$	molybdenum-99
$^{99\text{m}}\text{Tc}$	technetium-99m
$^{99\text{m}}\text{Tc-MDP}$	$^{99\text{m}}\text{Tc}$ -methylene diphosphonate
$^{99\text{m}}\text{Tc-sestamibi}$	$^{99\text{m}}\text{Tc}$ -methoxyisobutylisonitrile
AMT	$\alpha$ -methyl-L-tyrosine
BCH	2-amino-endo-bicycloheptane-2-carboxylic acid
BPB	( <i>S</i> )-[ <i>N</i> -2-( <i>N'</i> -benzylpropyl)amino]benzophenone
BSGI	breast-specific $\gamma$ -imaging
CT	computed tomography
DTPA	diethylenetriamine pentaacetic acid
EC	N,N'-ethylene-di-L-cysteine
EC-AMT	O-[3-(N-Ethylenedicysteine) propyl]- $\alpha$ -methyl tyrosine
EC-Tyrosine	O-[3-(N-Ethylenedicysteine) propyl]-L- tyrosine
HCC	human hepatocellular carcinoma
HPLC	High performance liquid chromatography
HYNIC	hydrazinenicotinamide
LAT/System L	L-type amino acid transporter system
logP	the partition coefficient value
MeAIB	N-methyl aminoisobutyric acid
$\text{N}_2\text{S}_2$	diaminodithiol
MRI	magnetic resonance imaging

N4 cyclam	1,4,8,11-tetra-azacyclotetradecane
N4-AMT	O-[3-(1,4,8,11-tetraazacyclotetradecan)-propyl]- $\alpha$ -methyl tyrosine
N4-Tyrosine	O-[3-(1,4,8,11-tetraazabicyclohexadecane)-propyl]-tyrosine
NMR	nuclear magnetic resonance
OSEM	ordered subset expectation maximization
PEM	positron emission mammography
PET	positron emission tomography
Pgp	P-glycoprotein
ROI	regions of interest
SNAT	the sodium-coupled neutral amino acid transporter
SPECT	single photon emission computed tomography
SUV	Standard uptake value
T/I	tumor-to-inflammation ratio
T/M	tumor-to-muscle ratio
$t_{1/2} \alpha$	half-life of the distribution phase
$t_{1/2} \beta$	half-life of the elimination phase

## **CHAPTER 1 Introduction**

### **I. Breast cancer and its diagnosis**

#### **a. Introduction**

Breast cancer is the most common malignancy among women in the United States. In 2010, a total of 207,090 new cases of invasive breast cancer, along with 54,010 new cases of non-invasive types, were expected to be diagnosed in women. Moreover, about 39,840 women were projected to die from this disease in the same year. According to the National Cancer Institute, the 5-year survival rate of breast cancer ranges from 23.4% in patients with stage IV disease to 98% in patients with stage I disease, highlighting the importance of early detection and diagnosis of breast cancer[1].

Molecular imaging serves as an essential tool in breast cancer diagnosis and staging, as well as provides a significant proportion of information for surgical management, radiation planning, chemotherapeutic assessment, and treatment response monitor of patients. In the present, positron emission tomography (PET), single photon emission computed tomography (SPECT), and their combinations with computed tomography (CT) or magnetic resonance imaging (MRI), are major functional molecular imaging modalities used in clinic. PET and SPECT radiotracers can target tumors based upon tumor-specific characteristics at molecular levels. The accumulating understanding of the breast cancer molecular biology has highlighted pivotal factors that are critical for breast cancer progression, which allows researchers to select suitable targets for developing tumor-specific radiotracers. For instance, given that sustained tumor growth demands elevated

glucose consumption for energy production in the lesion regions, PET radiotracer  $^{18}\text{F}$ -labeled glucose analog  $^{18}\text{F}$ -2-fluoro-2-deoxy-glucose ( $^{18}\text{F}$ -FDG) has commonly been used to visualize the glucose metabolism of breast cancer cells[2].  $^{18}\text{F}$ -labeled  $16\alpha$ - $17\beta$ -fluoroestradiol is used to image estrogen receptors, which are highly overexpressed in a large proportion of breast tumor tissues[3]. Many other radiotracers have been designed to image cell proliferation, cell apoptosis, angiogenesis and hypoxia of breast tumors. Since breast cancer treatment has become more individualized in compliance with the distinct biological characteristics of tumors from each patient, the more target-specific molecular imaging radiotracers may hold the key to guide treatment selection and evaluate treatment response in the early stages.

**b. Positron emission tomography (PET) and its radionuclides**

Positron emission tomography (PET) is a 3-D nuclear medicine imaging technique, which is based on detecting the annihilation radiation emitted from a certain positron-emitting radionuclide[2]. When the radionuclide decays, the positron annihilates an electron nearby, thus creates two 511 keV photons emitted opposite to each other (180 degree). This process is called “coincidence event”, which can be observed by PET detectors arranged in an array of full or partial ring around the patient body axis. Data are then reconstructed using standard algorithm. By using this coincidence-detection method, the traditional collimator can be eliminated, and therefore the spatial resolution and sensitivity can be highly improved.

Commonly used PET imaging radionuclides are listed in Table 1.1. In order to monitor a small bioactive molecule *in vivo* without altering its chemical structure, carbon-11 ( $^{11}\text{C}$ ) is often used as a label to substitute the stable carbon atom  $^{12}\text{C}$  in that molecule. Given that  $^{11}\text{C}$  has a half-life of only 20 minutes which has less commercial interest, fluorine-18 ( $^{18}\text{F}$ ) with a half-life of 110 minutes has been used alternatively. In fact,  $^{18}\text{F}$  is currently the most frequently used/developed PET radionuclide. In addition to  $^{11}\text{C}$ - and  $^{18}\text{F}$ -labeled biomarkers, there are some other short half-lived radiotracers such as  $^{15}\text{O}$ -labeled water and  $^{13}\text{N}$ -labeled ammonia that measure blood flow in the patient body[4]. Moreover, copper-64 ( $^{64}\text{Cu}$ ) and zirconium-89 ( $^{89}\text{Zr}$ ), because of their long half-life (12.7 h and 78.4 h, respectively), have been increasingly recognized in the past decade for labeling nanoparticles or slowly localizing antibodies[5]. Other than those cyclotron-produced PET radionuclides mentioned above, generator-produced gallium-68 ( $^{68}\text{Ga}$ ) and rubidium-82 ( $^{82}\text{Rb}$ ) have also shown high potentials in PET imaging. The advantage of in-house generator produced radionuclides is that the generator itself serves as a top-of-the-bench source for short half-lived radionuclides in the places that are located far from the cyclotron facility. Besides, it is quite simple to access radionuclides from the generator, and less expensive compared to cyclotron-produced radionuclides.

### **c. PET-based radiotracers for breast cancer imaging in clinic**

$^{18}\text{F}$ -FDG, a glucose analogue, has become the most common and attractive radiotracer for PET. Both  $^{18}\text{F}$ -FDG and glucose are transported across the cell

membrane by glucose transporters.  $^{18}\text{F}$ -FDG is phosphorylated by hexokinase to  $^{18}\text{F}$ -FDG-6-phosphate, whereas glucose is phosphorylated to glucose-6-phosphate. Unlike glucose-6-phosphate,  $^{18}\text{F}$ -FDG-6-phosphate cannot be further metabolized and therefore is trapped and accumulated steadily in tumor cells[2]. Hence,  $^{18}\text{F}$ -FDG is able to provide high sensitivity for detecting, staging, and re-staging tumors by imaging high glucose metabolic rates in tumor cells. For breast cancer cells, increased glucose utilization is caused by the overexpression of the glucose transporters Glut-1 and Glut-3 and by increased hexokinase activity[6]. The rate-limiting step in the uptake of  $^{18}\text{F}$ -FDG in breast cancer appears to be the phosphorylation process by hexokinase, particularly hexokinase I[6].

Although  $^{18}\text{F}$ -FDG-PET generally has high sensitivity and specificity in detecting malignancies, whole-body  $^{18}\text{F}$ -FDG-PET is not quite suitable for primary breast cancer diagnosis, especially for low-grade tumors and tumors smaller than 1 cm in diameter[7]. In addition, it is not appropriate to use  $^{18}\text{F}$ -FDG for breast cancer screening[8]. For locoregional staging of breast cancer,  $^{18}\text{F}$ -FDG-PET has shown high sensitivity in axillary staging of patients with late stage cancer, but it is not sensitive enough in detecting early-stage micrometastases and small tumor-infiltrated axillary lymph nodes[9]. Nevertheless,  $^{18}\text{F}$ -FDG-PET appears to be suitable for distant (systemic) staging; it is also well suited for staging of locally advanced breast cancer, which usually has a large primary tumor (>5 cm in diameter) or advanced axillary disease without clinically apparent distant metastases[10]. Moreover, several studies have demonstrated that  $^{18}\text{F}$ -FDG-PET is superior to traditional bone scintigraphy in the detection of osteolytic and



intramedullary metastases but is inferior in the detection of primary osteoblastic lesions[11]. An increasing number of studies have used  $^{18}\text{F}$ -FDG-PET to evaluate treatment responses. Although  $^{18}\text{F}$ -FDG has not yet been recommended as a routine assessment agent, accumulated  $^{18}\text{F}$ -FDG uptake has been proven to be an accurate early predictor of poor response to therapy. In a study showing that high  $^{18}\text{F}$ -FDG uptake was associated with a low blood flow or perfusion rate in tumors, the locally advanced breast cancer patients with high uptake were more likely to have poor response and early relapse[12].

Given its low specificity, many radiotracers have been developed as an alternative to  $^{18}\text{F}$ -FDG. Table 1.2 summarizes the PET-based radiotracers that currently applied for breast cancer imaging, according to the categories of the tumor-specific targets to which they are aimed at.

Table 1.1. Radionuclides commonly used in PET imaging.

Radionuclide	Half-life	Production
$^{11}\text{C}$	20.4 min	Cyclotron
$^{13}\text{N}$	9.97 min	Cyclotron
$^{15}\text{O}$	2.03 min	Cyclotron
$^{18}\text{F}$	109.7 min	Cyclotron
$^{61}\text{Cu}$	204.5 min	Cyclotron
$^{64}\text{Cu}$	12.8 h	Cyclotron
$^{89}\text{Zr}$	78.4 h	Cyclotron
$^{62}\text{Cu}$	9.7 min	Generator
$^{68}\text{Ga}$	68 min	Generator
$^{82}\text{Rb}$	1.25 min	Generator

**Table 1.2. PET-based radiotracers used to detect breast cancer in humans, by tumor-specific target.**

Target	PET Radiotracer
Perfusion	$^{15}\text{O}-\text{H}_2\text{O}$
Glucose metabolism	$^{18}\text{F}$ -FDG
Hormone receptor	$^{18}\text{F}$ -FES $^{18}\text{F}$ -fluorotamoxifen 21- $^{18}\text{F}$ fluoro-16 $\alpha$ -ethyl-19-norprogesterone 16 $\beta$ - $^{18}\text{F}$ -fluoromoxestol
HER2	$^{89}\text{Zr}$ -trastuzumab
Cell proliferation	$^{18}\text{F}$ -FLT
Angiogenesis	$^{18}\text{F}$ -galacto-RGD $^{18}\text{F}$ -AH111585 $^{89}\text{Zr}$ -bevacizumab
Amino acid transporters and protein synthesis	$^{11}\text{C}$ -methionine $^{11}\text{C}$ -tyrosine <i>O</i> -(2- $^{18}\text{F}$ fluoroethyl)-l-tyrosine
Epidermal growth factor receptor	$^{11}\text{C}$ -Iressa
Hypoxia	$^{18}\text{F}$ -fluoromisonidazole $^{18}\text{F}$ -fluoroetanidazole $^{18}\text{F}$ -fluoroazomycin-arabioside $^{64}\text{Cu}$ -diacetyl-bis-N4-methylthiosemicarbazone
Apoptosis	$^{18}\text{F}$ -annexin V
Membrane synthesis	$^{11}\text{C}$ -choline $^{18}\text{F}$ -fluorocholine
Bone	$^{18}\text{F}$ -fluoride

**d. Planar scintigraphic imaging, single photon emission computed tomography (SPECT) and their radionuclides**

Planar scintigraphic imaging uses one gamma camera to capture and determine gamma-ray emitting photons directly from the labeling radionuclide in a particular angle. The energy of the radionuclide for planar scintigraphic imaging is generally from 70 to 364 keV (Table 1.3).

**Table 1.3. Radionuclides commonly used in SPECT imaging.**

Radionuclide	Decay Mode	Half-life	Emitted Photon Energy [keV]
$^{99m}\text{Tc}$	IT	6.01 h	140 (87.7%)
$^{201}\text{Tl}$	EC	73.0 h	71 (47%), 135 (3%), 167 (10%)
$^{123}\text{I}$	EC	13.2 h	159 (83.3%)
$^{131}\text{I}$	$\text{B}^-$	8.02 d	364 (81.2%)
$^{111}\text{In}$	EC	67.4 h	171(90.3%), 245 (94%)
$^{67}\text{Ga}$	EC	78.3 h	93 (37%), 184 (20.4%), 300 (16.6%)

**IT: isomeric transition**

**EC: electron capture**

Different from planar scintigraphic imaging, a typical single photon emission computed tomography (SPECT) system consists of one or more rotating gamma camera(s) to obtain multiple projection images from different views around the patient, and a computer algorithm for 3D image reconstruction. A collimator is required to collect the  $\gamma$ -ray photons that are emitted from the patient body only in a particular direction[13].

Technetium-99m ( $^{99m}\text{Tc}$ ,  $t_{1/2} = 6.02$  h) is the most common radionuclide for planar and SPECT imaging. It emits a 140 keV gamma ray in 89% abundance, which can be detected by NaI detectors. In addition, it is produced with in-house generator that contains the parent nuclide molybdenum-99 ( $^{99}\text{Mo}$ ), and does not require the cyclotron. Since the chemistry of diagnostic radionuclide  $^{99m}\text{Tc}$  is very similar to that of the therapeutic radioisotope rhenium-188 ( $^{188}\text{Re}$ ), they could be labeled to the same ligand, which leads to the diagnostic/therapeutic matched pair[14].

Although the resolution and sensitivity of SPECT is not as good as PET scan due to its physical nature, SPECT and SPECT/CT still play important and irreplaceable roles in nuclear imaging area. First of all, SPECT radiopharmaceuticals are comparatively easier and less costly to produce. In addition, given that most SPECT radionuclides have longer half-life than that of PET radionuclides, SPECT offers more possibility to broaden the observational time window that allows the doctors to monitor biological processes *in vivo* several hours or even days after radiopharmaceutical administration. Furthermore, only limited facilities around the world can afford complete armamentarium of PET instruments

and cyclotron for the local production of short-lived positron-emitters. Clinical data have shown that 15.9 million SPECT procedures were performed in 2007, while only 1.6 million of PET procedures were performed, in comparison[15].

**e. Planar and SPECT-based radiotracers for breast cancer imaging in clinic**

To date, the most common radiotracer used for SPECT and planar scintigraphic imaging such as scintimammography is  $^{99m}\text{Tc}$ -methoxyisobutylisonitrile ( $^{99m}\text{Tc}$ -MIBI or  $^{99m}\text{Tc}$ -sestamibi). Scintimammography has been increasingly used to assess the suspicious lesions of patients with a negative or indeterminate mammography in the clinic[16]. This small lipophilic cation was originally developed as a myocardial perfusion agent. The first report of its application in breast cancer detection was by Aktolun et al. in 1992[17]. The cellular uptake mechanisms of  $^{99m}\text{Tc}$ -sestamibi still remain unclear; however, its uptake is driven by a negative transmembrane potential and most of the radioactivity is found in the mitochondria[18].  $^{99m}\text{Tc}$ -sestamibi scintimammography shows higher sensitivity (85%) and specificity (87%) than the traditional mammography, and its sensitivity is independent of breast density[19]. In addition,  $^{99m}\text{Tc}$ -sestamibi is a substrate of the transmembrane P-glycoprotein (Pgp), which is a member of the MDR/TAP subfamily that is involved in the multidrug resistance. Therefore, the uptake, clearance, and retention of  $^{99m}\text{Tc}$ -sestamibi have been investigated as predictors of response to chemotherapy in human breast cancer[20]. In a study of 45 patients with primary breast cancer, Cayre et al concluded that a negative  $^{99m}\text{Tc}$ -sestamibi

scintimammography predicted chemoresistance with a specificity of 100%. Besides,  $^{99m}\text{Tc}$ -sestamibi uptake was inversely correlated to the expression of multidrug resistance protein MDR1 ( $P < 0.05$ ) in invasive ductal carcinomas[21].

Nevertheless,  $^{99m}\text{Tc}$ -sestamibi scintimammography demonstrates relatively low sensitivity in detecting the nonpalpable lesions or tumors smaller than 1 cm[22]. Therefore, the high resolution small field-of-view breast-specific  $\gamma$ -imaging (BSGI) has been developed as an alternative. Similar to positron emission mammography (PEM), the single-head detector used in BSGI is mounted opposite to a compression plate, so the patient's breast is compressed between detector and plate. According to a 6-year BSGI study performed by Hruska et al. at Mayo Clinic, the sensitivity of BSGI for tumors larger than 1 cm was 97%, while that for tumors smaller than 1 cm was 74%[23]. When comparing BSGI with PEM, although the average sensitivity of PEM (93%) is slightly higher than that of BSGI (89%), BSGI has a much higher negative predictive value (100%) than that of PEM (88%)[24]. Thus, both of the imaging modalities have great detection ability in existing studies, and there is no proven clinically significant advantage to either modality over the other so far.

Although not majorly used, several other radiotracers have been successfully developed as alternatives to  $^{99m}\text{Tc}$ -sestamibi. Table 1.4 summarizes the radiotracers that currently applied to SPECT and planar scintigraphic imaging of breast cancer, categorized according to the tumor-specific targets to which they are aimed at.

**Table 1.4. Planar and SPECT-based radiotracers used to detect breast cancer in humans, by tumor-specific target.**

<b>Target</b>	<b>SPECT or Gamma Imaging Radiotracer</b>
<b>Perfusion</b>	Thallium-201 <sup>99m</sup> Tc-sestamibi <sup>99m</sup> Tc-tetrofosmin
<b>Glucose metabolism</b>	<sup>99m</sup> Tc-ethylenedicycysteine- <i>N</i> -acetylglucosamine
<b>Hormone receptor</b>	<sup>123</sup> I-16 $\alpha$ -estradiol
<b>HER2</b>	<sup>111</sup> In-trastuzumab
<b>Angiogenesis</b>	<sup>99m</sup> Tc-NC100692 <sup>111</sup> In-bevacizumab
<b>Amino acid transporters and protein synthesis</b>	<sup>99m</sup> Tc-methionine L-3- <sup>123</sup> I- $\alpha$ -methyltyrosine
<b>Apoptosis</b>	<sup>99m</sup> Tc-EC-annexin V
<b>Somatostatin receptors</b>	<sup>111</sup> In-diethylenetriamine pentaacetic acid-octreotide
<b>Bone</b>	<sup>99m</sup> Tc-MDP <sup>67</sup> Ga-citrate



## **II. Amino acid transporter systems**

### **a. Introduction**

Amino acids cross the cell membranes via various amino acid transporter systems based on their structures. The mammalian amino acid transporter systems can be classified as neutral, acidic or basic classes according to the substrates they transport. Each of the classes can be further divided into Na<sup>+</sup>-dependent and Na<sup>+</sup>-independent transporter subclasses[25]. To date, more than 20 systems have been identified (Table 1.5), and the major systems that are present in all tissues are the Na<sup>+</sup>-dependent system A and ASC, as well as the Na<sup>+</sup>-independent system L[26-28]. Transport of an amino acid generally depends on the difference between its intra- and extra-cellular concentration, and is frequently associated with counter-transport of a second amino acid, whose gradient is controlled by one or more of the Na<sup>+</sup>-dependent systems.

In tumor cells, amino acid transporters are generally upregulated to facilitate their increasing amino acid uptake[29, 30]. In addition to functioning as the basic building blocks of proteins, amino acids are also important sources of carbon and nitrogen in the synthesis of purine and pyrimidine nucleotides, amino sugars, and glutathione, which are the essential elements for rapid proliferation of tumor cells[31]. Therefore, the rate of amino acid uptake and transport, rather than the protein synthesis rate, is very crucial for tumor cells[32, 33].

The development of amino acid-based imaging probes has focused on radiolabeling the substrates of those amino acid transporter systems, especially for system L and/or A given that they are the two major transport systems in

mammalian cells. Here, we introduce systems A and L, their molecular biology and transport mechanisms.

**Table 1.5. Major amino acid transporter systems in mammalian.**

		Transporter System	Substrate	Transporter	Family
Neutral	Na <sup>+</sup> -dependent	A	Ala, Pro, N-methyl amino acids	ATA1-3	SLC38
		ASC	Ala, Ser, Thr, Cys, (Gln)	ASCT1,2	SLC1
		B <sup>0</sup>	Broad substrate selectivity		
		B-system	B-Ala, Tau	Taut	SLC6
		G	Gly, Sar	GLYT1,2	SLC6
		N	Gln, Asn, His	SN1,2	SLC38
		γ <sup>+</sup> L	Neutral and basic amino acids	γ <sup>+</sup> LAT1-4F2hc, γ <sup>+</sup> LAT2-4F2hc	SLC7
	Na <sup>+</sup> -independent	asc	Ala, Ser, Thr, Cys	Asc-1-4F2hc, Asc-2-?	SLC7
		b <sup>0,+</sup>	Neutral and basic amino acids	BAT1/b <sup>0,+</sup> AT-rBAT	SLC7
		L	Large neutral amino acids	LAT1-4-4F2hc,	SLC7
		T	Aromatic amino acids	TAT1	SLC16
Basic	Na <sup>+</sup> -dependent	B <sup>0,+</sup>	Neutral and basic amino acids	ATB <sup>0,+</sup>	SLC6
	Na <sup>+</sup> -independent	b <sup>0,+</sup>	Neutral and basic amino acids	BAT1/b <sup>0,+</sup> AT-rBAT	SLC7
		γ <sup>+</sup>	Basic amino acids	CAT1-4	SLC7
		γ <sup>+</sup> L	Neutral and basic amino acids	γ <sup>+</sup> LAT1-4F2hc, γ <sup>+</sup> LAT2-4F2hc	SLC7
Acidic	Na <sup>+</sup> -dependent	X <sub>AG</sub> <sup>-</sup>	L-Glu, L-/D-Asp	EAAC1, GLT-1, GLAST, EAAT4,5	SLC1
	Na <sup>+</sup> -independent	x <sub>C</sub> <sup>-</sup>	Cys/Glu exchange	xCT-4F2hc	SLC7

**SLC: solute carrier family, a naming of transporter families by Human Gene**

**Nomenclature Committee.**

**b. System A**

System A is a  $\text{Na}^+$ -dependent system that transports small neutral aliphatic amino acids. It can uniquely recognize and transport N-methylated amino acids, and thus, N-methyl aminoisobutyric acid (MeAIB) is used as a system A specific inhibitor to determine its substrates. It can also be characterized by tolerance of  $\text{Li}^+$  substitution for  $\text{Na}^+$ , and by the property of trans-inhibition[34]. System A is pH sensitive and displays hormonal and adaptive regulation[35]. It has three subtypes: SNAT1 (the sodium-coupled neutral amino acid transporter 1), SNAT2, and SNAT4. Some of these subtypes are considered to be associated with cancers. For instance, Kondoh et al. demonstrated that SNAT1 mRNA expression in human hepatocellular carcinoma (HCC) cell lines was significantly higher than that of normal liver tissue. In addition, the expression of SNAT1 was significantly activated in HCC tissues as well as in premalignant cirrhotic livers from HCC patients[36].

**c. System L**

System L (L-type amino acid transporter system, or LAT) is a  $\text{Na}^+$ -independent system for transporting large neutral amino acids such as branched or aromatic amino acids. It exchanges one amino acid from the extracellular compartment with one amino acid from the intracellular compartment (Fig. 1.1). LAT has broad substrate selectivity and four subtypes named LAT1-4, respectively. LAT1 and LAT2 have similar structures and their amino acid sequences show 50% identity in human. Both of them form heterodimeric complexes via a disulfide bond and comprise of a 12-transmembrane catalytic light chain and a type-II glycoprotein

heavy chain called 4F2hc (Fig. 1.1). Different from LAT1 and LAT2, the subtypes LAT3 and LAT 4 can function without 4F2hc; however, since both of them were identified recently, little is known about their molecular properties and functions. Among four subtypes, only LAT1 shows increased transport activity and plays an important role in proliferating cells such as placenta and tumor cells. LAT1 upregulation has been observed in various cancer types as well as tumor cell lines, thus, is considered as a diagnostic and prognostic biomarker for cancers[37-40]. LAT1 transports not only amino acids, but also some hormones such as thyroxine and triiodothyronine, as well as other drugs such as L-DOPA for Parkinson's disease and melphalan for cancer treatment[41]. BCH (2-amino-endo-bicycloheptane-2-carboxylic acid), a specific inhibitor of LAT, is often used to determine whether a certain compound like amino acid-based radiotracer is LAT substrate[42].

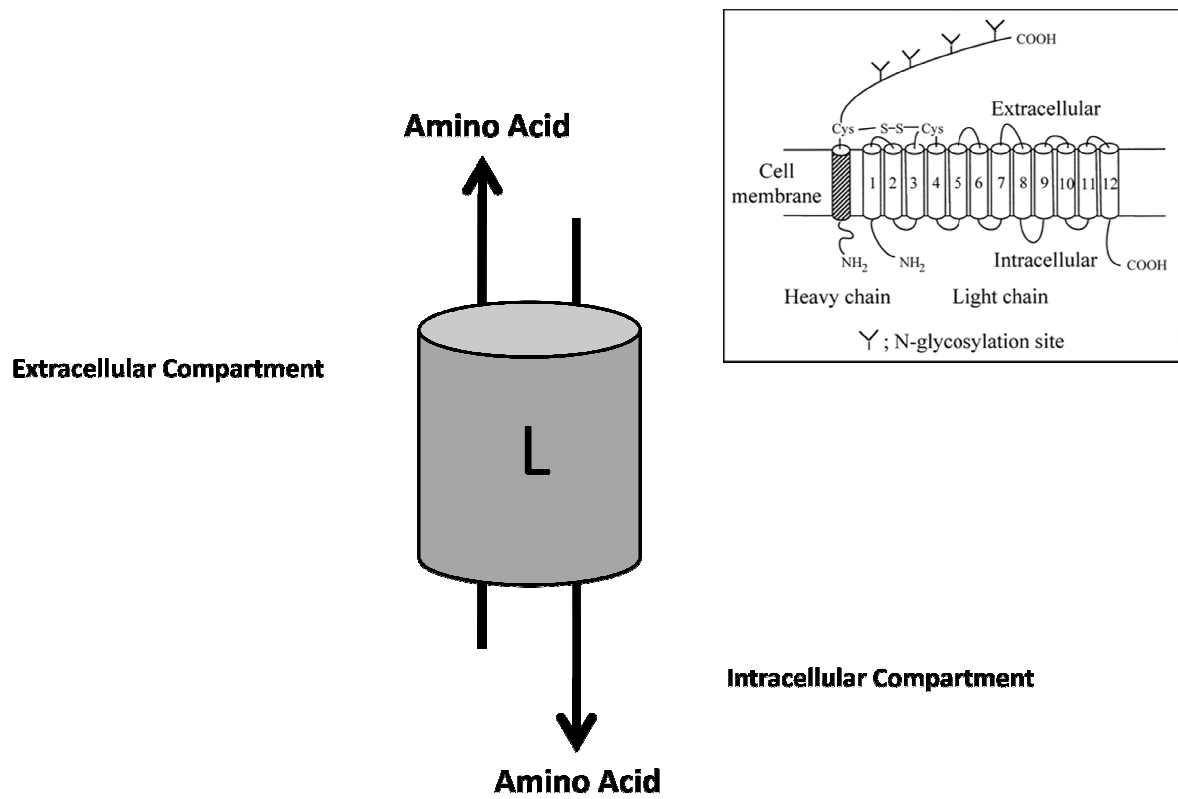


Figure 1.1. Predicted structure of L-type amino acid transporter LAT-1 and its transport mechanism.

### III. Tyrosine-based radiotracers for tumor imaging

#### a. $^{11}\text{C}$ -labeled tyrosine analogue

Theoretically, all amino acids can be labeled with  $^{11}\text{C}$  since all of them contain at least two carbons (the carboxyl carbon and the  $\alpha$ -carbon) that can serve as labeling sites. Although  $^{11}\text{C}$  is adequate for amino acid-based PET imaging, which typically has peak tumor uptake 15-20 min after *i.v.* injection, the 20 min half-life of  $^{11}\text{C}$  restricts its use only to the institutions that have an onsite cyclotron, and thus, makes it clinically impractical[43].

L-[1- $^{11}\text{C}$ ]-tyrosine ( $^{11}\text{C}$ -Tyr) is a reliable amino acid-based PET probe for tumor detection and quantification in multiple types of malignancies, including brain[44], breast[45], head and neck cancers[46], and soft tissue sarcomas[47]. Since  $^{11}\text{C}$ -Tyr is largely incorporated into proteins, it has been used as an appropriate probe for protein synthesis rate quantification. Same as its precursor tyrosine,  $^{11}\text{C}$ -Tyr has been proven to enter the tumor cells predominantly via amino acid transport system L.

There are mainly three approaches to synthesize  $^{11}\text{C}$ -Tyr: via the Bücherer-Strecker reaction[48], an enzymatic route[49], and the robotic synthesis using isocyanide method[50].  $^{11}\text{C}$ -Tyr can be obtained within 50-60 min in a high purity (>98%) through each method, however, the overall radiochemical yield by robotic synthesis was relatively lower than the other two methods (10% vs. 40-60%). Regardless of its low synthetic yield, the robotic synthesis is preferable because it is a convenient procedure for routine  $^{11}\text{C}$ -Tyr production and can avoid high dose radiation exposure and contamination.

To date, many studies have been conducted to compare the imaging potentials between  $^{11}\text{C}$ -Tyr and  $^{18}\text{F}$ -FDG.  $^{11}\text{C}$ -Tyr appears to be better than  $^{18}\text{F}$ -FDG for breast cancer imaging because of its lower uptake in fibrocystic disease[45].  $^{11}\text{C}$ -Tyr-PET showed higher specificity (95% vs. 88%), accuracy (95% vs. 88%), and positive predictive value (63% vs. 48%) than those of  $^{18}\text{F}$ -FDG-PET in detecting cervical lymph nodes of 11 patients with squamous cell carcinoma of the oral cavity[51]. Furthermore, prolactinomas could be clearly visualized by  $^{11}\text{C}$ -Tyr-PET, but not  $^{18}\text{F}$ -FDG-PET[52]. Kole et al. compared  $^{18}\text{F}$ -FDG and  $^{11}\text{C}$ -Tyr imaging potentials in patients with soft-tissue tumors before and after chemotherapy and found out that although  $^{18}\text{F}$ -FDG had a better indication of tumor grade,  $^{11}\text{C}$ -Tyr was more accurate in predicting proliferation and mitotic rate of the tumor lesions, especially after treatment[53]. In another study, Boer et al. have demonstrated a significant positive relationship between high  $^{11}\text{C}$ -Tyr uptake and poor survival rate of patients with laryngeal carcinoma under radiotherapy[54]. However,  $^{11}\text{C}$ -Tyr seems not suitable for visualizing the tumors with a low proliferation rate such as testicular nonseminoma germ-cell tumor[55].

**b.  $^{123}\text{I}$ -labeled tyrosine analogue**

The SPECT radionuclide  $^{123}\text{I}$  has a long half-life of 12.3 hr, which allows the imaging of slower biological processes taking place over the course of 1-2 days.

3- $^{123}\text{I}$ ]iodo- $\alpha$ -methyl-L-tyrosine ( $^{123}\text{I}$ -IMT) is a useful SPECT imaging probe for diagnostic evaluation and therapy planning to patients with brain tumors[56]. It can be synthesized by direct electrophilic iodination of  $\alpha$ -methyl-L-tyrosine (AMT) in the

presence of an oxidizing agent such as Chloramine-T[57] and Iodogen[58]. The average radiochemical yield ranges from 60-80%.

$^{123}\text{I}$ -IMT is dominantly transported by amino acid transport system L and not incorporated into proteins. It is eliminated via renal clearance, and the highest absorbed doses are observed in bladder, colon, and kidneys[59]. Although it was not ideal to determine prognosis and grade of gliomas,  $^{123}\text{I}$ -IMT-SPECT still succeeds to image the extent of cerebral gliomas as well as their recurrences, and to differentiate recurrences from radionecrosis[60-62]. For extracranial tumors,  $^{123}\text{I}$ -IMT-SPECT has been used to evaluate non-small cell lung cancer[63], head and neck cancer[64], melanoma[65], and soft tissue sarcomas[66]; however, most of those clinical results were similar or even inferior to those from  $^{18}\text{F}$ -FDG-PET. Plotkin et al. demonstrated that the positive predictive value in the diagnosis of relapsed head and neck cancer could be improved by integrating low-dose CT with  $^{123}\text{I}$ -IMT-SPECT[67, 68]. Therefore,  $^{123}\text{I}$ -IMT applied with combined SPECT/CT imaging is recommended for the future clinical studies.

Other than  $^{123}\text{I}$ -IMT, iodine-125-labeled 3- $^{125}\text{I}$ iodo- $\alpha$ -methyl-L-tyrosine was also synthesized and evaluated *in vitro* and *in vivo*[69-71], however, no clinical study has been reported so far.

### **c. $^{18}\text{F}$ -labeled tyrosine analogues**

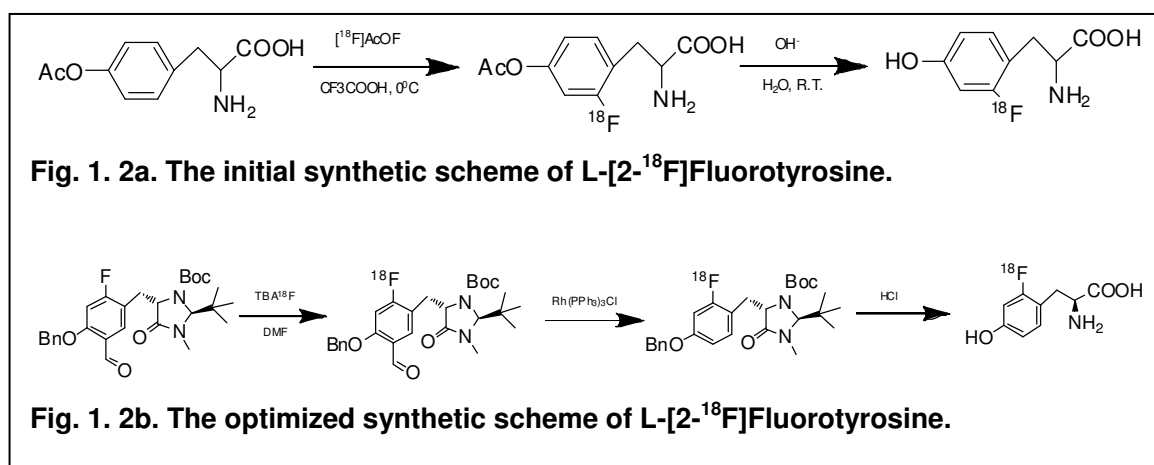
Compared to  $^{11}\text{C}$  with a 20 min short half-life,  $^{18}\text{F}$  has a 109.8 min half-life and thus can be remotely distributed to the institutions without an onsite cyclotron. An increasing number of  $^{18}\text{F}$ -labeled tyrosine analogues have been developed, and



their transport mechanisms as well as potentials to image tumors have been intensively under investigation. The three major  $^{18}\text{F}$ -labeled tyrosine-based radiotracers are discussed here.

## 1. L-2-[ $^{18}\text{F}$ ]fluorotyrosine ( $^{18}\text{F}$ -Tyr)

L-2-[ $^{18}\text{F}$ ]fluorotyrosine ( $^{18}\text{F}$ -Tyr) was first evaluated as a PET tracer of cerebral protein synthesis by Coenen et al in 1989[72]. The initial synthetic route is shown in Fig. 1. 2a . Briefly, [ $^{18}\text{F}$ ]acetylhypofluorite is used for electrophilic radiofluorination of O-acetyltyrosine in  $\text{CF}_3\text{COOH}$  as solvent at  $0^\circ\text{C}$ . After base-catalyzed hydrolysis of the acetyl moiety, the final product  $^{18}\text{F}$ -Tyr then can be isolated from the isomeric mixture via reverse phase HPLC with a specific activity of 10-20 GBq/mmol in a 17% yield[72]. Recently, Melean et al reported a new 3-step nucleophilic synthesis procedure starting with [ $^{18}\text{F}$ ]fluoride, and the total synthetic yield of  $^{18}\text{F}$ -Tyr was optimized up to 49% (Fig. 1. 2b).



$^{18}\text{F}$ -Tyr has been successfully used for detecting brain tumors[73]; however, it appears to be less sensitive for staging non-small cell lung cancer and lymphomas compared to  $^{18}\text{F}$ -FDG[74].

## **2. L-[3- $^{18}\text{F}$ ]- $\alpha$ -methyl tyrosine ( $^{18}\text{F}$ -FMT)**

Due to its lower physiological uptake in cortex than that of  $^{18}\text{F}$ -FDG, L-[3- $^{18}\text{F}$ ]- $\alpha$ -methyl tyrosine ( $^{18}\text{F}$ -FMT) was initially studied as a brain tumor imaging agent for PET by Inoue et al[75]. It was developed based on the same concept of its iodinated SPECT counterpart  $^{123}\text{I}$ -IMT, and hence, the metabolic behavior of  $^{18}\text{F}$ -FMT appears to be similar as that of  $^{123}\text{I}$ -IMT.  $^{18}\text{F}$ -FMT accumulates in the tumor cells solely via amino acid transporter system L, especially the LAT1 subtype, and shows no incorporation into proteins[76].

$^{18}\text{F}$ -FMT can be successfully synthesized following a simple and quick procedure designed by Tomiyoshi et al[77]. Briefly, [ $^{18}\text{F}$ ] $\text{F}_2$  gas is converted to  $^{18}\text{F}$ -labelled acetylhypofluorite, which is then bubbled into the solution containing 10 mg of L- $\alpha$ -methyltyrosine in 0.5 mL of trifluoroacetic acid (0 $^\circ\text{C}$ ). The radiochemical yield and purity of  $^{18}\text{F}$ -FMT were  $20.3\pm 5.1\%$  and  $99.4\pm 0.3\%$ , respectively.

In addition to its application in brain tumors,  $^{18}\text{F}$ -FMT has also been extensively investigated for its potential in detecting musculoskeletal tumor[78], maxillofacial tumor[79], oral squamous cell carcinoma[80], and non-small cell lung cancer[81-83]. In a study of 75 patients with musculoskeletal tumor, Watanabe et al concluded that although  $^{18}\text{F}$ -FDG may be better for tumor grading,  $^{18}\text{F}$ -FMT had higher specificity in differentiating between benign and malignant tumors[78]. In

another study of patients with untreated malignant maxillofacial tumor,  $^{18}\text{F}$ -FMT-PET had better contrast of tumor visualization to the surrounding normal structures than  $^{18}\text{F}$ -FDG-PET in 27 out of 36 patients[79]. Furthermore, Kaira et al demonstrated that  $^{18}\text{F}$ -FMT had no false-positives in detecting primary non-small cell lung cancer and lymph node metastasis. In addition, they showed that LAT1 expression was a strong prognostic factor in non-small cell lung cancer patients, and  $^{18}\text{F}$ -FMT uptake in the tumor lesions was positively correlated with LAT1 expression ( $p=0.890$ )[81, 82].

### 3. ***O*-(2- $^{18}\text{F}$ -Fluoroethyl)-L-Tyrosine ( $^{18}\text{F}$ -FET)**

*O*-(2- $^{18}\text{F}$ -fluoroethyl)-L-Tyrosine ( $^{18}\text{F}$ -FET) is a promising PET probe for diagnosis of brain tumors and extracranial squamous cell carcinomas[84]. Several strategies for  $^{18}\text{F}$ -FET synthesis have been reported.  $^{18}\text{F}$ -FET was initially prepared via a 2-step procedure, alkylation of the L-tyrosine di-potassium salt with [ $^{18}\text{F}$ ]fluoroethyltosylate (Fig. 1.3a)[85]. By following this procedure,  $^{18}\text{F}$ -FET could be obtained in about 50 min with an overall yield of 40% and the specific activity was  $>200$  GBq/ $\mu\text{mol}$ . However, this procedure is not suitable for automation because the separation and purification steps require HPLC. Later, the synthesis of  $^{18}\text{F}$ -FET was improved by the implementation of direct nucleophilic radiofluorination on protected alkyl tyrosine derivative, *O*-(2-tosyloxyethyl)-*N*-trityl-L-tyrosine *tert*-butylester (Fig. 1.3b). Although the radiochemical yield was much higher (60%), it took about 80 min for the entire process to complete due to the necessity of HPLC purification to remove the solvent and an aggressive TFA[86]. So far, the best

synthesis route of  $^{18}\text{F}$ -FET, which suits perfectly for automation modules, was reported by Krasikova et al in 2008[87]. It is a novel type of chiral enantiomerically pure labeling precursor based on Nill complex of a Schiff's base of (S)-[N-2-(N'-benzylpropyl)amino]benzophenone (BPB) with alkylated (S)-tyrosine, Ni-(S)-BPB-(S)-Tyr-OCH<sub>2</sub>CH<sub>2</sub>OTs (Fig. 1.3c). The overall synthesis time was 55 min, and the radiochemical yield was 40-45%.

$^{18}\text{F}$ -FET is primarily transported by the Na<sup>+</sup>-independent amino acid transport system L, as well as the Na<sup>+</sup>-dependent amino acid transporter system B<sup>0,+</sup> and B<sup>0</sup>.  $^{18}\text{F}$ -FET is not incorporated into proteins[85].

For the clinical studies,  $^{18}\text{F}$ -FET has always been compared to the same amino acid-based radiotracer  $^{11}\text{C}$ -MET, or the gold standard of tumor imaging tracer  $^{18}\text{F}$ -FDG. In a study of 16 patients with suspected primary or recurrent intracerebral tumors,  $^{18}\text{F}$ -FET-PET showed similar uptake and image contrast as those of  $^{11}\text{C}$ -MET[88]. However,  $^{18}\text{F}$ -FET accumulates to a significantly greater extent in tumor cells than in inflammatory cells when compared to  $^{18}\text{F}$ -FDG or  $^{11}\text{C}$ -MET, and therefore, shows better differentiation between tumor and inflammatory lesions *in vivo*[89, 90]. In fact, Popperl et al revealed that  $^{18}\text{F}$ -FET-PET could reliably distinguish post-therapeutic benign lesions, which may have a certain extent of inflammation, from tumor recurrence after initial treatment of both low- and high-grade gliomas[91]. In addition, Plotkin et al concluded that  $^{18}\text{F}$ -FET-PET was superior to  $^{18}\text{F}$ -FDG-PET for biopsy planning in patients with non-contrast-enhancing brain tumors diagnosed by MRI[92]. Although  $^{18}\text{F}$ -FET-PET itself already has high sensitivity (88-100%), specificity (88-92.9%), and positive predictive value

(84%) in glioma diagnosis[93-95], it is highly recommended to combine its application with MRI and MR spectroscopy[94]. Furthermore,  $^{18}\text{F}$ -FET appears to be suitable for the prognosis of glioma. Hutterer et al suggested that  $^{18}\text{F}$ -FET-PET might predict the failure of antiangiogenic treatment such as bevacizumab-irinotecan in patients with recurrent high-grade glioma[96]. Besides, Floeth et al suggested that the baseline amino acid uptake on  $^{18}\text{F}$ -FET-PET and a diffuse versus circumscribed tumor pattern on MRI were strong predictors for the outcomes of treatments to patients with low-grade glioma[97]. When the dynamic  $^{18}\text{F}$ -FET-PET imaging in patients with glioblastoma is quantified, the ratio of standard uptake value (SUV) to background may provide a more valuable predictive measurement of the clinical outcome rather than the conventional SUV or distribution volume[98].

Unlike  $^{18}\text{F}$ -FMT,  $^{18}\text{F}$ -FET is more dedicated in brain tumor imaging. Several studies were performed on the patients with head and neck cancer, however,  $^{18}\text{F}$ -FET imaging on those patients were not sensitive and specific enough to replace the  $^{18}\text{F}$ -FDG[99-101].

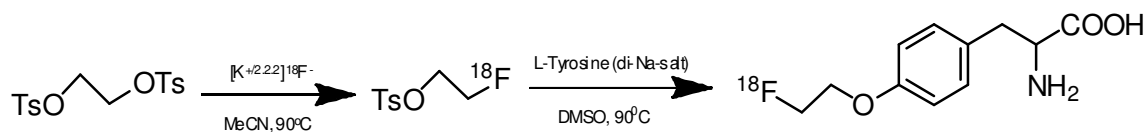


**Fig. 1.3a. The initial synthetic scheme of O-2-[ $^{18}\text{F}$ ]fluoroethyl-L-tyrosine.**

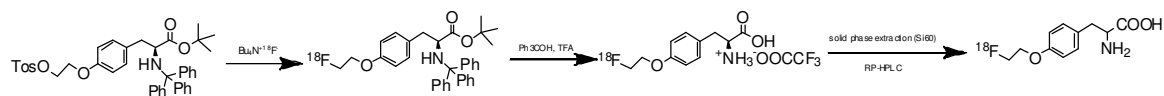


**Fig. 1.3b. The optimized synthetic scheme of O-2-[ $^{18}\text{F}$ ]fluoroethyl-L-tyrosine.**

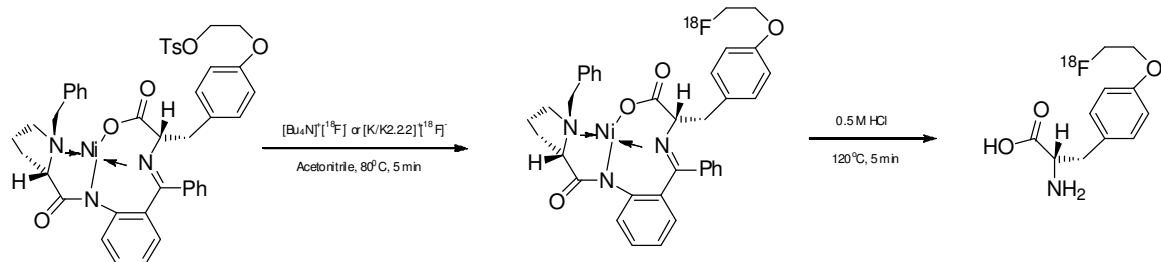


**Fig. 1.3c. The best synthetic scheme of O-2-[ $^{18}\text{F}$ ]fluoroethyl-L-tyrosine.**

#### IV. Technetium-99m and its coordination with chelators

Technetium-99m ( $^{99m}\text{Tc}$ ) -based radiopharmaceuticals have been developed for cancer diagnostics since the 1960's[102].  $^{99m}\text{Tc}$  is an ideal radioisotope for diagnostic imaging studies, because of its physical characteristics. It emits a 140 keV  $\gamma$ -ray in 89% abundance, which can be detected by NaI detectors with low energy high-resolution collimator in the standard gamma camera[103].  $^{99m}\text{Tc}$  has a half-life of 6.02 h, which is ideal for preparation of radiolabeled small ligands and proteins[14]. It can be produced with in-house generator that contains the parent nuclide molybdenum-99 ( $^{99}\text{Mo}$ ), and does not require a cyclotron[104]. In addition, technetium (Tc) is a second-row transition element in Group 7, right above rhenium (Re), which has the radioisotope rhenium-188 ( $^{188}\text{Re}$ ) for cancer therapeutic applications[103]. Therefore, Tc chemistry is very similar to that of Re, which forms a diagnostic/therapeutic matched pair. Furthermore, due to their identical coordination parameters with the same ligands, a Re complex is a good structural model for the corresponding  $^{99m}\text{Tc}$  complex because Re does not have any radioactivity and the structure of its complex can be confirmed safely [103].

N,N'-ethylene-di-L-cysteine (EC) has been used as a strong chelator to trap the radioisotopes such as  $^{99m}\text{Tc}$ ,  $^{188}\text{Re}$ , and gallium-68 ( $^{68}\text{Ga}$ )[105-107].  $^{99m}\text{Tc}$  labeled EC is used as a renal imaging agent, which shows identical imaging properties but higher plasma clearance than the most widely used clinical agent,  $^{99m}\text{Tc}$ -mercaptoacetyltriglycine ( $^{99m}\text{Tc}$ -MAG3)[107]. The rhenium complex of EC, Re-EC, has also been synthesized and the structure has been determined by single-crystal X-ray diffraction[107].

On the other hand, 1,4,8,11-tetra-azacyclotetradecane (N4 cyclam), one of the most common macrocyclic tetraamines, has also been reported as an efficient chelator for  $^{99m}\text{Tc}$  labeling[108, 109]. The  $^{99m}\text{Tc}$ -N4 complex is hexacoordinate with a *trans*-Tc (V)-dioxo core and positively charged (+1).

By taking the advantage of chelators such as EC and N4 cyclam, we can label the tumor-target ligands with several different radioisotopes for SPECT or PET imaging, and for the radiotherapeutic purposes, respectively.

## **V. Scope of the dissertation**

In this dissertation, four  $^{99m}\text{Tc}$ -labeled tyrosine derivatives have been synthesized and evaluated *in vitro* and *in vivo* for their imaging potentials in a breast cancer model (Fig. 1.4). We chose tyrosine and its derivative  $\alpha$ -methyl tyrosine (AMT) as the target ligands based on the preexisting promising clinical outcomes of application of their  $^{18}\text{F}$ -labeled analogues. In addition, the structures of tyrosine and AMT can be readily modified without changing their favorable biological characteristics. In order to radiolabel tyrosine and AMT with  $^{99m}\text{Tc}$ , we used chelators EC and N4 cyclam, which have been reported to have the ability to stably chelate with  $^{99m}\text{Tc}$ [108, 110]. By taking advantage of the chelator technology, we can label the same target ligand with different radioisotopes for various imaging modalities in tumor diagnosis, or label the ligand with the therapeutic radioisotopes for cancer treatment in future.

Our hypothesis is that  $^{99m}\text{Tc}$ -labeled tyrosine/AMT-based radiotracers provide great potential in breast cancer imaging by accumulating in tumor cells via the L-



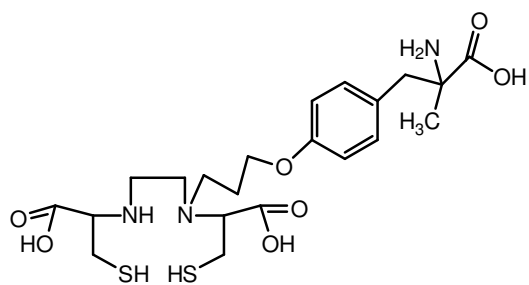
type amino acid transporter system (LAT), and they can well differentiate tumor from inflammation. To test this hypothesis in each radiotracer, three specific aims are addressed:

**Specific Aim 1.** Synthesize tyrosine/AMT-based precursor and label it with  $^{99m}\text{Tc}$ .

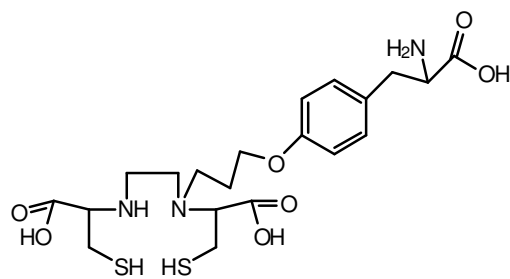
**Specific Aim 2.** Investigate the uptake kinetics and transport mechanisms of  $^{99m}\text{Tc}$ -labeled tyrosine/AMT-based radiotracer in rat mammary tumor cell line 13762.

**Specific Aim 3.** Assess the kinetics of  $^{99m}\text{Tc}$ -labeled tyrosine/AMT-based radiotracer accumulation in tumor and inflammation tissues in a rat mammary tumor model.

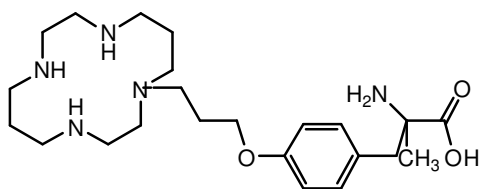
Chapter 1 has served as an introduction to the whole project. In Chapter 2-5, each chapter describes the synthesis and biological evaluation of one compound. Chapter 6 constitutes an overview of the project and compares four compounds based on the three specific aims that were presumed to be addressed.



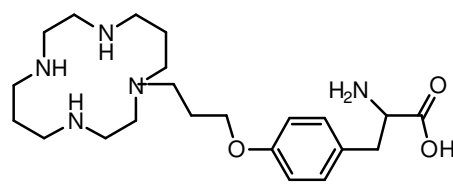
EC-AMT



EC-Tyrosine



N4-AMT



N4-Tyrosine

**Figure 1.4. Proposed structures of four tyrosine-based precursors.**

## CHAPTER 2 Development of $^{99m}\text{Tc}$ -EC-Tyrosine for breast cancer imaging

### I. Introduction

Currently  $^{18}\text{F}$ -FDG is the most common radiotracer for PET in tumor detection and staging. However,  $^{18}\text{F}$ -FDG has several limitations that give rise to false positive/negative diagnosis. For instance,  $^{18}\text{F}$ -FDG has poor contrast in brain tumor due to the high glucose uptake in both normal and neoplastic brain tissues[111], and it has poor differentiation of tumor from inflammatory tissue because of the high  $^{18}\text{F}$ -FDG uptake in granulocytes and macrophages[112, 113]. Therefore, radiolabeled amino acids have been developed as an alternative to  $^{18}\text{F}$ -FDG. Their use in tumor detection is based on an increased uptake of amino acids in tumor cells, which is assumed to reflect an enhanced amino acid transporter, metabolism, and protein synthesis[114]. In contrast to glucose analog  $^{18}\text{F}$ -FDG, the uptake of amino acids in macrophages and other inflammatory cells is lower, so amino acid-based radiotracers are considered to be more specific than  $^{18}\text{F}$ -FDG[84]. Among all radiolabeled amino acids, aromatic ones such as tyrosine and its derivatives are more suitable given their easier chemistry alterations and favorable biological characterizations. To date, tyrosine and its  $\alpha$ -methyl substituted analog AMT have been successfully labeled with  $^{11}\text{C}$ [115, 116],  $^{18}\text{F}$ [75, 81] and  $^{124/125}\text{I}$ [65] for PET imaging, as well as  $^{123/131}\text{I}$ [56] for SPECT imaging, respectively. Most of those radiolabeled tyrosine analogs show promising preclinical and clinical results in tumor imaging, particularly in brain tumor staging. In addition, they have been proven to accumulate into the tumor cells predominantly via LAT, which is the only

system that can transport large neutral amino acids with aromatic rings[38, 41]. LAT, especially its subtype LAT1, is an ideal target for tumor imaging because it is up-regulated and highly expressed in many cancer cell lines and positively correlated with tumor growth[117, 118].

Although the existing radiolabeled tyrosine and its derivatives have shown very promising clinical outcomes, most of them require an on-site cyclotron to produce the radioisotope, which is inconvenient and expensive. Besides, the half-life of the radioisotopes are either too short (i.e. 20 min for  $^{11}\text{C}$ ) or too long (i.e. 57.4 days for  $^{125}\text{I}$ ). Furthermore, iodine-labeled compounds are not stable *in vivo* because of deiodination. So far,  $^{18}\text{F}$  has the most appropriate half-life (110 min), however, the radiosynthesis yield of  $^{18}\text{F}$ -labeled compounds appear to be relatively low because of its electrophilic fluorination step. Therefore, it is desirable to develop a radiotracer with simpler chemistry and affordable isotope, which can be used clinically in most major medical facilities.  $^{99\text{m}}\text{Tc}$  has favorable physical characteristics for diagnostic imaging studies. It emits a 140 keV gamma ray in 89% abundance, which is commonly used by gamma camera and SPECT. Its relatively long half-life (6.02 h) can provide serial images which overcomes the drawback of Fluorine-18 [103]. The chelator EC is known to chelate  $^{99\text{m}}\text{Tc}$  stably owing to the efficient binding of the oxotechnetium group to two thiols and two amine nitrogen atoms of EC[107]. By taking the advantage of using the chelator EC, we could label several other radioisotopes such as Gallium-68, Indium-111, or Rhenium-188 with the same ligand for diagnostic and therapeutic applications in future[105, 107]. Here, we report the synthesis of  $^{99\text{m}}\text{Tc}$ -labeled tyrosine using EC as a chelator, and its

potential in breast tumor imaging is evaluated.

## II. Materials and methods

### Chemicals and Analysis

EC was purchased from Taiwan Hopax Chems, Mfg, Co., Ltd. (Kaohsiung, Taiwan). All other chemicals of analytical grades and solvents of HPLC grade were obtained from Sigma-Aldrich (St. Louis, MO). Nuclear magnetic resonance (NMR) was performed on Bruker 300MHz Spectrometer (Bruker BioSpin Corporation, Billerica, MA), and mass spectra were performed on Waters Q-TOF Ultima Mass Spectrometer (Milford, MA) at the chemistry core facility at the University of Texas MD Anderson Cancer Center (UTMDACC; Houston, TX). Chemical shifts were reported in  $\delta$  (ppm) and  $J$  values in Hertz. Sodium pertechnetate ( $\text{Na}^{99\text{m}}\text{TcO}_4$ ) was obtained from  $^{99}\text{Mo}/^{99\text{m}}\text{Tc}$  generator by Mallinckrodt (Hazelwood, MO).  $^{18}\text{F}$ -FDG was obtained from Department of Nuclear Medicine at UTMDACC.

### Synthesis of Precursor EC-Tyrosine

#### a) *N-t-Butoxycarbonyl-O-[3-Br-propyl]-L-tyrosine methyl ester (compound 1).*

N-*t*-Butoxycarbonyl-L-tyrosine methyl ester (25 g; 0.085 mol) was dissolved in acetone (300 mL). 1,3-dibromopropane (17.3 mL; 0.169 mol) and  $\text{K}_2\text{CO}_3$  (58 g; 0.420 mol) were added under nitrogen. The reaction mixture was refluxed at 80 °C overnight. After cooling and filtration, the solvent was removed under reduced pressure, and the residue was dissolved in chloroform. The residue was washed

with water and dried with anhydrous  $\text{MgSO}_4$ . The product was purified by column chromatography using a silica gel column, eluted with hexane/ethyl acetate (2:1 v/v) to yield 33.3 g (94.6%).  $\text{Ms}(\text{m/z})$ : 440.09  $[\text{M}+\text{Na}]^+$ .

**b) *N-t-Butoxycarbonyl-O-[3-(N-Ethylenedicysteine) propyl]-L- tyrosine (compound 2).***

EC (4.7 g, 17.6 mmol) was dissolved in water (50 mL), and the pH was adjusted to pH 8-9 by NaOH (1N). Compound 1 (5.1 g, 12.3 mmol) in ethanol (100 mL) was added to the above solution, followed by adding  $\text{K}_2\text{CO}_3$  (12.13 g, 88 mmol). Reaction mixture was then heated at 80 °C overnight. After cooling, the solvent was removed under reduced pressure, and the residue was dissolved in chloroform (50 mL). The residue was washed with water, dried with anhydrous  $\text{MgSO}_4$ , and evaporated to dryness. Without further purification, the compound 2 was used for following steps.

**c) *O-[3-(N-Ethylenedicysteine) propyl]-L- tyrosine (EC-Tyrosine) (compound 3).***

The crude product of compound 2 (2.5 g, 4.24 mmol) was dissolved in ethanol (50 mL). Hydrobromic acid (48%, 4.5 mL) was added dropwisely to the solution over 30-min period at room temperature with stirring. After filtration, the white solid was washed with ethanol and recrystallized in water to yield 1.73 g.

**Radiolabeling of EC-Tyrosine and EC with  $^{99\text{m}}\text{Tc}$**

EC-Tyrosine (1 mg) was dissolved in 0.2 mL sterile water, followed by adding tin (II) chloride (0.1 mL, 1 mg/mL). For EC labeling, EC (0.5 mg) was dissolved in 0.2mL sterile water by adding 10  $\mu$ L of 1N NaOH (pH=9). Required amount of Na<sup>99m</sup>TcO<sub>4</sub> was added to EC or EC-Tyrosine solution (pH 7.4). Radiochemical purity was determined by radio-HPLC (High performance liquid chromatography; Waters, Milford, MA), eluted with acetonitrile: water (7:3) using a flow rate of 0.5 mL/min.

### **Determination of the Partition Coefficient**

To determine the lipophilicity, 20  $\mu$ L of <sup>99m</sup>Tc-EC-Tyrosine was added into an equal volume mixture of 1-octanol and sterile water in a centrifuge tube. The mixture was vortexed at room temperature for 1 min and then centrifuged at 5000 rpm for 5 min. From each phase, 0.1 mL of the aliquot was taken out and the radioactivity was measured by gamma counter (Cobra Quantum; Packard, MN). The measurement was repeated for three times, and care was taken to avoid cross contamination between the phases. The partition coefficient value, expressed as logP, was calculated using the following equation:

$$\text{LogP} = \text{Log} (\text{radioactivity in 1-octanol layer} / \text{radioactivity in sterile water layer})$$

### ***In Vitro* Cellular Uptake Studies**

Rat breast tumor cell line 13762 (American Type Culture Collection, Rockville, MD) was selected and the same cell line was used to create the animal model for *in vivo* evaluation. Cells were maintained in Dulbecco's modified Eagle's medium and nutrient mixture F-12 Ham (DMEM/F12; GIBCO, Grand Island, NY) at 37 °C in a

humidified atmosphere containing 5% CO<sub>2</sub>. Cells were plated onto 6-well tissue culture plates (2x10<sup>5</sup> cells/well) and incubated with <sup>99m</sup>Tc-EC-Tyrosine (0.05 mg/well, 8 uCi/well), the negative control <sup>99m</sup>Tc-EC (0.025 mg/well, 8 uCi/well), or <sup>18</sup>F-FDG (8 uCi/well) for 0-4 h. After incubation, cells were washed with ice-cold PBS twice and detached by treating them with 0.5 mL of trypsin for 5 min. Cells were then collected and the radioactivity was measured with gamma counter. Data were expressed in mean ±S.D. percent of cellular uptake (%Uptake) in triplicate.

### ***In Vitro* Competitive Inhibition Study**

To investigate the transport mechanisms of <sup>99m</sup>Tc-EC-Tyrosine, the competitive inhibition study using L-tyrosine was conducted. Rat breast tumor cells were co-incubated with <sup>99m</sup>Tc-EC-Tyrosine (8 µg/well, 8 µCi/well) and L-tyrosine for up to 1 h. A set of concentrations of L-tyrosine (10x, 50x, and 100x of the EC-Tyrosine concentration) were used. After incubation, cells were washed with ice-cold PBS twice and detached by treating them with 0.5 mL of trypsin for 5 min. Cells were then collected and the radioactivity was measured by gamma counter. Data were expressed in mean ±S.D. percent of cellular uptake (%Uptake) in triplicate.

### **Blood Clearance**

All animal work was carried out in the Small Animal Imaging Facility (SAIF) at UTMDACC under a protocol approved by Institutional Animal Care and Use Committee (IACUC). For blood clearance analysis, three normal female Fischer 344 rats (150±25 g) (Harlan Sprague-Dawley, Indianapolis, IN) were intravenously



injected with 30  $\mu\text{Ci}$   $^{99\text{m}}\text{Tc}$ -EC-Tyrosine. Blood samples were drawn through lateral tail vein at several time-points from 5 min to 24 h ( $n=3/\text{rat}$ ) by microliter pipettes (10  $\mu\text{L}$ ). The blood samples were measured for radioactivity by gamma counter, and then were calculated as percentage of the injected dose per gram of blood (%ID/g).

### ***In Vivo* Tissue Distribution Study of $^{99\text{m}}\text{Tc}$ -EC-Tyrosine**

Tissue distribution studies of  $^{99\text{m}}\text{Tc}$ -EC-Tyrosine (study I,  $n=9$ ) and  $^{18}\text{F}$ -FDG (study II,  $n=9$ ) were conducted by using normal female Fischer 344 rats ( $150\pm 25$  g,  $n=18$ ). For each compound, the rats were divided into three groups for three time intervals (0.5, 2, 4 h for  $^{99\text{m}}\text{Tc}$ -EC-Tyrosine; 0.5, 1, 2 h for  $^{18}\text{F}$ -FDG;  $n=3/\text{time point}$ ). The injection activity was  $25\pm 0.5$   $\mu\text{Ci}/\text{rat}$  intravenously. At each time interval, the rats were sacrificed, and the selected tissues were excised, weighed and measured for radioactivity by gamma counter. Each sample was calculated as percentage of the injected dose per gram of tissue wet weight (%ID/g). Counts from a diluted sample of the original injection were used as reference.

### **Planar Scintigraphic Imaging Study**

Female Fischer 344 rats were inoculated subcutaneously with 0.1 mL of breast tumor cells 13762 suspension in PBS ( $10^5$  cells/rat) into the right legs. Planar scintigraphic imaging of  $^{99\text{m}}\text{Tc}$ -EC-Tyrosine was performed 12-14 days after inoculation when tumors reached approximately 1 cm in diameter. Planar scintigraphic images were obtained using M-CAM (Siemens Medical Solutions, Hoffman Estates, IL) equipped with a Low Energy High Resolution collimator.

Anesthetized breast tumor-bearing rats were injected intravenously with  $^{99m}\text{Tc}$ -EC-Tyrosine (0.3 mg/rat, 300  $\mu\text{Ci}$ /rat;  $n=3$ ). The images were acquired up to 4 h post-administration of tracers. Computer outlined regions of interest (ROIs in counts per pixel) between tumor and muscle were used to calculate tumor/muscle (T/M) ratios. Percentage of the injected dose (%ID) of tumor was also calculated from the reference standard, which was 1/10 of the original injection activity.

### ***In Vivo* Uptake Blocking Study**

To ascertain whether  $^{99m}\text{Tc}$ -EC-Tyrosine uptake is mediated specifically by LAT, *in vivo* blocking studies using the unlabeled L-Tyrosine as the competitive inhibitor was conducted. The same animal model used in the planar scintigraphic imaging study was employed. Unlabeled L-Tyrosine (50 mg/kg) dissolved in 0.3 mL saline (pH adjusted to 2-3) was administered intravenously to mammary tumor-bearing rats 1 h prior to  $^{99m}\text{Tc}$ -EC-Tyrosine injection. Planar scintigraphic images were acquired up to 4 h, and ROIs of liver, kidneys, tumor, and muscle were used to calculate the ratios of liver/muscle, kidney/muscle, and tumor/muscle, respectively. In addition, %IDs of liver, kidneys, tumor, and muscle were calculated from the reference standard, which was 1/10 of the original injection activity. The results were compared with those from the rats injected with  $^{99m}\text{Tc}$ -EC-Tyrosine alone (control).

### **Tumor and Inflammation Uptake Comparison *In Vivo***

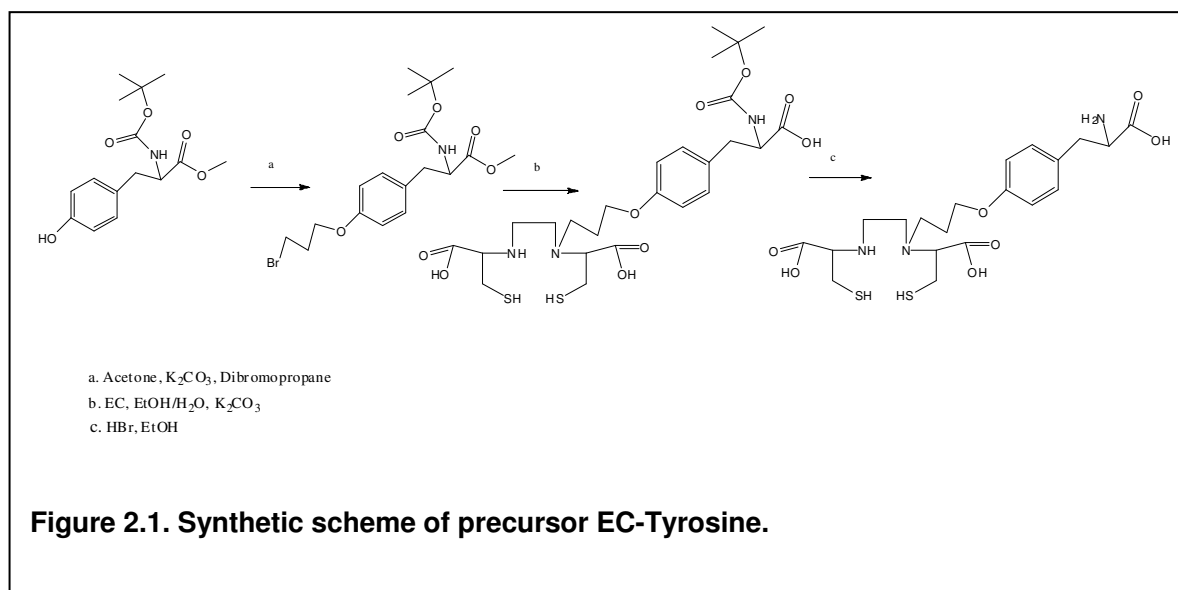
To investigate whether  $^{99m}\text{Tc}$ -EC-Tyrosine can differentiate tumor from the inflammatory tissue, a rat model bearing both mammary tumor and turpentine oil-induced inflammation was created. 13762 rat mammary tumor cells ( $10^5$  cells/0.1 mL PBS/rat) were inoculated into the right calf muscles of the female Fischer 344 rats. After the tumors reached to 1 cm in diameter, turpentine oil (0.1 mL/rat) was injected into the left calf muscles of the rats to induce inflammation. The anesthetized rats ( $n=3$ ) were injected intravenously with  $^{99m}\text{Tc}$ -EC-Tyrosine 24 h after the turpentine injection. Planar scintigraphic images were acquired up to 4 h, and ROIs of tumor, inflammation, and muscle were used to calculate the tumor-to-muscle ratios (T/Ms), inflammation-to-muscle ratios (I/Ms), and tumor-to-inflammation ratios (T/Is), respectively. Same animal model was used to evaluate  $^{18}\text{F}$ -FDG. Micro-PET imaging of  $^{18}\text{F}$ -FDG was performed using R4 micro-PET scanner (Concorde Microsystems, TN). The rats were injected intravenously with  $^{18}\text{F}$ -FDG (500  $\mu\text{Ci}$ /rat,  $n=3$ ), and dynamic PET scans were obtained for 90 min with a spatial resolution of 2.2 mm. PET images were reconstructed by using the ordered subset expectation maximization (OSEM) algorithm. T/Ms, I/Ms and T/Is ratios were calculated based on the regional radioactivity concentrations ( $\mu\text{Ci}/\text{cm}^3$ ) that were estimated from the average pixels within ROIs drawn around the tumor, inflammation or muscle on transverse slices of the reconstructed image sets.

### **III. Results**

#### **Chemistry and radiochemistry**

The synthetic scheme of precursor EC-Tyrosine is shown in Fig. 2.1. The structure and purity of EC-Tyrosine were confirmed by  $^1\text{H}$ - and  $^{13}\text{C}$ - NMR, mass spectra, and HPLC, respectively. The total synthesis yield of EC-Tyrosine was 79.5% (3-step). The  $^1\text{H}$ - and  $^{13}\text{C}$ -NMR results were  $^1\text{H}$ -NMR ( $\text{D}_2\text{O}$ ,  $\delta/\text{ppm}$ ): 7.01 (d, 2H, phenyl ring), 6.79 (d, 2H, phenyl ring), 3.94 (dd, 2H, O- $\text{CH}_2$ ), 3.27(t, 2H, CHN), 2.87 (d, 2H,  $\text{PhCH}_2$ -), 2.68-2.40(m, 8H,  $-\text{CH}_2$ -), 1.88(m, 2H, C- $\text{CH}_2$ -C).  $^{13}\text{C}$ -NMR ( $\text{D}_2\text{O}$ ,  $\delta/\text{ppm}$ ): 182.22, 182.22, 180.16, 156.69, 130.85, 130.50, 130.50, 114.85, 114.85, 66.89, 62.66, 57.35, 57.35, 46.28, 39.61, 34.29, 28.31, 28.20.

Precursor EC-Tyrosine could be labeled with  $^{99\text{m}}\text{Tc}$  with high radiochemical purities ( $> 95\%$ ). The partition coefficient value ( $\log P$ ) of  $^{99\text{m}}\text{Tc}$ -EC-Tyrosine was  $-2.02 \pm 0.168$ .



### ***In Vitro* Cellular Uptake Studies**

The cellular uptake kinetics of  $^{99m}\text{Tc}$ -EC-Tyrosine,  $^{99m}\text{Tc}$ -EC, and  $^{18}\text{F}$ -FDG using 13762 rat breast tumor cells is shown in Fig. 2.2. The uptake of  $^{99m}\text{Tc}$ -EC-Tyrosine into the tumor cells increased rapidly, and reached 1.02%Uptake at 4 h. In addition, the %Uptake of  $^{99m}\text{Tc}$ -EC-Tyrosine was much higher than that of  $^{18}\text{F}$ -FDG and the negative control  $^{99m}\text{Tc}$ -EC.

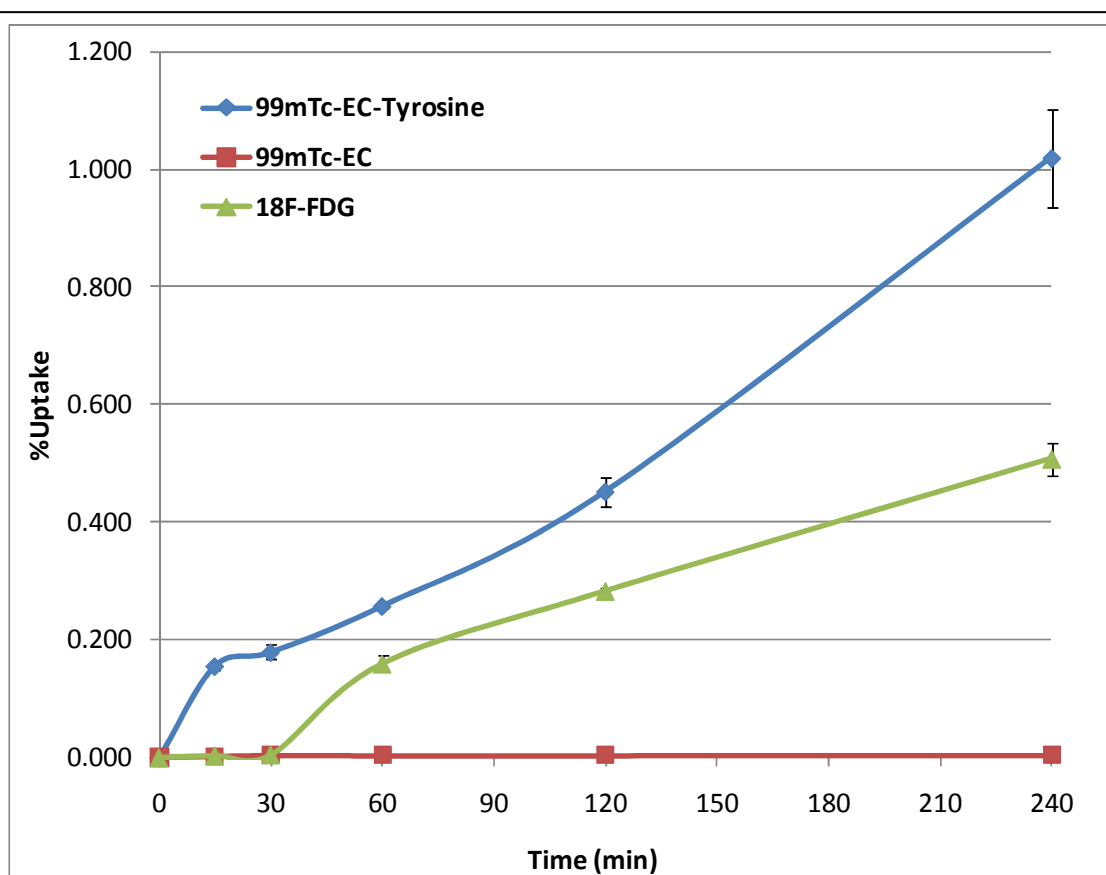


**Figure 2.2.** Time course of  $^{99m}\text{Tc}$ -EC-Tyrosine,  $^{99m}\text{Tc}$ -EC and  $^{18}\text{F}$ -FDG uptake in rat breast tumor cell line 13762 (0– 240 min). Data are expressed in mean  $\pm$  S.D. percentage of cellular uptake (%Uptake).

## Competitive Inhibition Study of $^{99m}\text{Tc}$ -EC-Tyrosine

After incubated with L-tyrosine at 10-100 times as high as the concentrations of EC-Tyrosine,  $^{99m}\text{Tc}$ -EC-Tyrosine showed a significantly decreased uptake, especially for 50 and 100 times concentration groups (Fig. 2.3). These results suggest that  $^{99m}\text{Tc}$ -EC-Tyrosine is transported at least partially via the same transporter system LAT as L-tyrosine is.

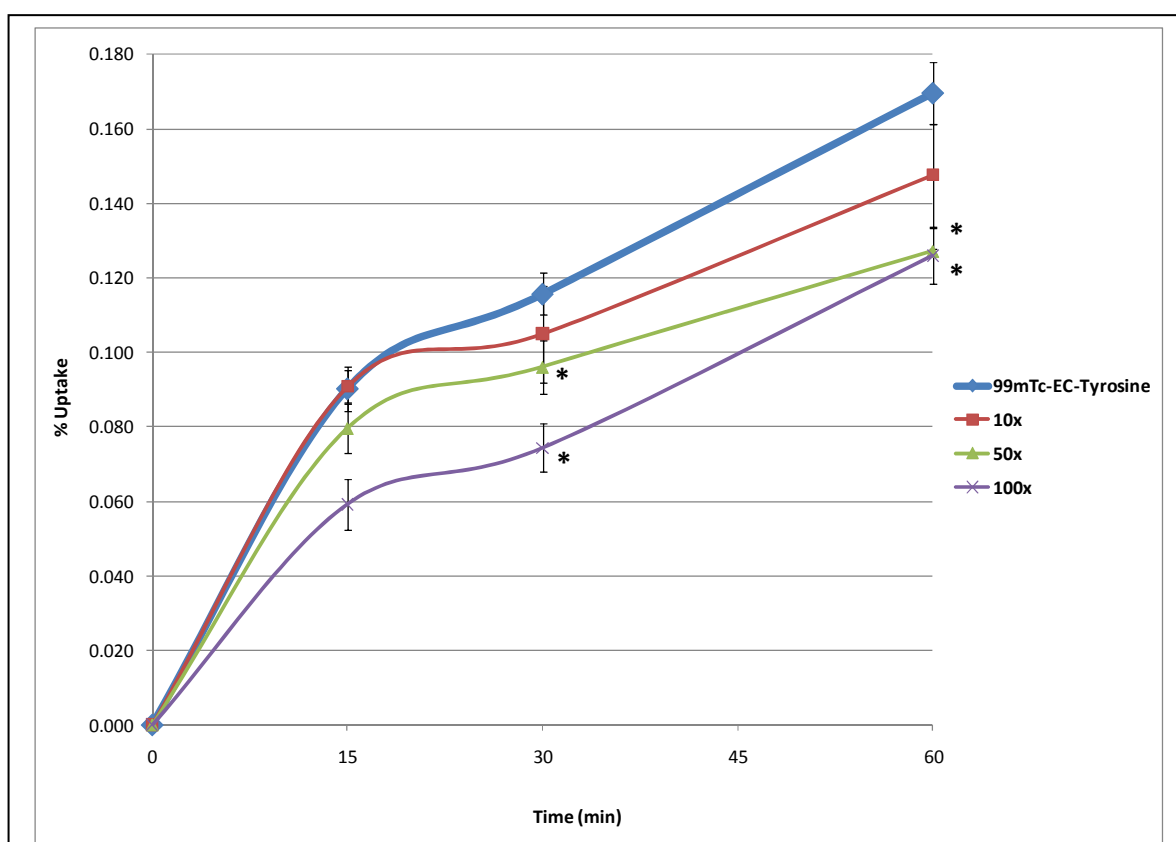
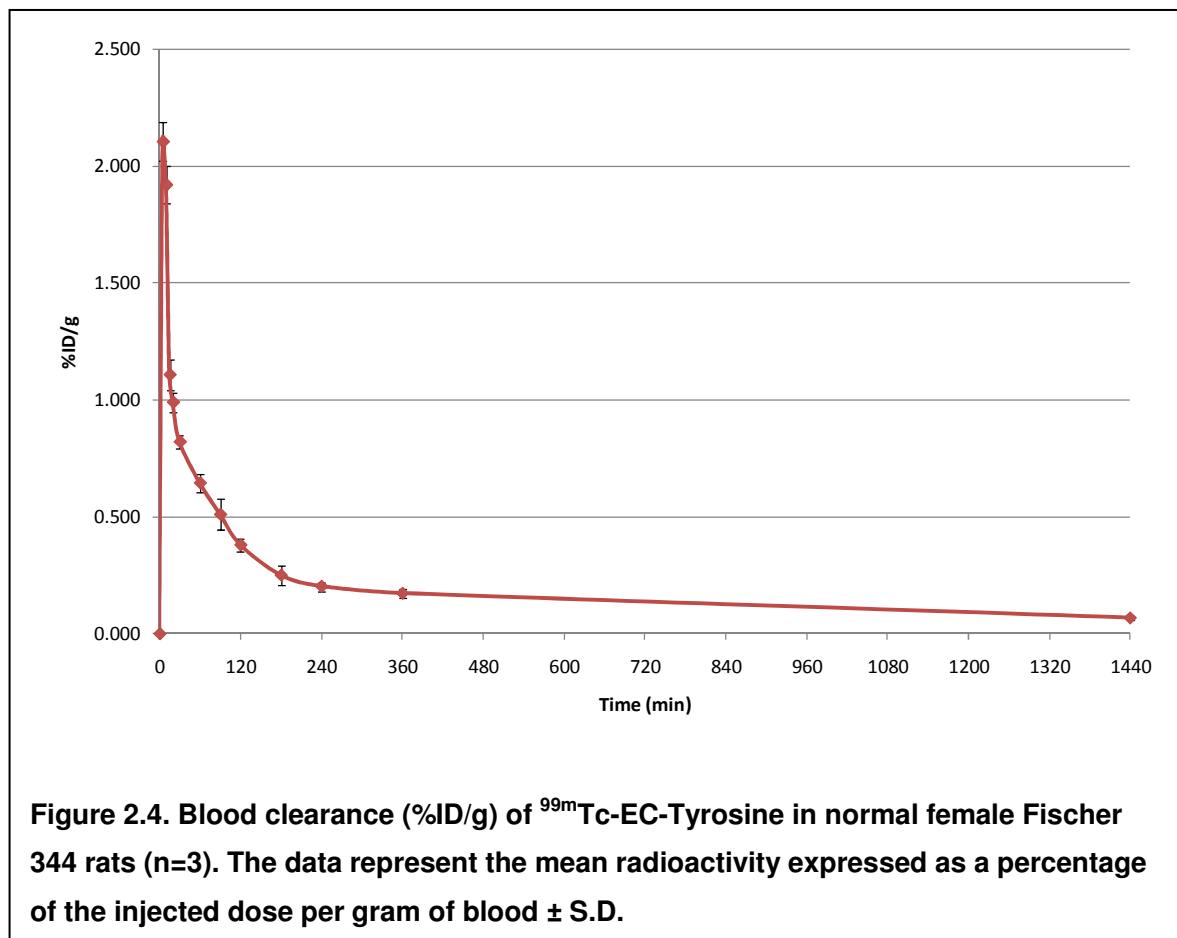


**Figure 2.3. Competitive inhibition uptake of  $^{99m}\text{Tc}$ -EC-Tyrosine by L-tyrosine in rat breast tumor cell line 13762 up to 1 h. A set of concentrations of L-tyrosine [10X–100X of EC-Tyrosine concentration (8 mg/well)] were used. Data are expressed in mean  $\pm$  S.D. percentage of cellular uptake (%Uptake).**

**\*P<0.05 compared with the control group.**

## Blood clearance

The blood clearance curve for  $^{99m}\text{Tc}$ -EC-Tyrosine in normal Fischer 344 rats (n=3) is shown in Fig. 2.4. The plasma half-life of the distribution phase ( $t_{1/2 \alpha}$ ) was  $13.68 \pm 1.067$  min, and that of the elimination phase ( $t_{1/2 \beta}$ ) was  $117.51 \pm 5.727$  min.



### ***In Vivo* Tissue Distribution Study of <sup>99m</sup>Tc-EC-Tyrosine**

The tissue distribution results of <sup>99m</sup>Tc-EC-Tyrosine and <sup>18</sup>F-FDG in the normal Fischer 344 rats are shown in Tables 2.1 and 2.2, respectively. Low thyroid and stomach uptake of <sup>99m</sup>Tc-EC-Tyrosine was observed, suggesting its high stability *in vivo*. In addition, kidneys had high uptake of <sup>99m</sup>Tc-EC-Tyrosine at all time-points.

**Table 2.1. Biodistribution of <sup>99m</sup>Tc-EC-Tyrosine in normal Fischer 344 female rats.**

<b>%ID/g</b>	<b>30 MIN</b>	<b>120 MIN</b>	<b>240 MIN</b>
<b>blood</b>	0.96 ±0.076	0.41 ±0.039	0.23 ±0.006
<b>heart</b>	0.24 ±0.007	0.12 ±0.011	0.08 ±0.009
<b>lung</b>	0.47 ±0.041	0.33 ±0.001	0.20 ±0.025
<b>thyroid</b>	0.43 ±0.036	0.24 ±0.001	0.11 ±0.002
<b>pancreas</b>	0.21 ±0.018	0.17 ±0.016	0.10 ±0.007
<b>liver</b>	1.47 ±0.045	2.42 ±0.075	0.97 ±0.007
<b>spleen</b>	0.47 ±0.054	1.41 ±0.117	0.62 ±0.036
<b>kidney</b>	11.12 ±0.545	16.50 ±0.395	11.13 ±0.234
<b>stomach</b>	0.27 ±0.006	0.19 ±0.002	0.08 ±0.000
<b>intestine</b>	1.13 ±0.009	0.33 ±0.023	0.17 ±0.017
<b>muscle</b>	0.10 ±0.009	0.05 ±0.006	0.03 ±0.000
<b>bone&amp;joint</b>	0.28 ±0.021	0.10 ±0.003	0.07 ±0.009
<b>brain</b>	0.04 ±0.003	0.01 ±0.001	0.01 ±0.001

Each rat received <sup>99m</sup>Tc-EC-Tyrosine (25 µCi, intravenously). Each value is percent of injected dose per gram weight (n= 3)/time interval. Each data represents mean of three measurements with standard deviation.



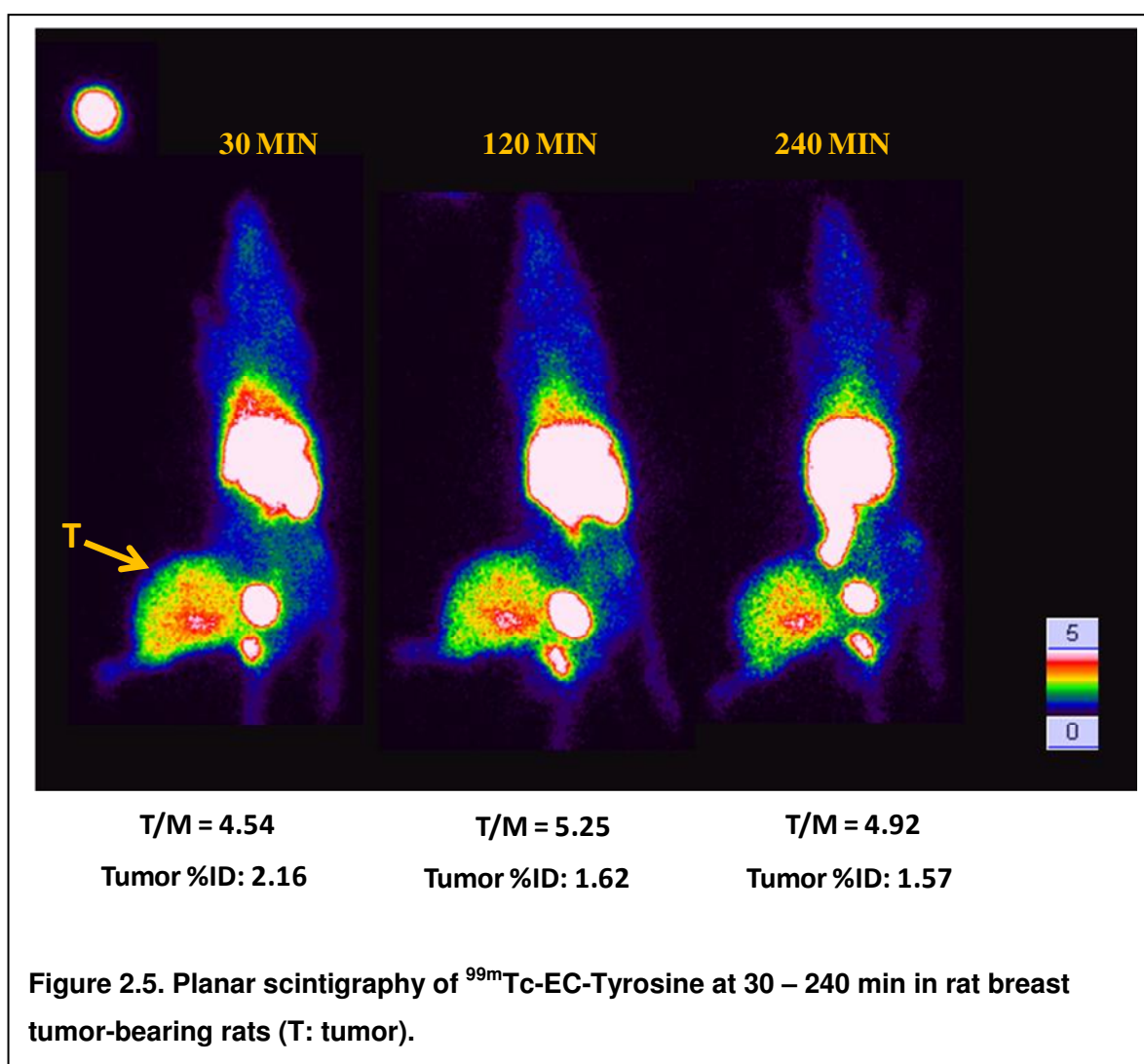
**Table 2.2. Biodistribution of  $^{18}\text{F}$ -FDG in normal Fischer 344 female rats.**

<b>%ID/g</b>	<b>30 MIN</b>	<b>60 MIN</b>	<b>120 MIN</b>
<b>blood</b>	0.40±0.042	0.13±0.006	0.06±0.002
<b>heart</b>	1.57±0.056	1.38±0.126	1.08±0.068
<b>lung</b>	0.55±0.056	0.42±0.024	0.46±0.027
<b>thyroid</b>	1.07±0.080	1.04±0.040	1.05±0.069
<b>pancreas</b>	0.26±0.028	0.21±0.006	0.20±0.016
<b>liver</b>	0.40±0.048	0.16±0.006	0.13±0.012
<b>spleen</b>	0.82±0.081	0.74±0.032	0.86±0.071
<b>kidney</b>	0.71±0.051	0.37±0.012	0.24±0.018
<b>stomach</b>	0.61±0.078	0.44±0.031	0.39±0.030
<b>intestine</b>	0.69±0.068	0.53±0.035	0.52±0.025
<b>muscle</b>	0.33±0.040	0.34±0.027	0.74±0.024
<b>bone&amp; joint</b>	0.33±0.036	0.44±0.065	0.50±0.034
<b>brain</b>	2.00±0.149	1.99±0.046	1.39±0.086

Each rat received  $^{18}\text{F}$ -FDG (25  $\mu\text{Ci}$ , intravenously). Each value is percent of injected dose per gram weight (n =3)/time interval. Each data represents mean of three measurements with standard deviation.

## Planar Scintigraphic Imaging Study

The selected planar scintigraphic images of  $^{99m}\text{Tc}$ -EC-Tyrosine at 30 min, 2h, and 4 h in breast tumor-bearing rats are shown in Fig. 2.5. Tumors were clearly detected by  $^{99m}\text{Tc}$ -EC-Tyrosine at all time-points. The T/M ratios at 30 min, 2h, and 4 h were 4.54, 5.25, and 4.92, respectively. Tumor %IDs at these three time-points were 2.16%, 1.62%, and 1.57%, respectively (Fig. 2.5).



## ***In Vivo* Uptake Blocking Study**

The liver, kidneys, tumor, and muscle %IDs, as well as the ratios of these organs to muscle before and after *in vivo* blocking by unlabeled L-Tyrosine were listed in Table 2.3 and 2.4. The organ-to-muscle ratios of  $^{99m}\text{Tc}$ -EC-Tyrosine after using the blocking agent L-tyrosine decreased at all time intervals compared to the control group. However, this observation was not because of the decreased uptake of liver, kidneys or tumor, but due to the increased  $^{99m}\text{Tc}$ -EC-Tyrosine uptake by muscle (Table 2.3).  $^{99m}\text{Tc}$ -EC-Tyrosine uptake at tumor site could only be blocked at 30 min, suggesting that  $^{99m}\text{Tc}$ -EC-Tyrosine and unlabeled L-Tyrosine might be uptaken via the same amino acid transporter LAT very rapidly.

**Table 2.3. Percentage of injected dose (%ID) of selected organs before and after *in vivo* blocking of  $^{99m}\text{Tc}$ -EC-Tyrosine by unlabeled L-Tyrosine in mammary tumor-bearing rats. Red font indicates the decreased %ID when compared to the corresponding control group. Blue shading indicates  $P < 0.05$  when compared to the corresponding control group (n=3/group/time interval).**

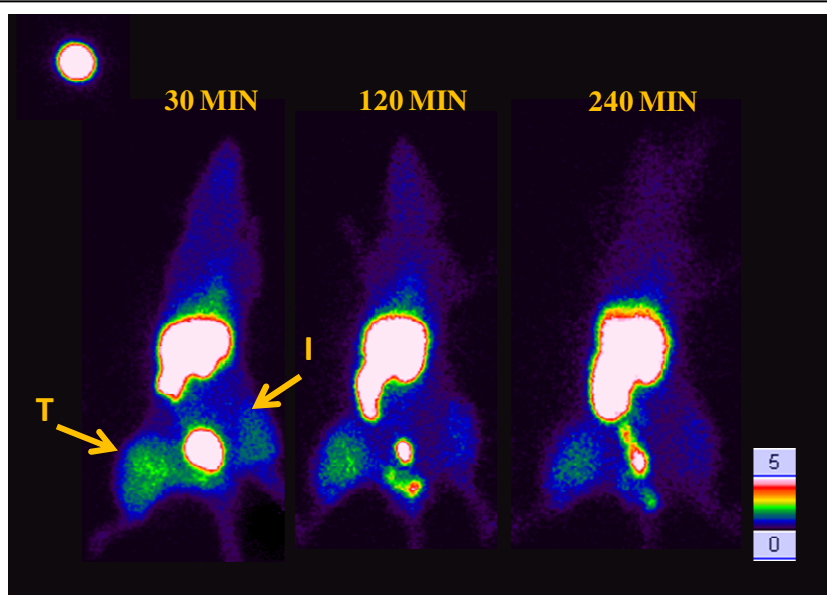
%ID	30 min			2 hr			4hr		
	Control	Block	Decrease	Control	Block	Decrease	Control	Block	Decrease
Liver	6.23±0.34	6.67±0.42	-7.06%	6.06±0.27	5.11±0.12	15.68%	5.90±0.54	5.62±0.51	4.75%
Kidney	11.36±0.53	9.87±0.61	13.12%	9.73±0.31	8.36±0.29	14.08%	7.46±0.21	10.62±0.17	-42.36%
Tumor	1.36±0.08	1.28±0.15	5.88%	0.82±0.06	0.95±0.09	-15.85%	0.69±0.11	0.83±0.05	-20.29%
Muscle	0.32±0.03	0.58±0.05	-81.25%	0.24±0.06	0.36±0.05	-50.00%	0.15±0.02	0.23±0.04	-53.33%

**Table 2.4. Selected organ to muscle ratios before and after *in vivo* blocking of  $^{99m}\text{Tc}$ -EC-Tyrosine by unlabeled L-Tyrosine in mammary tumor-bearing rats. Red font indicates the decreased %ID when compared to the corresponding control group. Blue shading indicates  $P < 0.05$  when compared to the corresponding control group (n=3/group/time interval).**

Ratio	30 min			2 hr			4hr		
	Control	Block	Decrease	Control	Block	Decrease	Control	Block	Decrease
Liver/Muscle	19.7±1.1	11.5±0.6	41.62%	61.7±1.7	14.2±0.4	76.99%	39.7±2.4	24.7±1.6	37.78%
Kidney/Muscle	36.0±1.4	17.0±1.2	52.78%	99.1±3.2	23.3±2.4	76.49%	50.2±3.4	46.6±3.1	7.17%
Tumor/Muscle	4.25±0.12	2.21±0.23	48.00%	3.42±0.25	2.64±0.29	22.81%	4.64±0.06	3.64±0.35	21.55%

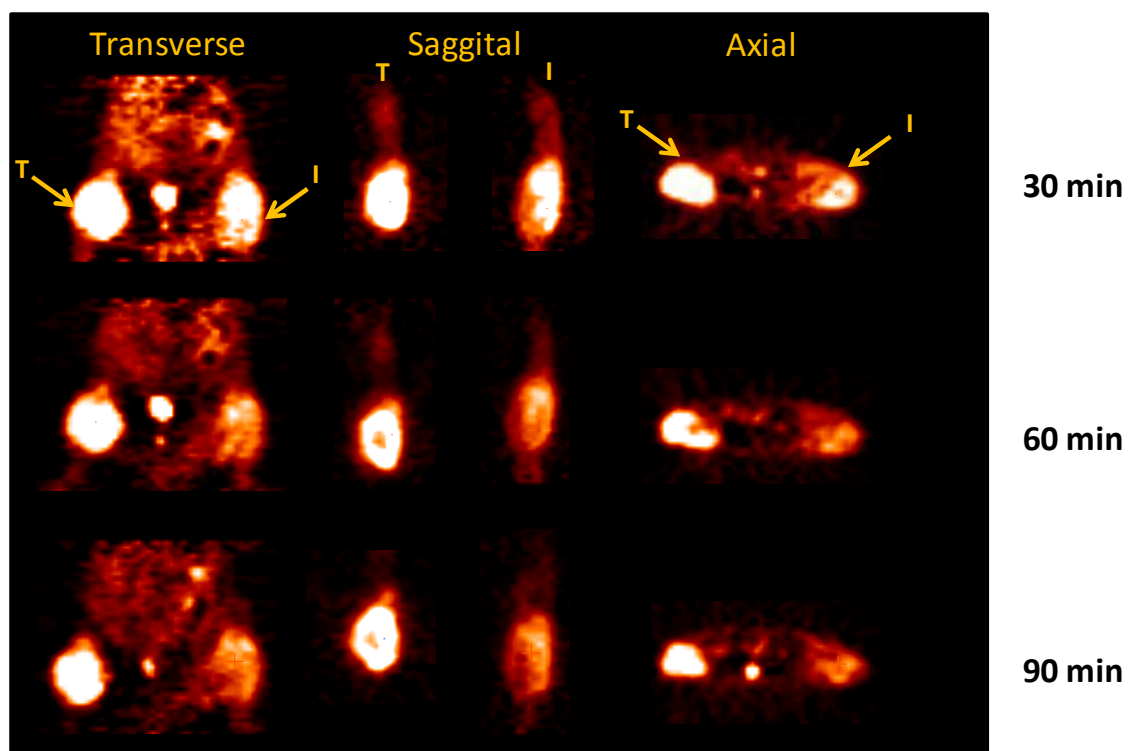
## Tumor and Inflammation Uptake Comparison *In Vivo*

The representative planar scintigraphic images of  $^{99m}\text{Tc}$ -EC-Tyrosine, as well as the micro-PET images of  $^{18}\text{F}$ -FDG in breast tumor and inflammation-bearing rats are shown in Fig. 2.6 and Fig. 2.7, respectively. The T/M of  $^{99m}\text{Tc}$ -EC-Tyrosine at each time interval was much higher than I/M. In addition, the T/I of  $^{99m}\text{Tc}$ -EC-Tyrosine at the last time-point was even higher than that of  $^{18}\text{F}$ -FDG (2.47 vs. 1.80), which suggested that  $^{99m}\text{Tc}$ -EC-Tyrosine could differentiate tumor from inflammation very well.



	30 min	2 hr	4 hr
T/M	4.30	8.36	4.64
I/M	3.02	4.31	1.88
T/I	1.43	1.94	2.47

**Figure 2.6. Planar scintigraphic images of  $^{99m}\text{Tc}$ -EC-Tyrosine at 30 – 240 min in rat breast tumor and inflammation-bearing rats (T: tumor, I: inflammation). The tumor-to-muscle ratios (T/Ms), inflammation-to-muscle ratios (I/Ms), and tumor-to-inflammation ratios (T/Is) are listed below the figure.**



	30 min	60 min	90 min
T/M	5.88	7.54	4.90
I/M	3.43	3.77	2.72
T/I	1.71	1.99	1.80

**Figure 2.7.** microPET images of  $^{18}\text{F}$ -FDG at 30 – 90 min in rat breast tumor and inflammation-bearing rats (T: tumor, I: inflammation). The tumor-to-muscle ratios (T/Ms), inflammation-to-muscle ratios (I/Ms), and tumor-to-inflammation ratios (T/Is) are listed below the figure.

## IV. Discussion

In the present study, we report the synthesis of  $^{99m}\text{Tc}$ -labeled tyrosine using EC as a chelator, and its potentials in breast cancer diagnosis by using the breast tumor models *in vitro* and *in vivo* are evaluated.

For chemical synthesis, the precursor EC-Tyrosine was successfully synthesized with an overall yield of 79.5%. Since the starting material N-*t*-Butoxycarbonyl-L-tyrosine methyl ester was commercially available, it took only three steps to obtain the final product EC-Tyrosine. The mild aqueous solution instead of the traditional organic solution was used for the coupling reaction of EC with N-*t*-Butoxycarbonyl-O-[3-Br-propyl]-L-tyrosine methyl ester (compound 1), which is a very efficient method. In this reaction, the molar ratio of EC and N-*t*-Butoxycarbonyl-O-[3-Br-propyl]-L-tyrosine methyl ester (compound 1) was controlled accurately in 2:1 in order to avoid each EC conjugating with more than one Tyrosine. The structure of EC-Tyrosine was well confirmed with the NMR and mass spectra results; therefore, tyrosine was assured to be conjugated with EC specifically on the nitrogen atom, but not on the sulfur atom.

When the precursor EC-Tyrosine was labeled with  $^{99m}\text{Tc}$ , the radiochemical purity was more than 95%. Since  $^{99m}\text{Tc}$ -EC-Tyrosine is a kit-product and labeled without any further purification, the radiochemical yield was assumed to be identical to its radiochemical purity. The partition coefficient value (logP) of  $^{99m}\text{Tc}$ -EC-Tyrosine was slightly lower than its  $\alpha$ -methyl derivative  $^{99m}\text{Tc}$ -EC-AMT ( $-2.02 \pm 0.168$  vs.  $-1.14 \pm 0.072$ , reported in Chapter 3), which supports our hypothesis. It is well-known that the lower logP indicates the lower lipophilicity of the compound. In our

hypothesis, we speculated that the lipophilicity of tyrosine-based radiotracer could be increased by adding a methyl group on its  $\alpha$ -carbon.

In cellular uptake study,  $^{99m}\text{Tc}$ -EC-Tyrosine was taken up rapidly by rat mammary tumor cells, and the %Uptake of  $^{99m}\text{Tc}$ -EC-Tyrosine was significantly higher than that of the negative control  $^{99m}\text{Tc}$ -EC, suggesting high specificity of  $^{99m}\text{Tc}$ -EC-Tyrosine in tumor uptake. Besides,  $^{99m}\text{Tc}$ -EC-Tyrosine even has higher uptake than  $^{18}\text{F}$ -FDG in this *in vitro* breast cancer model. In competitive inhibition study,  $^{99m}\text{Tc}$ -EC-Tyrosine uptake was significantly inhibited by L-tyrosine at 50x and 100x concentrations, which suggests that  $^{99m}\text{Tc}$ -EC-Tyrosine is transported at least partially via the same transporter system LAT that L-tyrosine exploits. These findings were consistent with those of many other radiolabeled tyrosine analogs. For instance,  $^{11}\text{C}/^{14}\text{C}$ -tyrosine[119],  $^{123}\text{I}/^{125}\text{I}$ -labeled AMT[56, 120],  $^{18}\text{F}$ -labeled tyrosine[121], AMT[76], and fluoroethyltyrosine ( $^{18}\text{F}$ -FET) [114] have been proven to be predominantly transported via amino acid transporter LAT. Since the increased expression level of LAT has been observed in various types of tumors[38], upregulated LAT is a suitable target for tumor imaging.

For *in vivo* evaluation,  $^{99m}\text{Tc}$ -EC-Tyrosine had a relatively fast blood clearance in normal Fischer 344 rats (Fig. 2.4). Biodistribution study showed that  $^{99m}\text{Tc}$ -EC-Tyrosine had high uptake in kidneys of normal rats (Table 2.1), which was consistent with the imaging findings in the breast tumor-bearing rats (Fig. 2.5). This may partially due to the characteristics of EC given that  $^{99m}\text{Tc}$ -EC itself is known as a renal tubular imaging agent[122]. In addition, the similar results were observed in  $^{99m}\text{Tc}$ -labeled EC-chelated AMT analogue  $^{99m}\text{Tc}$ -EC-AMT (reported in Chapter 3).



Compared to  $^{99m}\text{Tc}$ -EC-AMT,  $^{99m}\text{Tc}$ -EC-Tyrosine had even higher kidney uptake, which may be owing to its lower lipophilicity. The compound with lower lipophilicity is more water soluble, therefore, is more likely to be metabolized and excreted by kidneys. Furthermore, Shikano et al. confirmed that the uptake of  $^{123}\text{I}$ -labeled AMT ( $^{123}\text{I}$ -AMT) into normal human renal proximal tubule epithelial cells could be significantly inhibited by BCH, an LAT specific inhibitor[123]. This result suggests that LAT is involved in radiolabeled tyrosine uptake in kidneys. To ascertain whether  $^{99m}\text{Tc}$ -EC-Tyrosine uptake is mediated specifically by LAT, the *in vivo* uptake blocking studies using the unlabeled L-Tyrosine as the competitive inhibitor were conducted (Table 2.3 and 2.4). Although the organ-to-muscle ratios of  $^{99m}\text{Tc}$ -EC-Tyrosine after using the blocking agent L-tyrosine decreased at all time intervals compared to the control group, this observation was caused by the increased  $^{99m}\text{Tc}$ -EC-Tyrosine uptake in muscle (Table 2.3).  $^{99m}\text{Tc}$ -EC-Tyrosine uptake at tumor site could only be blocked at 30 min, suggesting that  $^{99m}\text{Tc}$ -EC-Tyrosine and unlabeled L-Tyrosine might be uptaken via the same amino acid transporter LAT very rapidly. These *in vivo* findings were coherent with the *in vitro* competitive inhibition results.

The most important finding in our study was the high suitability of  $^{99m}\text{Tc}$ -EC-Tyrosine to differentiate tumor from inflammation. The T/M of  $^{99m}\text{Tc}$ -EC-Tyrosine at each time-point was much higher than I/M. In addition, the T/I of  $^{99m}\text{Tc}$ -EC-Tyrosine at the last time-point was even higher than that of  $^{18}\text{F}$ -FDG (2.47 vs. 1.80). Since one of the biggest limitations of  $^{18}\text{F}$ -FDG in clinic is that it cannot distinguish tumor from inflammatory site very well,  $^{99m}\text{Tc}$ -EC-Tyrosine may promise an ideal alternative to  $^{18}\text{F}$ -FDG in future.

In summary, EC-Tyrosine was synthesized and labeled with  $^{99m}\text{Tc}$  readily and efficiently with high radiochemical purity. *In vitro* cellular uptake study demonstrated that  $^{99m}\text{Tc}$ -EC-Tyrosine transport involved amino acid transporter system LAT. Due to its simple chemical synthesis procedure, high cost effectiveness of the isotope, and comparatively high tumor/muscle uptake ratios in planar imaging,  $^{99m}\text{Tc}$ -EC-Tyrosine has great potential for breast cancer imaging, especially in differential diagnosis of tumor from inflammation. By taking the advantages of the coordination capability of chelator, EC-Tyrosine could chelate various radioisotopes for either imaging or therapy in the future.

## **CHAPTER 3    Development of $^{99m}\text{Tc}$ -EC-AMT for breast cancer imaging (partially adapted from [124])**

### **I.      Introduction**

$^{18}\text{F}$ -FDG-PET is a gold standard for tumor detection and staging in clinic. Unfortunately,  $^{18}\text{F}$ -FDG has several limitations that give rise to false positive/negative diagnosis and poor predictive value of tumor response to chemo/radio therapy[125].  $^{18}\text{F}$ -FDG has poor contrast in brain tumor due to the high uptake of glucose in both normal and neoplastic brain tissues[111], and it has poor differentiation of tumor from inflammatory tissue, because of the high uptake of  $^{18}\text{F}$ -FDG in granulocytes and macrophages[112, 113]. Radiolabeled amino acids show relatively low accumulation in normal tissues, rather high accumulation in tumor tissue, and rapid blood clearance[32]. These radiolabeled amino acids are attractive, since the main determinant of their uptake is amino acid transporters that are generally upregulated in cancer cells[76, 126]. Upregulated amino acid transporters indirectly reflect elevated cell proliferation[127], and assessment of their activities promises potential applications in differential diagnosis and prediction of early treatment response. Among all radiolabeled amino acids, aromatic amino acids are more suitable for tumor imaging due to easier chemical modification and characterization. However, aromatic amino acids tend to be decarboxylated[128], which reduces its ability to enter cells via amino acid transporters. Placing a methyl group at the alpha position could slower its metabolic process, thus, extensive amount of effort was directed towards the  $^{18}\text{F}$ - and  $^{123/124}\text{I}$ -labeled  $\alpha$ -carbon-methylated aromatic amino acids such as 2- $^{18}\text{F}$ fluoromethyl-L-phenylalanine[129],

2- and 3-L-[ $^{18}\text{F}$ ]fluoro- $\alpha$ -methyl tyrosine ( $^{18}\text{F}$ -FAMT)[75, 81, 130], and  $^{123}\text{I}$ -labeled L-3-[ $^{123}\text{I}$ ]iodo- $\alpha$ -methyltyrosine ( $^{123}\text{I}$ -AMT)[56].

Clinical study in lung cancer patients showed that  $^{18}\text{F}$ -FAMT had no false-positives in detecting primary tumors and lymph node metastases, and was able to improve the diagnostic performance in non-small cell lung cancer[81].  $^{18}\text{F}$ -FAMT has been proven to be transported into the tumor cells solely via the LAT system, especially the LAT1 subtype[76]. LAT is the only system that can transport large neutral amino acids with aromatic rings such as tyrosine, phenylalanine, and tryptophan[38, 41]. LAT family is known to form heterodimers, which contain a chaperone-like heavy chain 4F2hc, and a 12-time transmembrane light chain that is unique to each subtype[117]. Previous clinical studies showed that uptake of  $^{18}\text{F}$ -FAMT in tumors was positively correlated with LAT1 expression and cell proliferation[81]. Although application of  $^{18}\text{F}$ -FAMT-PET shows very promising clinical results, its radiosynthesis yield is relatively low, and the cost of using PET isotope  $^{18}\text{F}$  is prohibitive. Therefore, it is desirable to develop a radiotracer with simpler chemistry and affordable isotope, which can be used clinically in most major medical facilities.

$^{99\text{m}}\text{Tc}$  is an ideal radioisotope for diagnostic imaging studies, due to its physical characteristics. It emits a 140 keV gamma ray in 89% abundance [103], which is commonly used by SPECT. The half-life of  $^{99\text{m}}\text{Tc}$  is 6.02 h, which can provide serial images and therefore overcome the drawback of  $^{18}\text{F}$ . Diaminodithiol ( $\text{N}_2\text{S}_2$ ) compounds are known to form considerably stable Tc (V) O-complexes owing to the efficient binding of the oxotechnetium group to two thiols and two amine nitrogen

atoms[107]. EC is the most successful example of  $N_2S_2$  chelates[106, 131]. Previously, we reported that EC-conjugates can be labeled with  $^{99m}\text{Tc}$  via a peptide bond efficiently with high radiochemical purity, and the complex remains stable[131]. Here, we report the synthesis of  $^{99m}\text{Tc}$ -labeled AMT using EC as a chelator and evaluation of its potential use in breast tumor imaging.

## II. Materials and methods

### Chemicals and Analysis

All chemicals and sources used here were previously described in Chapter 2.

### Synthesis of Precursor EC-AMT

#### a) *$\alpha$ -Methyl tyrosine ethylester (compound 1).*

Thionyl chloride (18 mL; 0.24 mol) was added to  $\alpha$ -methyltyrosine (15.0 g; 0.08 mol) in anhydrous ethanol (100 mL) at 0 °C. The mixture was refluxed at 80-90 °C overnight with stirring. After cooling, the solvent was evaporated *in vacuo* to dryness. A saturated solution of  $\text{NaHCO}_3$  (150 mL) was added to the residue. White solid was filtered and washed with water and recrystallized in ethanol and water to yield 15.7 g (91.7%). MS(m/z): 224.23  $[\text{M}]^+$ .

#### b) *N-t-Butoxycarbonyl- $\alpha$ -methyltyrosineethylester (compound 2).*

Compound 1 (15.48 g; 69.35 mmol) was dissolved in anhydrous dichloromethane (200 mL). Di-tert-butyl dicarbonate (15.14 g; 69.35 mmol) and  $\text{NaHCO}_3$  (58.3 g, 0.69 mol) were added. Reaction mixture was stirred overnight at

50 °C, and the white solid was removed by filtration. The solution was washed with water and dried over anhydrous  $\text{MgSO}_4$ . The product was purified by column chromatography using a silica gel column, and eluted with hexane/ethyl acetate (5:2 v/v) to yield 8.97 g (40%). MS(m/z): 346.16  $[\text{M}+\text{Na}]^+$ .

**c) *N*-t-Butoxycarbonyl-O-[3-Br-propyl]- $\alpha$ -methyl tyrosine ethylester (compound 3).**

Compound 2 (9.42 g; 0.029 mol) was dissolved in acetone (200 mL). 1,3-dibromopropane (11.0 mL; 0.115 mol) and  $\text{K}_2\text{CO}_3$  (10.0 g; 0.178 mol) were added under nitrogen. The reaction mixture was refluxed at 70-80 °C overnight. After cooling and filtration, the solvent was removed under reduced pressure, and the residue was dissolved in chloroform. The residue was washed with water and dried with anhydrous  $\text{MgSO}_4$ . The product was purified by column chromatography using a silica gel column, eluted with hexane/ethyl acetate (4:1 v/v) to yield 11.0 g (86%). Ms(m/z): 445.10  $[\text{M}]^+$ .

**d) *N*-t-Butoxycarbonyl-O-[3-(N-Ethylenedicysteine) propyl]- $\alpha$ -methyl tyrosine (compound 4).**

EC (3.33 g, 12.4 mmol) was dissolved in water (50 mL), and the pH was adjusted to pH 9-10 by NaOH (1N). Compound 3 (3.86 g, 8.69 mmol) in ethanol (80 mL) was added to the above solution, followed by adding  $\text{K}_2\text{CO}_3$  (8.6 g, 62.2 mmol). Reaction mixture was then heated at 90 °C overnight. After cooling, the solvent was removed under reduced pressure, and the residue was dissolved in chloroform (50

mL). The residue was washed with water, dried with anhydrous  $\text{MgSO}_4$ , and evaporated to dryness. Without further purification, the compound 4 was used for following steps.

**e) *O*-[3-(*N*-Ethylenedicysteine) propyl]- $\alpha$ -methyl tyrosine (EC-AMT) (compound 5).**

The crude product of compound 4 (2.5 g, 0.04 mol) was dissolved in dichloromethane (50 mL). Hydrobromic acid (48%, 4.5 mL) was added dropwisely to the solution over 30 min periods at room temperature with stirring. After filtration, the white solid was washed with ethanol and recrystallized in water to yield 2.08g (86%).

**f) *Rhenium*- *O*-[3-(*N*-Ethylenedicysteine) propyl]- $\alpha$ -methyl tyrosine (Re-EC-AMT) (compound 6).**

An ethanol solution (10 mL) containing trichlorooxobis (triphenylphosphine) rhenium (V) (110 mg, 0.13 mmol) was added to an aqueous solution (10 mL) with EC-AMT (66 mg, 0.13 mmol) and potassium hydroxide (120 mg, 1.3 mmol), followed by refluxing at 90 °C for 1 h. The color of reaction mixture changed from green to yellow. After cooling and filtration, the ethanol was removed *in vacuo*. The remaining aqueous solution was acidified to pH 4 with 1N HCl. The yellow solid product (Re-EC-AMT) formed immediately was collected and recrystallized from water. Ms (m/z): 739.29  $[\text{M}+\text{HCl}]^+$ .

### **Radiolabeling of EC-AMT and EC with $^{99m}\text{Tc}$**

EC-AMT (1 mg) was dissolved in 0.2 mL sterile water, followed by adding tin (II) chloride (0.1 mL, 1 mg/mL). For EC labeling, EC (0.5 mg) was dissolved in 0.2 mL sterile water by adding 10  $\mu\text{L}$  of 1N NaOH (pH=9). Required amount of  $\text{Na}^{99m}\text{TcO}_4$  was added to EC or EC-AMT solution (pH 7.4). Radiochemical purity was determined by radio-HPLC (High performance liquid chromatography; Waters, Milford, MA), eluted with acetonitrile: water (7:3) using a flow rate of 0.5 mL/min.

### **Determination of the Partition Coefficient**

To determine the lipophilicity, 20  $\mu\text{L}$  of  $^{99m}\text{Tc}$ -EC-AMT was added into an equal volume mixture of 1-octanol and sterile water in a centrifuge tube. The mixture was vortexed at room temperature for 1 min and then centrifuged at 5000 rpm for 5 min. From each phase, 0.1 mL of the aliquot was taken out and the radioactivity was measured by gamma counter (Cobra Quantum; Packard, MN). The measurement was repeated for three times, and care was taken to avoid cross contamination between the phases. The partition coefficient value, expressed as logP, was calculated using the following equation:

$$\text{LogP} = \text{Log} (\text{radioactivity in 1-octanol layer} / \text{radioactivity in sterile water layer})$$

### ***In Vitro* Cellular Uptake Studies**

Rat breast tumor cell line 13762 (American Type Culture Collection, Rockville, MD) was selected and the same cell line was used to create the animal model for *in vivo* evaluation. Cells were maintained in Dulbecco's modified Eagle's medium and



nutrient mixture F-12 Ham (DMEM/F12; GIBCO, Grand Island, NY) at 37 °C in a humidified atmosphere containing 5% CO<sub>2</sub>. Cells were plated onto 6-well tissue culture plates (2x10<sup>5</sup> cells/well) and incubated with <sup>99m</sup>Tc-EC-AMT (0.05 mg/well, 8 uCi/well), <sup>99m</sup>Tc-EC (0.025 mg/well, 8 uCi/well) or <sup>18</sup>F-FDG (8 uCi/well) for 0-4 h. After incubation, cells were washed with ice-cold PBS twice and detached by treating them with 0.5 mL of trypsin for 5 min. Cells were then collected and the radioactivity was measured with gamma counter (Cobra Quantum; Packard, MN). Data were expressed in mean ±S.D. percent of cellular uptake (%Uptake) in triplicate.

#### **Competitive Inhibition Study of <sup>99m</sup>Tc-EC-AMT**

To investigate the transport mechanisms of <sup>99m</sup>Tc-EC-AMT, the competitive inhibition study using L-tyrosine was conducted. Rat breast tumor cells were co-incubated with <sup>99m</sup>Tc-EC-AMT (8 µg/well, 8 µCi/well) and L-tyrosine for up to 1 h. A set of concentrations of L-tyrosine (10x, 50x, and 100x of the EC-AMT concentration) were used. After incubation, cells were washed with ice-cold PBS twice and detached by treating them with 0.5 mL of trypsin for 5 min. Cells were then collected and the radioactivity was measured by gamma counter. Data were expressed in mean ±S.D. percent of cellular uptake (%Uptake) in triplicate.

#### **Blood Clearance**

All animal work was carried out in the Small Animal Imaging Facility (SAIF) at UTMDACC under a protocol approved by Institutional Animal Care and Use

Committee (IACUC). For blood clearance analysis, three normal female Fischer 344 rats ( $150 \pm 25$  g) (Harlan Sprague-Dawley, Indianapolis, IN) were intravenously injected with  $30 \mu\text{Ci } ^{99\text{m}}\text{Tc-EC-AMT}$ . Blood samples were drawn through lateral tail vein at several time-points from 5 min to 24 h ( $n=3/\text{rat}$ ) by microliter pipettes ( $10 \mu\text{L}$ ). The blood samples were measured for radioactivity by gamma counter, and then were calculated as percentage of the injected dose per gram of blood ( $\% \text{ID/g}$ ).

### ***In vivo* Tissue Distribution Studies**

Tissue distribution studies of  $^{99\text{m}}\text{Tc-EC-AMT}$  (study I,  $n=9$ ) and  $^{18}\text{F-FDG}$  (study II,  $n=9$ ) were conducted by using normal female Fischer 344 rats ( $150 \pm 25$  g,  $n=18$ ). For each compound, the rats were divided into three groups for three time intervals (0.5, 2, 4 h for  $^{99\text{m}}\text{Tc-EC-AMT}$ ; 0.5, 1, 2 h for  $^{18}\text{F-FDG}$ ;  $n=3/\text{time point}$ ). The injection activity was  $25 \pm 0.5 \mu\text{Ci/rat}$  intravenously. At each time interval, the rats were sacrificed, and the selected tissues were excised, weighed and measured for radioactivity by gamma counter. Each sample was calculated as percentage of the injected dose per gram of tissue wet weight ( $\% \text{ID/g}$ ). Counts from a diluted sample of the original injection were used as reference.

### **Planar Scintigraphic Imaging Study**

Female Fischer 344 rats were inoculated subcutaneously with 0.1 mL of breast tumor cells 13762 suspension in PBS ( $10^5$  cells/rat) into the right legs. Planar scintigraphic imaging of  $^{99\text{m}}\text{Tc-EC-AMT}$  was performed 12-14 days after inoculation when tumors reached approximately 1 cm in diameter. Planar scintigraphic images

were obtained using M-CAM (Siemens Medical Solutions, Hoffman Estates, IL) equipped with a Low Energy High Resolution collimator. Anesthetized breast tumor-bearing rats were injected intravenously with  $^{99m}\text{Tc}$ -EC-AMT (0.3 mg/rat, 300  $\mu\text{Ci}$ /rat;  $n=3$ ). The images were acquired up to 4 h post-administration of tracers. Computer outlined regions of interest (ROIs in counts per pixel) between tumor and muscle were used to calculate tumor/muscle (T/M) ratios. Percentage of the injected dose (%ID) of tumor was also calculated from the reference standard, which was 1/10 of the original injection activity.

### ***In Vivo* Uptake Blocking Study**

To ascertain whether  $^{99m}\text{Tc}$ -EC-AMT uptake is mediated specifically by LAT, *in vivo* blocking studies using the unlabeled L-Tyrosine as the competitive inhibitor was conducted. The same animal model used in the planar scintigraphic imaging study was employed. Unlabeled L-Tyrosine (50 mg/kg) dissolved in 0.3 mL saline (pH adjusted to 2-3) was administered intravenously to mammary tumor-bearing rats 1 h prior to  $^{99m}\text{Tc}$ -EC-AMT injection. Planar scintigraphic images were acquired up to 4 h, and ROIs of liver, kidneys, tumor, and muscle were used to calculate the ratios of liver/muscle, kidney/muscle, and tumor/muscle, respectively. In addition, %IDs of liver, kidneys, tumor, and muscle were calculated from the reference standard, which was 1/10 of the original injection activity. The results were compared with those from the rats injected with  $^{99m}\text{Tc}$ -EC-AMT alone (control).

### **Tumor and Inflammation Uptake Comparison *In Vivo***

To investigate whether  $^{99m}\text{Tc}$ -EC-AMT can differentiate tumor from the inflammatory tissue, a rat model bearing both mammary tumor and turpentine oil-induced inflammation was created. 13762 rat mammary tumor cells ( $10^5$  cells/0.1 mL PBS/rat) were inoculated into the right calf muscles of the female Fischer 344 rats. After the tumors reached to 1 cm in diameter, turpentine oil (0.1 mL/rat) was injected into the left calf muscles of the rats to induce inflammation. The anesthetized rats ( $n=3$ ) were injected intravenously with  $^{99m}\text{Tc}$ -EC-AMT 24 h after the turpentine injection. Planar scintigraphic images were acquired up to 4 h, and ROIs of tumor, inflammation, and muscle were used to calculate the tumor-to-muscle ratios (T/Ms), inflammation-to-muscle ratios (I/Ms), and tumor-to-inflammation ratios (T/Is), respectively. Same animal model was used to evaluate  $^{18}\text{F}$ -FDG. Micro-PET imaging of  $^{18}\text{F}$ -FDG was performed using R4 micro-PET scanner (Concorde Microsystems, TN). The rats were injected intravenously with  $^{18}\text{F}$ -FDG (500  $\mu\text{Ci}$ /rat,  $n=3$ ), and dynamic PET scans were obtained for 90 min with a spatial resolution of 2.2 mm. PET images were reconstructed by using the ordered subset expectation maximization (OSEM) algorithm. T/Ms, I/Ms and T/Is ratios were calculated based on the regional radioactivity concentrations ( $\mu\text{Ci}/\text{cm}^3$ ) that were estimated from the average pixels within ROIs drawn around the tumor, inflammation or muscle on transverse slices of the reconstructed image sets.

### **III. Results**

#### **Chemistry**

EC-AMT was synthesized via a five-step procedure. The synthetic scheme is

shown in Fig.3.1. The structures and purities of EC-AMT and Re-EC-AMT were confirmed by  $^1\text{H}$ - and  $^{13}\text{C}$ - NMR, mass spectra, and HPLC. For EC-AMT, the  $^1\text{H}$ - and  $^{13}\text{C}$ -NMR results were  $^1\text{H}$  NMR ( $\text{D}_2\text{O}$ ,  $\delta/\text{ppm}$ ): 7.10 (d, 2H, phenyl ring), 6.79 (d, 2H, phenyl ring), 3.96 (dd, 2H, O-CH<sub>2</sub>), 3.09(t, 1H, CHN), 2.87 (d, 2H, PhCH<sub>2</sub>-), 2.68-2.40(m, 8H, -CH<sub>2</sub>-), 1.88(m, 2H, C-CH<sub>2</sub>-C), 1.13[s, 9H, C(CH<sub>3</sub>)<sub>3</sub>].  $^{13}\text{C}$  NMR ( $\text{D}_2\text{O}$ ,  $\delta/\text{ppm}$ ): 184.22, 180.16, 156.69, 131.11, 130.40, 114.65, 66.90, 62.69, 59.31, 57.28, 46.33, 45.47, 34.29, 28.35, 28.23, 25.76, 16.85. For Re-EC-AMT, the  $^1\text{H}$ - and  $^{13}\text{C}$ -NMR results are  $^1\text{H}$  NMR ( $\text{D}_2\text{O}$ ,  $\delta/\text{ppm}$ ): 7.02 (d, 2H, phenyl ring), 6.87 (d, 2H, phenyl ring), 4.05 (t, 2H, O-CH<sub>2</sub>), 3.17-3.00(m, 3H, CHN, PhCH<sub>2</sub>), 2.73-2.50 (m, 8H, -CH<sub>2</sub>-), 1.96(m, 2H, C-CH<sub>2</sub>-C), 1.38[s, 3H, CH<sub>3</sub>].

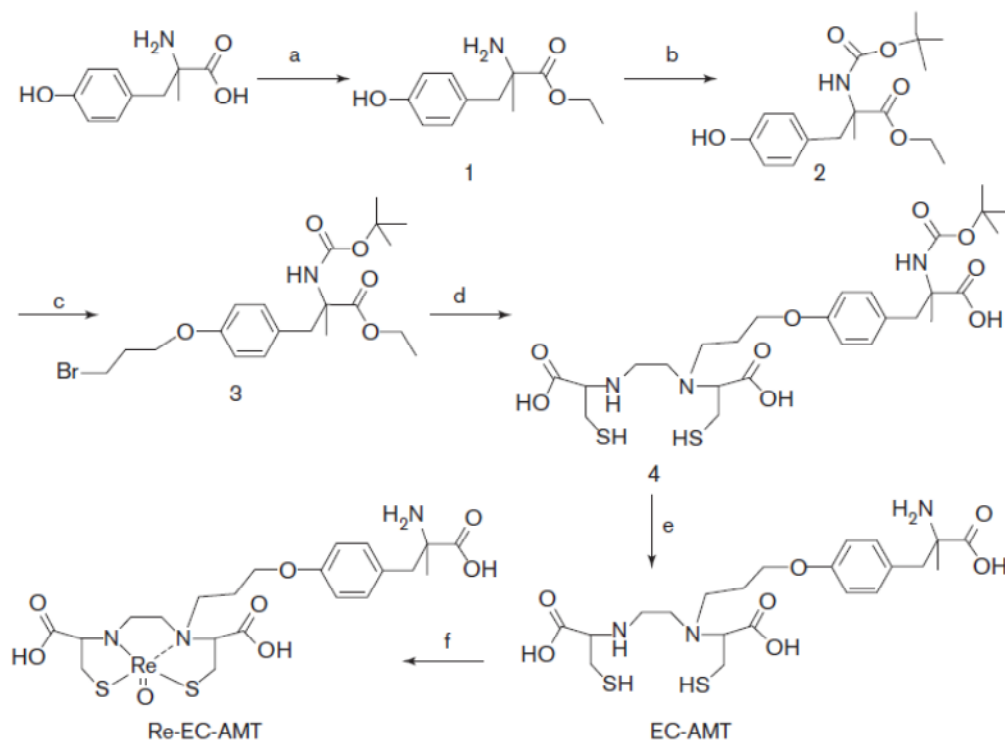


**Figure 3.1. Synthetic scheme of precursor EC-AMT and cold standard reference compound rhenium (Re) EC-AMT.**

$^{99m}\text{Tc}$ -labeled EC-AMT was obtained with high radiochemical purity (95%) (Fig. 3.2). The retention time of  $^{99m}\text{Tc}$ -EC-AMT matched to that of the cold reference standard Re-EC-AMT (Fig. 3.2). The partition coefficient value ( $\log P$ ) of  $^{99m}\text{Tc}$ -EC-AMT was  $-1.14 \pm 0.072$ .

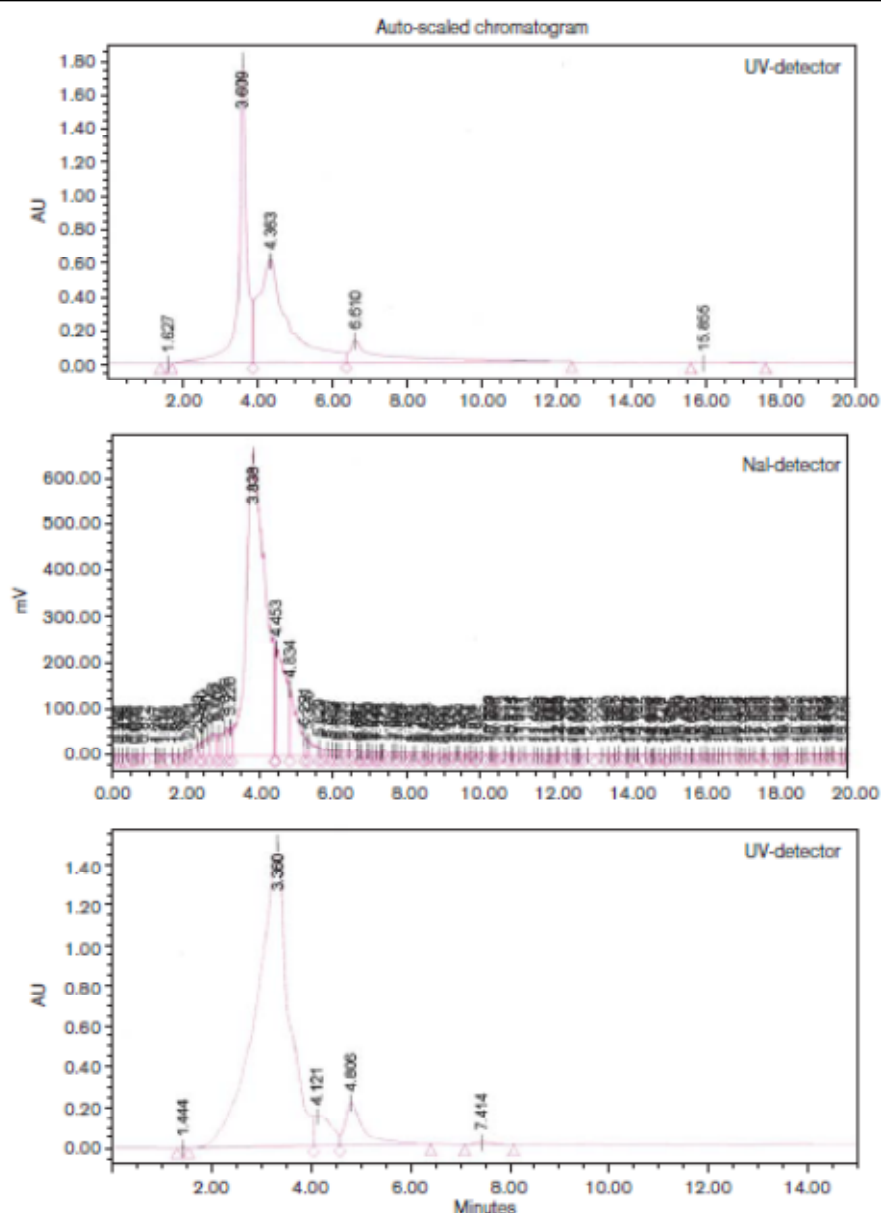


**Figure 3.2.** High performance liquid chromatography analysis of  $^{99m}\text{Tc}$ -EC-AMT and Re-EC-AMT at a flow rate of 0.5 mL/min using a C-18 reverse column under UV absorbance of 274 nm.

### ***In Vitro* Cellular Uptake Studies**

The cellular uptake kinetics of  $^{99m}\text{Tc}$ -EC-AMT,  $^{99m}\text{Tc}$ -EC, and  $^{18}\text{F}$ -FDG using rat breast tumor cell line 13762 is shown in Fig. 3.3. The uptake of  $^{99m}\text{Tc}$ -EC-AMT into the 13762 mammary tumor cells increased rapidly, and reached 1.85%Uptake at 4 h. In addition, the %Uptake of  $^{99m}\text{Tc}$ -EC-AMT was dramatically higher than that of  $^{18}\text{F}$ -FDG and the negative control  $^{99m}\text{Tc}$ -EC.

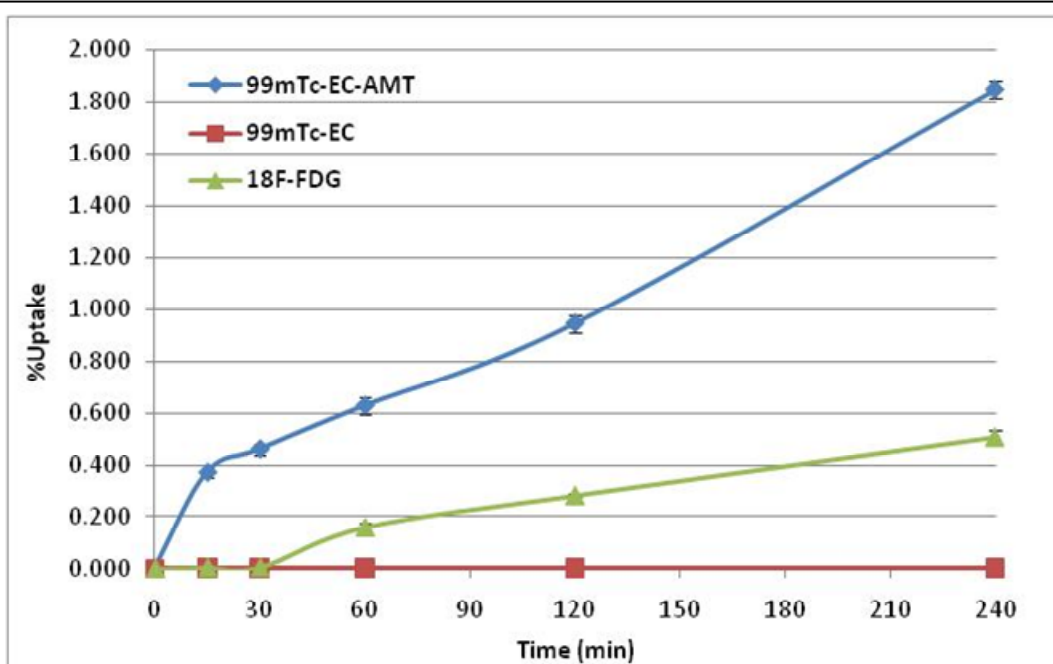


**Figure 3.3.** Time course of  $^{99m}\text{Tc}$ -EC-AMT,  $^{99m}\text{Tc}$ -EC and  $^{18}\text{F}$ -FDG uptake in rat breast tumor cell line 13762 (0– 240 min). Data are expressed in mean  $\pm$  S.D. percentage of cellular uptake (%Uptake).



### Competitive Inhibition Study of $^{99m}\text{Tc}$ -EC-AMT

After incubating the 13762 rat mammary tumor cells with L-tyrosine at 10-100 times as high as the concentrations of EC-AMT, these tumor cells showed a significantly decrease in  $^{99m}\text{Tc}$ -EC-AMT uptake (Fig. 3.4). These results suggest that  $^{99m}\text{Tc}$ -EC-AMT is transported at least partially via the same transporter system LAT that L-tyrosine exploits.

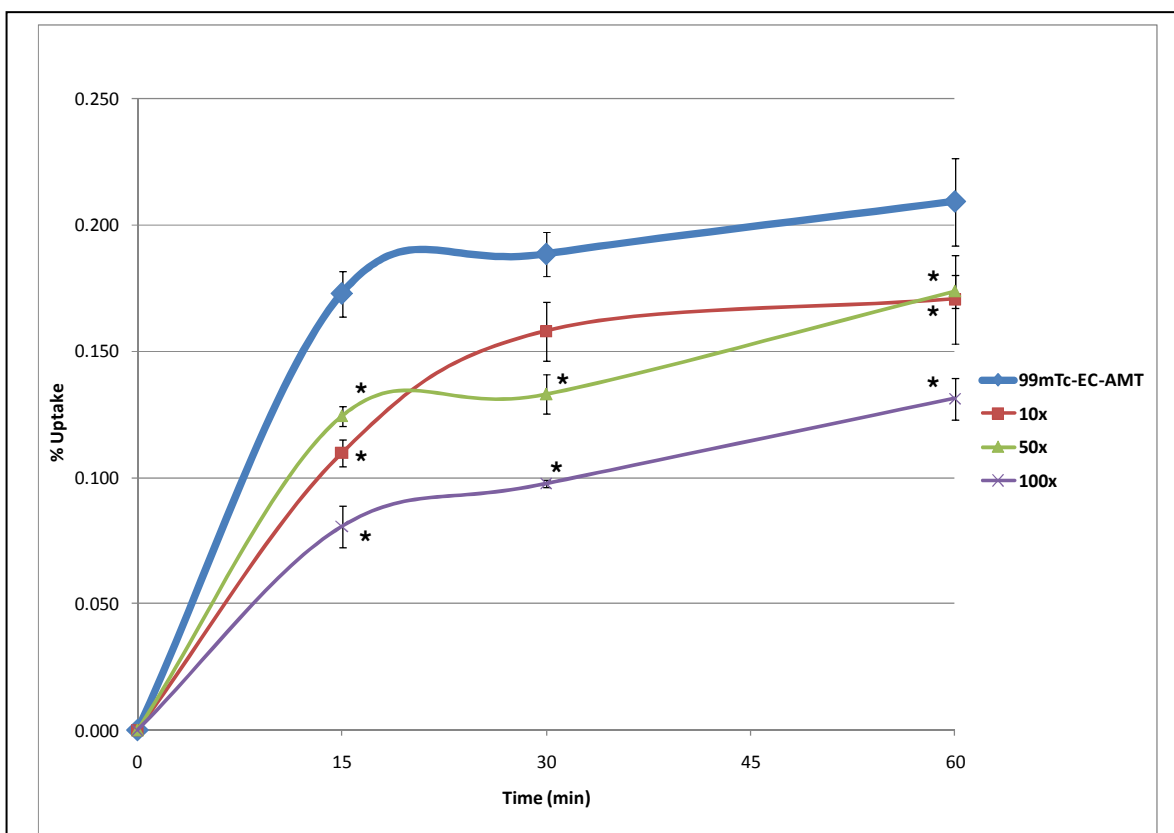


**Figure 3.4. Competitive inhibition uptake of  $^{99m}\text{Tc}$ -EC-AMT by L-tyrosine in rat breast tumor cell line 13762 up to 1 h. A set of concentrations of L-tyrosine [10X–100X of EC-AMT concentration (8 mg/well)] were used. Data are expressed in mean  $\pm$  S.D. percentage of cellular uptake (%Uptake).**

**\*P<0.05 compared with the control group.**

## Blood Clearance

The blood clearance curve for  $^{99m}\text{Tc}$ -EC-AMT in normal Fischer 344 rats ( $n=3$ ) is shown in Fig. 3.5. The plasma half-life of the distribution phase ( $t_{1/2} \alpha$ ) was  $9.41 \pm 0.202$  min, and that of the elimination phase ( $t_{1/2} \beta$ ) was  $98.75 \pm 5.377$  min.

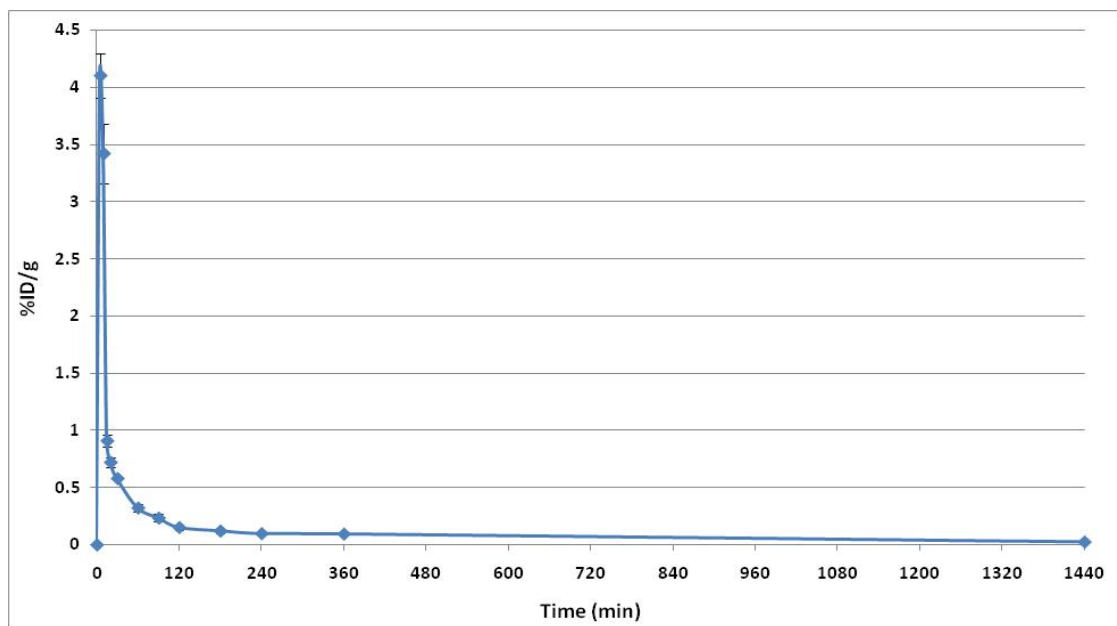


**Figure 3.5. Blood clearance (%ID/g) of  $^{99m}\text{Tc}$ -EC-AMT in normal female Fischer 344 rats ( $n=3$ ). The data represent the mean radioactivity expressed as a percentage of the injected dose per gram of blood  $\pm$  S.D.**

### ***In Vivo* Tissue Distribution Studies**

The tissue distribution results of  $^{99m}\text{Tc}$ -EC-AMT and  $^{18}\text{F}$ -FDG in the normal Fischer 344 rats are shown in Tables 3.1 and 3.2, respectively. Low thyroid and stomach uptake of  $^{99m}\text{Tc}$ -EC-AMT was observed, suggesting its high stability *in vivo*.

**Table 3.1. Biodistribution of  $^{99m}\text{Tc}$ -EC-AMT in normal Fischer 344 female rats.**

<b>%ID/g</b>	<b>30 MIN</b>	<b>120 MIN</b>	<b>240 MIN</b>
<b>blood</b>	0.64 $\pm$ 0.047	0.41 $\pm$ 0.019	0.17 $\pm$ 0.004
<b>heart</b>	0.19 $\pm$ 0.005	0.11 $\pm$ 0.004	0.05 $\pm$ 0.002
<b>lung</b>	0.44 $\pm$ 0.038	0.29 $\pm$ 0.012	0.14 $\pm$ 0.004
<b>thyroid</b>	0.28 $\pm$ 0.029	0.22 $\pm$ 0.038	0.09 $\pm$ 0.008
<b>pancreas</b>	0.15 $\pm$ 0.016	0.10 $\pm$ 0.003	0.06 $\pm$ 0.001
<b>liver</b>	2.03 $\pm$ 0.180	1.48 $\pm$ 0.079	1.07 $\pm$ 0.155
<b>spleen</b>	0.56 $\pm$ 0.053	0.54 $\pm$ 0.027	0.48 $\pm$ 0.054
<b>kidney</b>	8.56 $\pm$ 0.966	9.01 $\pm$ 0.212	8.43 $\pm$ 0.171
<b>stomach</b>	0.28 $\pm$ 0.070	0.12 $\pm$ 0.006	0.08 $\pm$ 0.012
<b>intestine</b>	0.89 $\pm$ 0.107	0.81 $\pm$ 0.490	0.13 $\pm$ 0.009
<b>muscle</b>	0.10 $\pm$ 0.017	0.05 $\pm$ 0.001	0.02 $\pm$ 0.001
<b>bone&amp; joint</b>	0.09 $\pm$ 0.016	0.07 $\pm$ 0.010	0.06 $\pm$ 0.005
<b>brain</b>	0.02 $\pm$ 0.003	0.02 $\pm$ 0.003	0.01 $\pm$ 0.001

Each rat received  $^{99m}\text{Tc}$ -EC-AMT (25  $\mu\text{Ci}$ , intravenously). Each value is percent of injected dose per gram weight (n= 3)/time interval. Each data represents mean of three measurements with standard deviation.

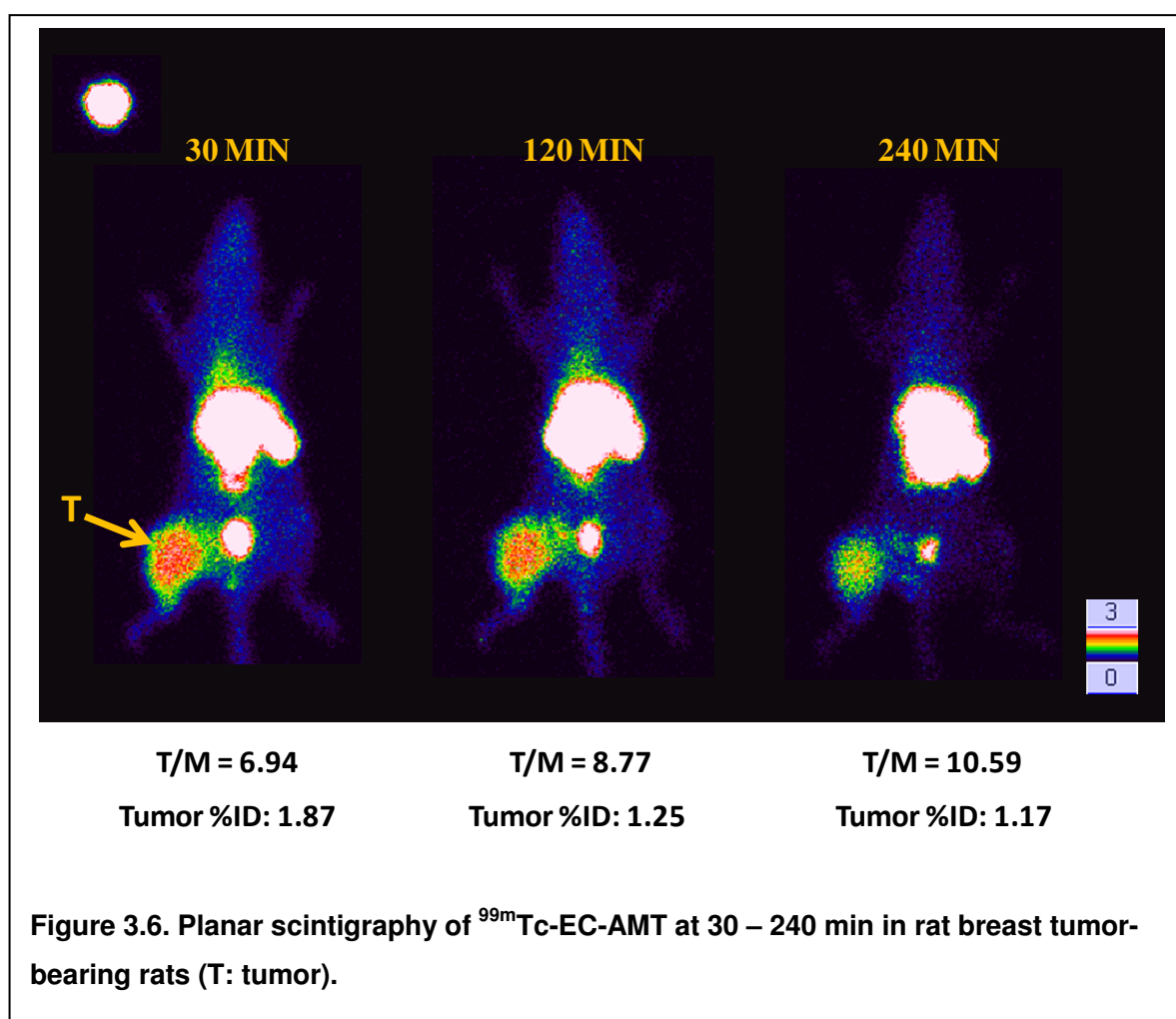
**Table 3.2. Biodistribution of  $^{18}\text{F}$ -FDG in normal Fischer 344 female rats.**

<b>%ID/g</b>	<b>30 MIN</b>	<b>60 MIN</b>	<b>120 MIN</b>
<b>blood</b>	0.40±0.042	0.13±0.006	0.06±0.002
<b>heart</b>	1.57±0.056	1.38±0.126	1.08±0.068
<b>lung</b>	0.55±0.056	0.42±0.024	0.46±0.027
<b>thyroid</b>	1.07±0.080	1.04±0.040	1.05±0.069
<b>pancreas</b>	0.26±0.028	0.21±0.006	0.20±0.016
<b>liver</b>	0.40±0.048	0.16±0.006	0.13±0.012
<b>spleen</b>	0.82±0.081	0.74±0.032	0.86±0.071
<b>kidney</b>	0.71±0.051	0.37±0.012	0.24±0.018
<b>stomach</b>	0.61±0.078	0.44±0.031	0.39±0.030
<b>intestine</b>	0.69±0.068	0.53±0.035	0.52±0.025
<b>muscle</b>	0.33±0.040	0.34±0.027	0.74±0.024
<b>bone&amp; joint</b>	0.33±0.036	0.44±0.065	0.50±0.034
<b>brain</b>	2.00±0.149	1.99±0.046	1.39±0.086

Each rat received  $^{18}\text{F}$ -FDG (25  $\mu\text{Ci}$ , intravenously). Each value is percent of injected dose per gram weight (n =3)/time interval. Each data represents mean of three measurements with standard deviation.

## Planar Scintigraphic Imaging Study

The selected planar scintigraphic images of  $^{99m}\text{Tc}$ -EC-AMT at 30 min, 2h, and 4 h in breast tumor-bearing rats are shown in Fig. 3.6. Tumors were clearly detected by  $^{99m}\text{Tc}$ -EC-AMT at all time-points. The T/M ratios at 30 min, 2h, and 4 h were 6.94, 8.77, and 10.59, respectively. Tumor %IDs at these three time-points were 1.87%, 1.25%, and 1.17%, respectively (Fig. 3.6).



### ***In Vivo* Uptake Blocking Study**

The liver, kidneys, tumor, and muscle %IDs, as well as the ratios of these organs to muscle before and after *in vivo* blocking by unlabeled L-Tyrosine were listed in Table 3.3 and 3.4. At 30 min,  $^{99m}\text{Tc}$ -EC-AMT uptake in liver, kidney, and tumor decreased by 9.8%, 47.9%, and 23.9% respectively by using the blocking agent L-Tyrosine. However, after 90 min, no significant blocking effect was observed. (Results at 4 h are not shown). These results suggest that  $^{99m}\text{Tc}$ -EC-AMT at least partially utilizes the same transport system LAT as L-Tyrosine does, and is taken by tumor rapidly.

**Table 3.3. Percentage of injected dose (%ID) of selected organs before and after *in vivo* blocking of  $^{99m}\text{Tc}$ -EC-AMT by unlabeled L-Tyrosine in mammary tumor-bearing rats. Red font indicates the decreased %ID when compared to the corresponding control group. Blue shading indicates  $P < 0.05$  when compared to the corresponding control group (n=3/group/time interval).**

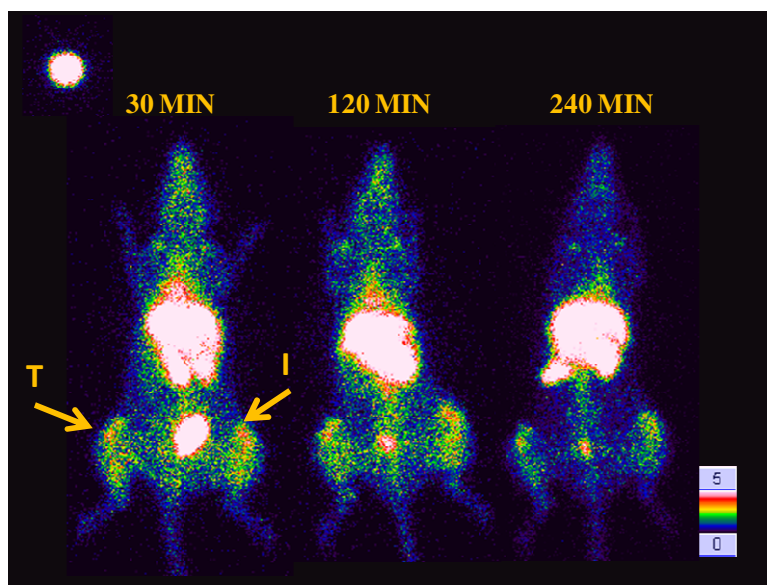
%ID	30 min			2 hr			4hr		
	Control	Block	Decrease	Control	Block	Decrease	Control	Block	Decrease
Liver	6.98±0.44	6.91±0.56	1.00%	8.02±0.21	6.47±0.16	19.33%	6.66±0.53	5.41±0.15	18.77%
Kidney	28.0±1.6	16.0±2.6	42.86%	34.2±3.6	25.3±4.0	26.02%	23.5±1.7	20.2±0.6	14.04%
Tumor	1.28±0.04	1.07±0.09	16.41%	0.77±0.08	0.74±0.05	3.90%	0.68±0.09	0.70±0.11	-2.94%
Muscle	0.28±0.03	0.30±0.03	-7.14%	0.21±0.03	0.20±0.04	4.76%	0.13±0.01	0.13±0.02	0.00%

**Table 3.4. Selected organ to muscle ratios before and after *in vivo* blocking of  $^{99m}\text{Tc}$ -EC-AMT by unlabeled L-Tyrosine in mammary tumor-bearing rats. Red font indicates the decreased %ID when compared to the corresponding control group. Blue shading indicates  $P < 0.05$  when compared to the corresponding control group (n=3/group/time interval).**

Ratio	30 min			2 hr			4hr		
	Control	Block	Decrease	Control	Block	Decrease	Control	Block	Decrease
Liver/Muscle	25.4±1.8	22.9±1.5	9.84%	38.7±1.8	34.7±0.9	10.34%	50.6±3.3	41.5±2.1	26.90%
Kidney/Muscle	101.8±1.7	53.0±1.2	47.94%	165.3±5.7	135.9±10.3	17.79%	178.7±14.4	154.5±6.9	8.19%
Tumor/Muscle	4.64±0.54	3.54±0.32	23.71%	3.74±0.16	3.70±0.23	1.07%	5.15±0.17	5.33±0.41	-7.52%

### Tumor and Inflammation Uptake Comparison *In Vivo*

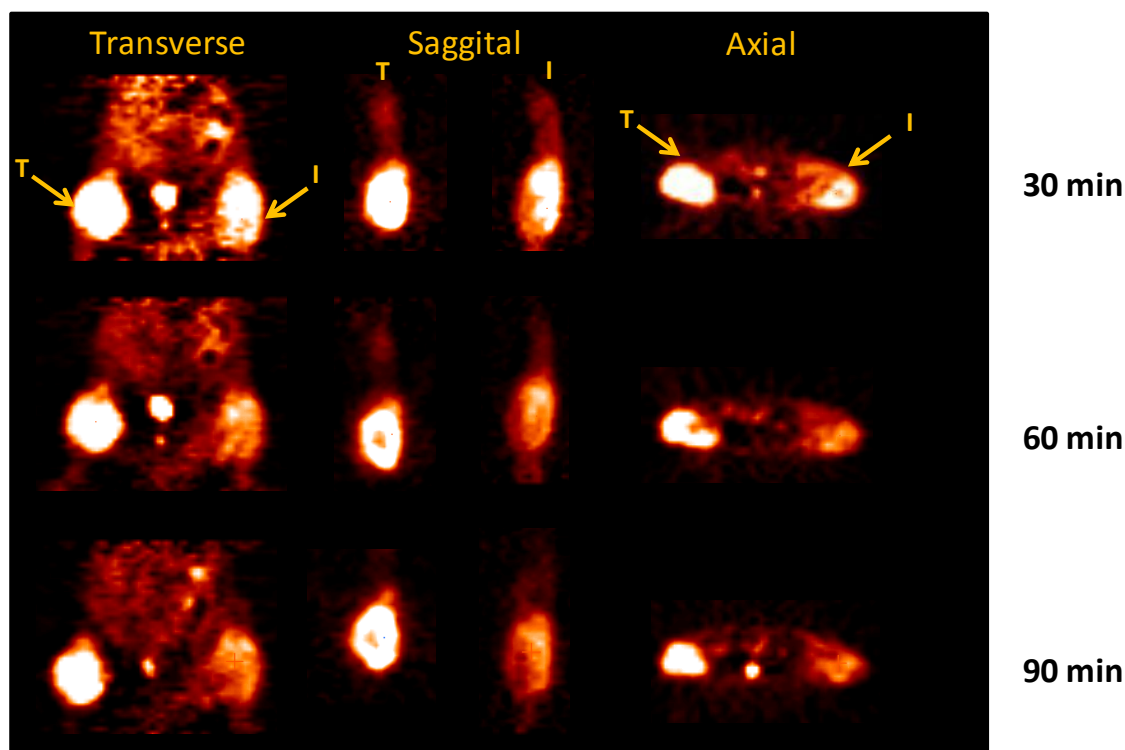
The representative planar scintigraphic images of  $^{99m}\text{Tc}$ -EC-AMT, as well as the micro-PET images of  $^{18}\text{F}$ -FDG in breast tumor and inflammation-bearing rats are shown in Fig. 3.7 and Fig. 3.8, respectively. The T/M of  $^{99m}\text{Tc}$ -EC-AMT at each time-point was relatively lower than I/M ratio. Furthermore, the T/I of  $^{99m}\text{Tc}$ -EC-AMT was also lower than that of  $^{18}\text{F}$ -FDG. These results suggested that  $^{99m}\text{Tc}$ -EC-AMT could not differentiate tumor from inflammation very well in this tumor model.



	30 min	2 hr	4 hr
T/M	2.68	2.51	2.75
I/M	3.17	3.10	3.02
T/I	0.84	0.81	0.91

**Figure 3.7.** Planar scintigraphic images of  $^{99m}\text{Tc}$ -EC-AMT at 30 – 240 min in rat breast tumor and inflammation-bearing rats (T: tumor, I: inflammation). The tumor-to-muscle ratios (T/Ms), inflammation-to-muscle ratios (I/Ms), and tumor-to-inflammation ratios (T/Is) are listed below the figure.





	30 min	60 min	90 min
T/M	5.88	7.54	4.90
I/M	3.43	3.77	2.72
T/I	1.71	1.99	1.80

**Figure 3.8. microPET images of  $^{18}\text{F}$ -FDG at 30 – 90 min in rat breast tumor and inflammation-bearing rats (T: tumor, I: inflammation). The tumor-to-muscle ratios (T/Ms), inflammation-to-muscle ratios (I/Ms), and tumor-to-inflammation ratios (T/Is) are listed below the figure.**

#### IV. Discussion

The present study investigated the imaging capability of  $^{99m}\text{Tc}$ -EC-AMT in breast tumor models *in vitro* and *in vivo*. For chemical synthesis, the precursor EC-AMT was successfully synthesized with an overall yield of 23%. Since the chelator EC was unprotected during the coupling reaction with AMT, each EC molecule could be conjugated with more than one AMT. Moreover, AMT might not only be conjugated with EC specifically on the nitrogen atom, but also on the sulfur atom. Those two potential problems could be readily solved by conducting the coupling reaction in the mild aqueous solution instead of the organic one. In addition, the molar ratio of EC and N-t-Butoxycarbonyl-O-[3-Br-propyl]- $\alpha$ -methyl tyrosine ethylester (compound 3) was controlled accurately in 2:1 under this aqueous solution. Furthermore, the structure of EC-AMT was well confirmed from the  $^1\text{H}$ -NMR and mass spectra results.

When label the precursor EC-AMT with  $^{99m}\text{Tc}$ , the radiochemical purity was 95%. In respect that  $^{99m}\text{Tc}$ -EC-AMT is a kit-product and labeled without any further purification, the radiochemical yield was assumed to be identical to its radiochemical purity (95%). Re-EC-AMT was synthesized as the reference standard for the structure confirmation of  $^{99m}\text{Tc}$ -EC-AMT. In periodic table, Tc is a second-row transition element in Group 7 and right above rhenium. Hence, Tc is very similar to Re in terms of chemistry, and they are known to have identical coordination parameters with the same ligand such as AMT[103]. From the HPLC results, the retention time of  $^{99m}\text{Tc}$ -EC-AMT matched to that of Re-EC-AMT, suggested the radiochemical structure of  $^{99m}\text{Tc}$ -EC-AMT was correct. In addition,

one radioisotopic form of Re,  $^{188}\text{Re}$ , is commonly used for the internal radionuclide therapy[132]. Therefore,  $^{188}\text{Re}$ -EC-AMT might be valuable in the treatment of breast cancer, while  $^{99\text{m}}\text{Tc}$ -EC-AMT could be used to diagnose the cancer and monitor treatment response in the future.

In cellular uptake study,  $^{99\text{m}}\text{Tc}$ -EC-AMT was taken up rapidly by rat mammary tumor cells, and the %Uptake of  $^{99\text{m}}\text{Tc}$ -EC-AMT was significantly higher than that of the negative control  $^{99\text{m}}\text{Tc}$ -EC, suggesting high specificity of  $^{99\text{m}}\text{Tc}$ -EC-AMT in tumor uptake. Besides,  $^{99\text{m}}\text{Tc}$ -EC-AMT has much higher uptake than  $^{18}\text{F}$ -FDG in this *in vitro* breast cancer model. In competitive inhibition study,  $^{99\text{m}}\text{Tc}$ -EC-AMT uptake could be significantly inhibited by L-tyrosine, which suggests that  $^{99\text{m}}\text{Tc}$ -EC-AMT is transported at least partially via the same transporter system LAT that L-tyrosine exploits. Our findings were consistent with other reported studies regarding radiolabeled tyrosine analogs. For instance,  $^{11}\text{C}/^{14}\text{C}$ -tyrosine[119],  $^{123}\text{I}/^{125}\text{I}$ -labeled AMT[56, 120],  $^{18}\text{F}$ -labeled tyrosine[121], AMT[76], and fluoroethyltyrosine ( $^{18}\text{F}$ -FET) [114] have been proven to be predominantly transported via amino acid transporter LAT. Increased expression level of LAT has been observed in various types of tumors[38], therefore, upregulated LAT is a suitable target for tumor imaging.

For *in vivo* evaluation,  $^{99\text{m}}\text{Tc}$ -EC-AMT had a relatively fast blood clearance in normal Fischer 344 rats (Fig. 3.5). Biodistribution study showed that  $^{99\text{m}}\text{Tc}$ -EC-AMT had high uptake in kidneys of normal rats (Table 3.1), which was consistent with the imaging results of breast tumor-bearing rats (Fig. 3.6). This may be due to the characteristics of EC given that  $^{99\text{m}}\text{Tc}$ -EC is a well-known renal tubular imaging agent[122]. In addition, Moore et al. reported that AMT itself, an inhibitor of tyrosine

hydroxylase, could not be excreted from kidneys and hence crystallized in the proximal tubules because of its poor solubility at the hydrogen ion concentrations of body fluids (pH 5-8)[133]. Furthermore, Shikano et al. confirmed that the uptake of  $^{123}\text{I}$ -labeled AMT ( $^{123}\text{I}$ -AMT) into normal human renal proximal tubule epithelial cells could be significantly inhibited by BCH, an LAT specific inhibitor[123]. This result suggests that LAT is involved in  $^{123}\text{I}$ -AMT uptake in kidneys. To ascertain whether  $^{99\text{m}}\text{Tc}$ -EC-AMT uptake is mediated specifically by LAT, we then conducted *in vivo* uptake blocking studies using the unlabeled L-Tyrosine as the competitive inhibitor (Table 3.3 and 3.4).  $^{99\text{m}}\text{Tc}$ -EC-AMT uptake in liver, kidney, and tumor were significantly blocked at early time-points, which suggested that both  $^{99\text{m}}\text{Tc}$ -EC-AMT and unlabeled L-Tyrosine were rapidly uptaken via amino acid transporter LAT. These *in vivo* findings were coherent with the *in vitro* competitive inhibition results.

In planar imaging studies shown in Fig. 3.6, tumors could be clearly detected by  $^{99\text{m}}\text{Tc}$ -EC-AMT at all time-points. Because of the washout of non-specific uptake, T/M ratios of  $^{99\text{m}}\text{Tc}$ -EC-AMT increased from 6.94 to 10.59, which were even much higher than those of  $^{18}\text{F}$ -FDG. The T/M ratios of  $^{18}\text{F}$ -FDG in the same animal model were 5.88, 7.54 and 2.87 for 30 min, 60 min and 120 min, respectively (images not shown). Nevertheless, we found that  $^{99\text{m}}\text{Tc}$ -EC-AMT was not superior to  $^{18}\text{F}$ -FDG in differentiating tumor from inflammation in this animal model because the T/Is of  $^{99\text{m}}\text{Tc}$ -EC-AMT were lower than those of  $^{18}\text{F}$ -FDG. In this study, we used turpentine to induce inflammation chemically. In future, we may need to create and test  $^{99\text{m}}\text{Tc}$ -EC-AMT in another animal model using radiation to induce inflammation so it can more similarly mimic the patients undergoing radiation therapy.

In summary, EC-AMT was synthesized and labeled with  $^{99m}\text{Tc}$  readily and efficiently with high radiochemical purity. *In vitro* cellular uptake study demonstrated that  $^{99m}\text{Tc}$ -EC-AMT transport involved amino acid transporter system LAT. Although it cannot differentiate breast tumor from chemical-induced inflammation very well,  $^{99m}\text{Tc}$ -EC-AMT has great potential for breast cancer imaging given its simple chemical synthesis procedure, more cost effectiveness of the isotope, and high tumor/muscle uptake ratios in planar imaging. By taking the advantages of the coordination capability of the chelator, EC-AMT could chelate various radioisotopes for either imaging or therapy in the future.

## **CHAPTER 4 Development of $^{99m}\text{Tc}$ -N4-Tyrosine for breast cancer imaging**

### **I. Introduction**

$^{18}\text{F}$ -FDG, an  $^{18}\text{F}$ -labeled glucose analog, is a gold standard for PET in cancer diagnosis[2]. However,  $^{18}\text{F}$ -FDG-PET has several limitations that give rise to false positive/negative diagnosis and poor predictive value of tumor response to chemo/radio therapy[125]. For instance,  $^{18}\text{F}$ -FDG cannot distinguish tumor from inflammatory or normal brain tissues because both sites have high glucose consumption. Therefore, radiolabeled amino acids have been developed as an alternative to  $^{18}\text{F}$ -FDG. Their use in tumor detection is based on an increased uptake of amino acids in tumor cells, which is assumed to reflect an enhanced amino acid transporter, metabolism, and protein synthesis[114]. Among all radiolabeled amino acids, aromatic ones such as tyrosine and its derivatives are more suitable given their easier chemistry alterations and favorable biological characterizations. To date, tyrosine and its  $\alpha$ -methyl substituted analog AMT have been successfully labeled with  $^{11}\text{C}$ [115, 116],  $^{18}\text{F}$ [75, 81] and  $^{124/125}\text{I}$ [65] for PET imaging, as well as  $^{123/131}\text{I}$ [56] for SPECT imaging, respectively. Most of those radiolabeled tyrosine analogs show promising preclinical and clinical results in tumor imaging, especially in brain tumor diagnosis. In addition, they have been proven to accumulate into the tumor cells predominantly via LAT, which is the only system that can transport large neutral amino acids with aromatic rings such as tyrosine, phenylalanine, and tryptophan[38, 41]. LAT, especially its subtype LAT1, is

an ideal target for tumor imaging because it is up-regulated and highly expressed in many cancer cell lines and correlated with tumor growth[117, 118].

Although the existing radiolabeled tyrosine and its derivatives have shown very promising clinical outcomes, most of them require an on-site cyclotron to produce the radioisotope, which is inconvenient and expensive. Besides, the half-life of the radioisotopes are either too short (i.e. 20 min for  $^{11}\text{C}$ ) or too long (i.e. 57.4 days for  $^{125}\text{I}$ ). Furthermore, iodine-labeled compounds are not stable *in vivo* because of deiodination. So far,  $^{18}\text{F}$  has the most appropriate half-life (110 min), however, the radiosynthesis yield of  $^{18}\text{F}$ -labeled radiotracers appear to be relatively low because of its electrophilic fluorination and tedious purification. Therefore, it is desirable to develop a radiotracer with simpler chemistry and affordable isotope, which can be used clinically in most major medical facilities.  $^{99\text{m}}\text{Tc}$  is an ideal radioisotope for diagnostic imaging studies, due to its physical characteristics. It emits a 140 keV gamma ray in 89% abundance [103], which is commonly used by gamma imaging and SPECT. The half-life of  $^{99\text{m}}\text{Tc}$  is 6.02 h, which can provide serial images and therefore overcome the drawback of  $^{18}\text{F}$ . Unlike most of the cyclotron-produced radionuclides that utilize the covalent chemistry for labeling,  $^{99\text{m}}\text{Tc}$  requires a “chelator” to conjugate the radioisotope with the target ligand. The nitrogen, oxygen and sulfur combination have been shown to be stable chelators for  $^{99\text{m}}\text{Tc}$  such as  $\text{N}_4$  (e.g. DOTA, cyclam-14),  $\text{N}_3\text{S}$  (e.g. MAG-3),  $\text{N}_2\text{S}_2$  (e.g. ECD),  $\text{NS}_3$ ,  $\text{S}_4$  (e.g. sulfur colloid), diethylenetriamine pentaacetic acid (DTPA),  $\text{O}_2\text{S}_2$  (e.g. DMSA), and hydrazinenicotinamide (HYNIC)[68, 101-105]. By taking the advantage of using the chelator, we could label several other radioisotopes such as Gallium-68, Indium-111,

or Rhenium-188 with the same ligand for diagnostic and therapeutic applications in future[105, 107]. Here, we report the synthesis of  $^{99m}\text{Tc}$ -labeled tyrosine using N4 cyclam as a chelator and evaluate its potential in breast tumor imaging.

## II. Materials and methods

### Chemicals and Analysis

All chemicals and sources used here were previously described in Chapter 2.

### Synthesis of Precursor N4-Tyrosine

#### a) *N-t-Butoxycarbonyl-O-[3-Br-propyl]-L-tyrosine methyl ester 1.*

N-*t*-Butoxycarbonyl-L-tyrosine methyl ester (25 g; 0.085 mol) was dissolved in acetone (300 mL). 1,3-dibromopropane (17.3 mL; 0.169 mol) and  $\text{K}_2\text{CO}_3$  (58 g; 0.420 mol) were added under nitrogen. The reaction mixture was refluxed at 80 °C overnight. After cooling and filtration, the solvent was removed under reduced pressure, and the residue was dissolved in chloroform. The residue was washed with water and dried with anhydrous  $\text{MgSO}_4$ . The product was purified by column chromatography using a silica gel column, eluted with hexane/ethyl acetate (2:1 v/v) to yield 33.3 g (94.6%). Ms (m/z): 440.09  $[\text{M}+\text{Na}]^+$ .

#### b) *N<sup>1</sup>, N<sup>4</sup>-dioxyl-1,4,8,11-tetraazabicyclotetradecane (N<sup>1</sup>,N<sup>4</sup>-cyclooxamide) 2.*

N4 cyclam (15.00 g; 74.88 mmol) was dissolved in 150 mL of anhydrous ethanol, and diethyl oxalate (10.94 g; 74.88 mmol) was added. The reaction mixture



was refluxed 18 h at 75 °C. The solvent was rotary evaporated and the crude product was recrystallized in acetone : ethanol to yield white crystals of N<sup>1</sup>,N<sup>4</sup>-dioxyl-1,4,8,11-1,5,8,12-tetraazabicyclotetradecane (N<sup>1</sup>,N<sup>4</sup>-cyclooxamide) **2** . Yield: 13.64 g (17.31 mmol, 72.00 %). Ms (m/z) = 255.33 [M]<sup>+</sup>.

**c)     *N*-t-Butoxycarbonyl-*O*-[3-( N<sup>1</sup>,N<sup>4</sup>-dioxyl-1,4,8,11-tetraazabicyclotetradecane)-propyl]- tyrosine methylester **3**.**

Compound **2** (0.625 g; 2.46 mmol) was dissolved in 20 mL of anhydrous DMF and reacted with a solution of compound **1** (1.06 g; 2.46 mmol) in 40 mL of DMF under nitrogen atmosphere. The mixture was refluxed at 75 °C for 18 hours, and then cooled to room temperature. The solvent was removed *in vacuo*. The residue was dissolved in 30 mL chloroform, washed with water and 12 mL of 1M Na<sub>2</sub>CO<sub>3</sub>, and then separated for the organic layer. The crude compound was purified via a silica gel column using chloroform: methanol (9:1) solution. Yield: 0.6489 g (1.052 mmol, 42.76%).

**d)     *O*-[3-(N<sup>1</sup>,N<sup>4</sup>-dioxyl-1,4,8,11-tetraazabicyclotetradecane)-propyl]-tyrosine methylester **4**.**

Compound **3** (0.6 g; 1 mmol) was dissolved in anhydrous dichloromethane (15 mL), and 2.5 mL of trifluoroacetic acid was added. The solution was stirred overnight at room temperature, and the solvents were removed *in vacuo*.

**e)     *O*-[3-(1,4,8,11-tetraazabicyclohexadecane)-propyl]-tyrosine (N4-Tyrosine) 5.**

Compound **4** (0.25 g; mmol) was dissolved in 5 mL water, and 2.5 mL of 10N NaOH was added to it. The solution was stirred and refluxed overnight at 90 °C, and the solvent was evaporated *in vacuo*. The crude compound was then dissolved in 5 mL water, and pH of the solution was neutralized to pH=7 by adding 5 M HCl. The final solution was lyophilized overnight to obtain white powder, which was then dissolved in 25 mL anhydrous methanol, filtered, evaporated, and lyophilized to obtain off-white powder.

**Radiolabeling of N4-Tyrosine with <sup>99m</sup>Tc**

N4-Tyrosine (1 mg) was dissolved in 0.2 mL sterile water, followed by adding tin (II) chloride (0.1 mL, 1 mg/mL). Required amount of Na<sup>99m</sup>TcO<sub>4</sub> was added to N4-Tyrosine solution. Radiochemical purity was determined by radio-HPLC (Waters, Milford, MA), eluted with acetonitrile: water (7:3) using a flow rate of 0.5 mL/min.

**Determination of the Partition Coefficient**

To determine the lipophilicity, 20 µL of <sup>99m</sup>Tc-N4-Tyrosine was added into an equal volume mixture of 1-octanol and sterile water in a centrifuge tube. The mixture was vortexed at room temperature for 1 min and then centrifuged at 5000 rpm for 5 min. From each phase, 0.1 mL of the aliquot was taken out and the radioactivity was measured by gamma counter (Cobra Quantum; Packard, MN). The measurement was repeated for three times, and care was taken to avoid cross

contamination between the phases. The partition coefficient value, expressed as logP, was calculated using the following equation:

$$\text{LogP} = \text{Log} (\text{radioactivity in 1-octanol layer} / \text{radioactivity in sterile water layer})$$

### ***In Vitro* Cellular Uptake Studies**

Rat breast tumor cell line 13762 (American Type Culture Collection, Rockville, MD) was selected because the same cell line was used to create the animal model for *in vivo* evaluation. Cells were maintained in Dulbecco's modified Eagle's medium and nutrient mixture F-12 Ham (DMEM/F12; GIBCO, Grand Island, NY) at 37 °C in a humidified atmosphere containing 5% CO<sub>2</sub>. Cells were plated onto 6-well tissue culture plates (2x10<sup>5</sup> cells/well) and incubated with <sup>99m</sup>Tc-N4-Tyrosine (0.05 mg/well, 8 uCi/well), <sup>99m</sup>Tc-N4 (0.025 mg/well, 8 uCi/well) or <sup>18</sup>F-FDG (8 uCi/well) for 0-4 h. After incubation, cells were washed with ice-cold PBS twice and detached by treating them with 0.5 mL of trypsin for 5 min. Cells were then collected and the radioactivity was measured with gamma counter (Cobra Quantum; Packard, MN). Data were expressed in mean ±S.D. percent of cellular uptake (%Uptake) in triplicate.

### ***In Vitro* Competitive Inhibition Study**

To investigate the transport mechanisms of <sup>99m</sup>Tc-N4-Tyrosine, the competitive inhibition study using L-tyrosine was conducted. Rat breast tumor cells were co-incubated with <sup>99m</sup>Tc-N4-Tyrosine (8 µg/well, 8 µCi/well) and L-tyrosine for up to 1 h. A set of concentrations of L-tyrosine (10-1000x of the N4-Tyrosine concentration)

were used. After incubation, cells were washed with ice-cold PBS twice and detached by treating them with 0.5 mL of trypsin for 5 min. Cells were then collected and the radioactivity was measured by gamma counter. Data were expressed in mean  $\pm$ S.D. percent of cellular uptake (%Uptake) in triplicate.

### **Blood Clearance**

All animal work was carried out in the Small Animal Imaging Facility (SAIF) at UTMDACC under a protocol approved by Institutional Animal Care and Use Committee (IACUC). For blood clearance analysis, three normal female Fischer 344 rats ( $150\pm 25$  g) (Harlan Sprague-Dawley, Indianapolis, IN) were intravenously injected with 30  $\mu$ Ci  $^{99m}\text{Tc}$ -N4-Tyrosine. Blood samples were drawn through lateral tail vein at several time-points from 5 min to 24 h ( $n=3/\text{rat}$ ) by microliter pipettes (10  $\mu$ L). The blood samples were measured for radioactivity by gamma counter, and then were calculated as percentage of the injected dose per gram of blood (%ID/g).

### ***In vivo* Tissue Distribution Studies**

Tissue distribution studies of  $^{99m}\text{Tc}$ -N4-Tyrosine (study I,  $n=9$ ) and  $^{18}\text{F}$ -FDG (study II,  $n=9$ ) were conducted by using normal female Fischer 344 rats ( $150\pm 25$  g,  $n=18$ ). For each compound, the rats were divided into three groups for three time intervals (0.5, 2, 4 h for  $^{99m}\text{Tc}$ -N4-Tyrosine; 0.5, 1, 2 h for  $^{18}\text{F}$ -FDG;  $n=3/\text{time point}$ ). The injection activity was  $25\pm 0.5$   $\mu$ Ci/rat intravenously. At each time interval, the rats were sacrificed, and the selected tissues were excised, weighed and measured for radioactivity by gamma counter. Each sample was calculated as percentage of

the injected dose per gram of tissue wet weight (%ID/g). Counts from a diluted sample of the original injection were used as reference.

### **Planar Scintigraphic Imaging Study**

Female Fischer 344 rats were inoculated subcutaneously with 0.1 mL of breast tumor cells 13762 suspension in PBS ( $10^5$  cells/rat) into the right legs. Planar scintigraphic imaging of  $^{99m}\text{Tc}$ -N4-Tyrosine was performed 12-14 days after inoculation when tumors reached approximately 1 cm in diameter. Planar scintigraphic images were obtained using M-CAM (Siemens Medical Solutions, Hoffman Estates, IL) equipped with a Low Energy High Resolution collimator. Anesthetized breast tumor-bearing rats were injected intravenously with  $^{99m}\text{Tc}$ -N4-Tyrosine (0.3 mg/rat, 300  $\mu\text{Ci}$ /rat; n=3). The images were acquired up to 4 h post-administration of tracers. Computer outlined regions of interest (ROIs in counts per pixel) between tumor and muscle were used to calculate tumor/muscle (T/M) ratios. Percentage of the injected dose (%ID) of tumor was also calculated from the reference standard, which was 1/10 of the original injection activity.

### ***In Vivo* Uptake Blocking Study**

To ascertain whether  $^{99m}\text{Tc}$ -N4-Tyrosine uptake is mediated specifically by LAT, *in vivo* blocking studies using the unlabeled L-Tyrosine as the competitive inhibitor was conducted. The same animal model used in the planar scintigraphic imaging study was employed. Unlabeled L-Tyrosine (50 mg/kg) dissolved in 0.3 mL saline (pH adjusted to 2-3) was administered intravenously to mammary tumor–

bearing rats 1 h prior to  $^{99m}\text{Tc}$ -N4-Tyrosine injection. Planar scintigraphic images were acquired up to 4 h, and ROIs of liver, kidneys, tumor, and muscle were used to calculate the ratios of liver/muscle, kidney/muscle, and tumor/muscle, respectively. In addition, %IDs of liver, kidneys, tumor, and muscle were calculated from the reference standard, which was 1/10 of the original injection activity. The results were compared with those from the rats injected with  $^{99m}\text{Tc}$ -N4-Tyrosine alone (control).

### **Tumor and Inflammation Uptake Comparison *In Vivo***

To investigate whether  $^{99m}\text{Tc}$ -N4-Tyrosine can differentiate tumor from the inflammatory tissue, a rat model bearing both mammary tumor and turpentine oil-induced inflammation was created. 13762 rat mammary tumor cells ( $10^5$  cells/0.1 mL PBS/rat) were inoculated into the right calf muscles of the female Fischer 344 rats. After the tumors reached to 1 cm in diameter, turpentine oil (0.1 mL/rat) was injected into the left calf muscles of the rats to induce inflammation. The anesthetized rats (n=3) were injected intravenously with  $^{99m}\text{Tc}$ -N4-Tyrosine 24 h after the turpentine injection. Planar scintigraphic images were acquired up to 4 h, and ROIs of tumor, inflammation, and muscle were used to calculate the tumor-to-muscle ratios (T/Ms), inflammation-to-muscle ratios (I/Ms), and tumor-to-inflammation ratios (T/Is), respectively. Same animal model was used to evaluate  $^{18}\text{F}$ -FDG. Micro-PET imaging of  $^{18}\text{F}$ -FDG was performed using R4 micro-PET scanner (Concorde Microsystems, TN). The rats were injected intravenously with  $^{18}\text{F}$ -FDG (500  $\mu\text{Ci}$ /rat, n=3), and dynamic PET scans were obtained for 90 min with

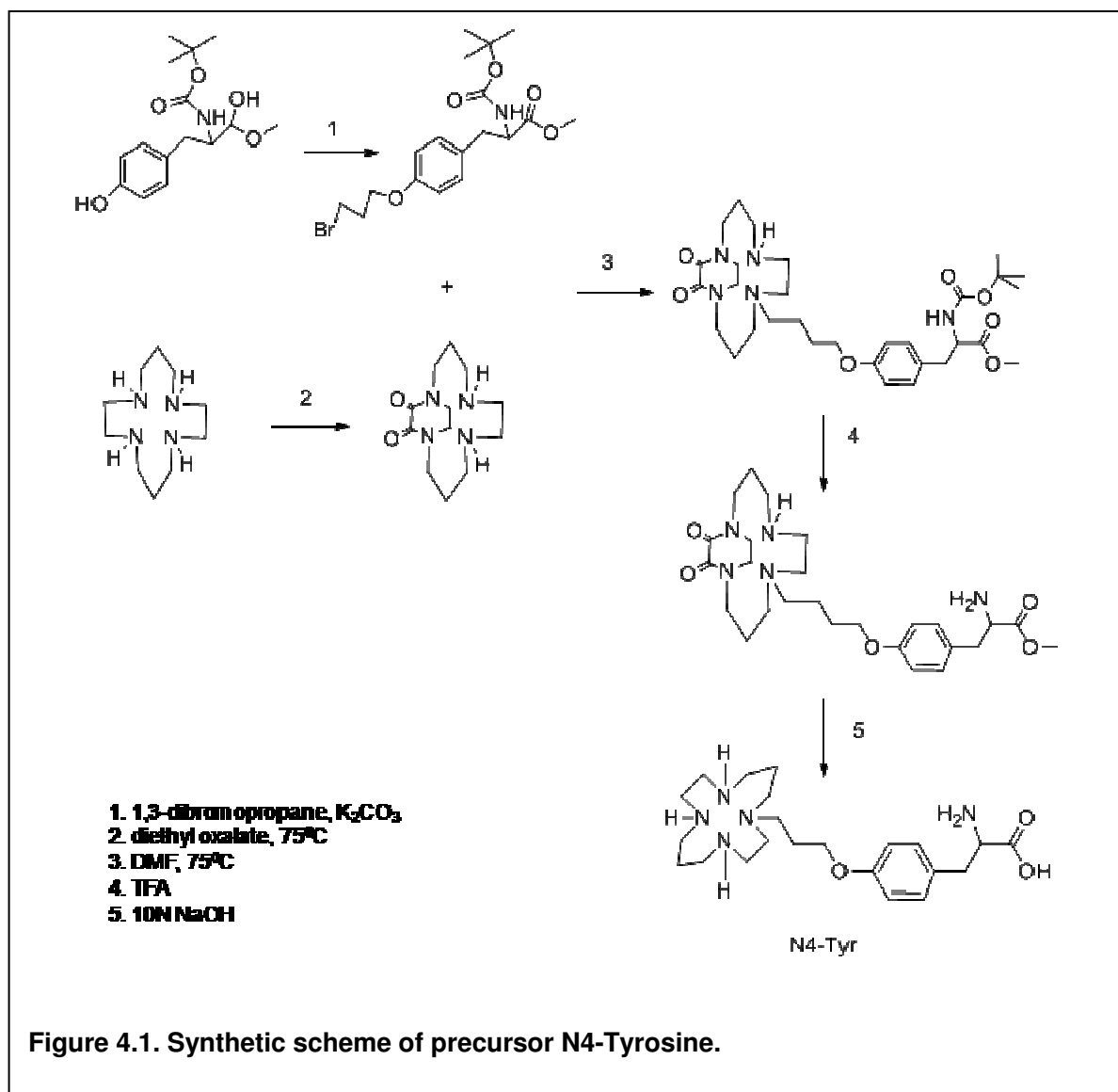
a spatial resolution of 2.2 mm. PET images were reconstructed by using the ordered subset expectation maximization (OSEM) algorithm. T/Ms, I/Ms and T/Is ratios were calculated based on the regional radioactivity concentrations ( $\mu\text{Ci}/\text{cm}^3$ ) that were estimated from the average pixels within ROIs drawn around the tumor, inflammation or muscle on transverse slices of the reconstructed image sets.

### III. Results

#### Chemistry and Radiochemistry

Precursor N4-Tyrosine was synthesized via a five-step procedure and the total synthesis yield was 38%. The synthetic scheme is shown in Fig.4.1. The structure and purity of N4-Tyrosine was confirmed by  $^1\text{H}$ - and  $^{13}\text{C}$ - NMR, mass spectra, and HPLC. The  $^1\text{H}$ - and  $^{13}\text{C}$ -NMR results were  $^1\text{H}$ - NMR ( $\text{D}_2\text{O}$ ,  $\delta/\text{ppm}$ ): 7.18 (d, 2H, phenyl ring), 6.95 (d, 2H, phenyl ring), 4.073 (t, 2H, O-CH<sub>2</sub>), 3.43(t, 1H, CHN), 2.28-3.00 (m, 2OH, OCH<sub>2</sub> and NCH<sub>2</sub>-), 1.87-1.91(m, 2H, C-CH<sub>2</sub>-C), 1.68-1.79(m, 4H, C-CH<sub>2</sub>-C).  $^{13}\text{C}$ - NMR ( $\text{D}_2\text{O}$ ,  $\delta/\text{ppm}$ ):162.88,156.72, 130.76, 117.57, 115.25, 68.55, 57.29, 53.91, 51.56, 49.95, 49.17, 48.96, 48.24, 48.03, 46.80, 45.73, 45.35, 39.27, 24.90, 24.31, 23.87.

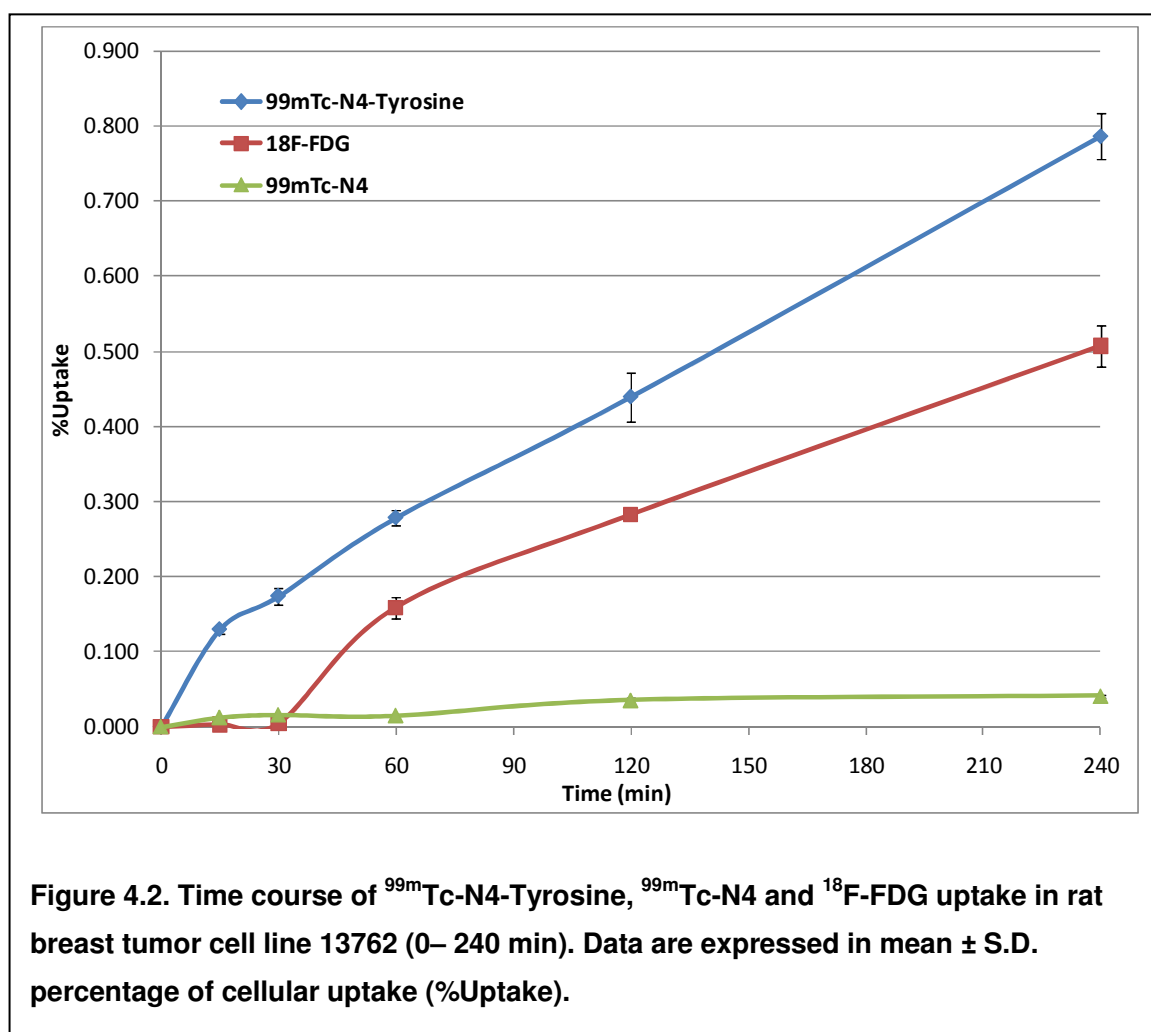
Precursor N4-Tyrosine could be labeled with  $^{99\text{m}}\text{Tc}$  successfully in a high radiochemical purity (>96%). The logP of  $^{99\text{m}}\text{Tc}$ -N4-Tyrosine was  $-2.83\pm0.082$ .





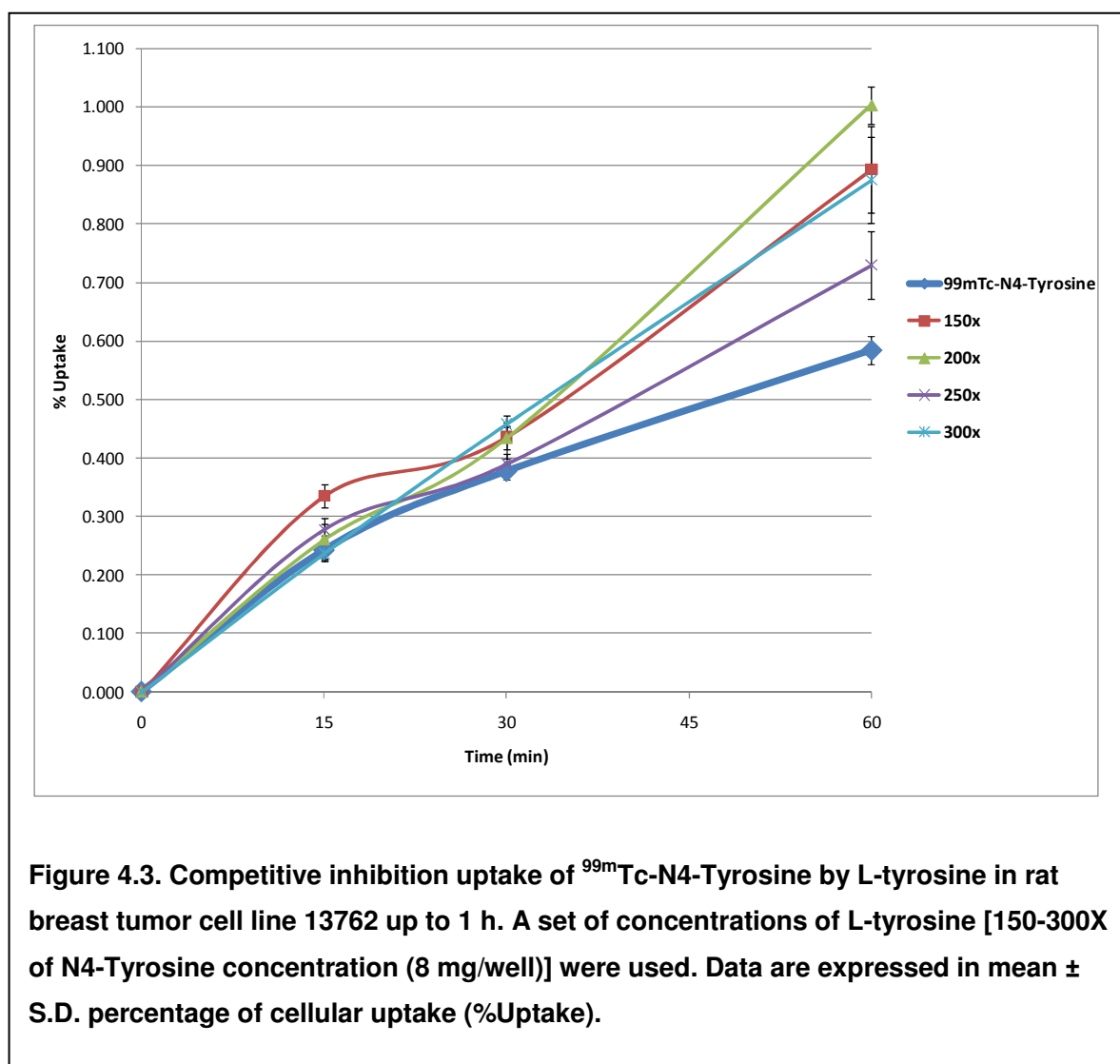
### ***In Vitro* Cellular Uptake Studies**

The cellular uptake kinetics of  $^{99m}\text{Tc}$ -N4-Tyrosine,  $^{99m}\text{Tc}$ -N4, and  $^{18}\text{F}$ -FDG using rat breast tumor cells is shown in Fig. 4.2. There was a drastically increased uptake for  $^{99m}\text{Tc}$ -N4-Tyrosine at 15-240 min, but not for  $^{99m}\text{Tc}$ -N4 chelator itself, which suggested that  $^{99m}\text{Tc}$ -N4-Tyrosine can enter and accumulate into tumor cells rapidly and specifically. In addition, the %Uptake of  $^{99m}\text{Tc}$ -N4-Tyrosine was relatively higher than that of  $^{18}\text{F}$ -FDG.



### Competitive Inhibition Study of $^{99m}\text{Tc}$ -N4-Tyrosine

After co-incubated with L-tyrosine at 10-1000 times as high as the concentrations of N4-Tyrosine,  $^{99m}\text{Tc}$ -N4-Tyrosine did not show any significantly decreased uptake at all concentrations. The  $^{99m}\text{Tc}$ -N4-Tyrosine uptakes of selected concentrations are shown in Fig. 4.3. These results suggest that  $^{99m}\text{Tc}$ -N4-Tyrosine may not share the same LAT transporter system as L-Tyrosine.



## Blood Clearance

The blood clearance curve for  $^{99m}\text{Tc}$ -N4-Tyrosine in normal Fischer 344 rats (n=3) is shown in Fig. 4.4. The plasma half-life of the distribution phase ( $t_{1/2} \alpha$ ) was  $9.31 \pm 0.759$  min, and that of the elimination phase ( $t_{1/2} \beta$ ) was  $90.14 \pm 1.901$  min.

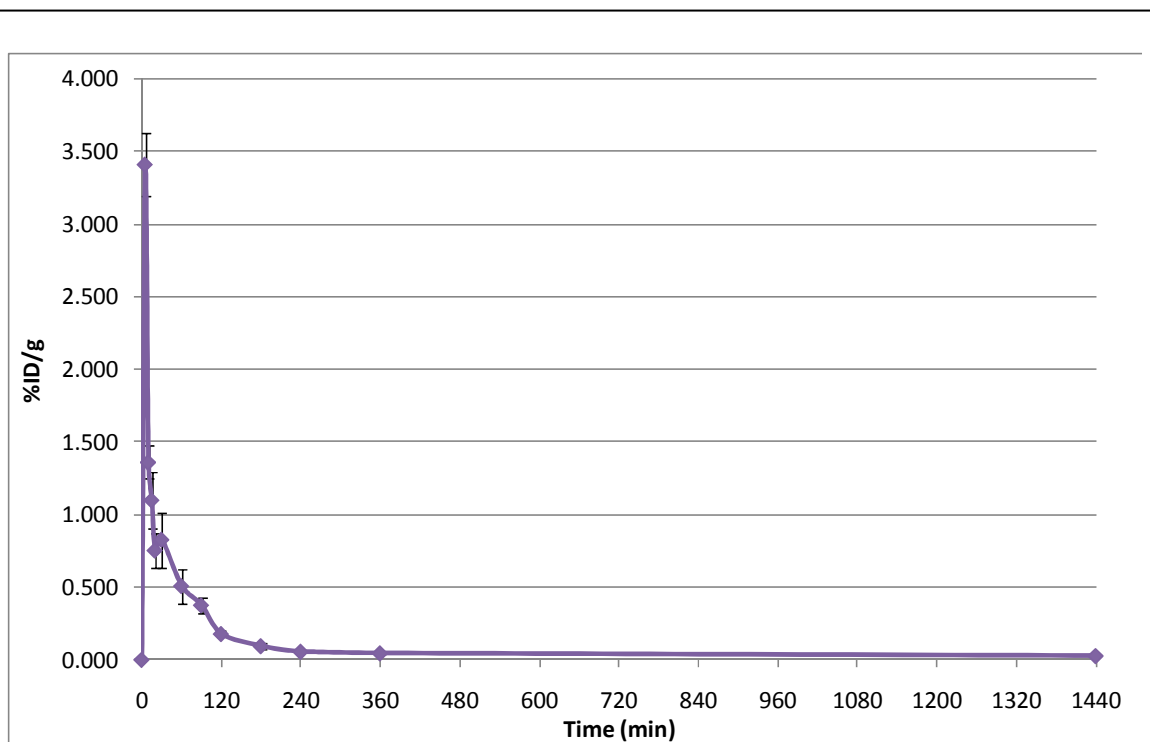


**Figure 4.4. Blood clearance (%ID/g) of  $^{99m}\text{Tc}$ -N4-Tyrosine in normal female Fischer 344 rats (n=3). The data represent the mean radioactivity expressed as a percentage of the injected dose per gram of blood  $\pm$  S.D.**

### ***In Vivo* Tissue Distribution Studies**

The tissue distribution results of  $^{99m}\text{Tc}$ -N4-Tyrosine and  $^{18}\text{F}$ -FDG in the normal Fischer 344 rats are shown in Tables 4.1 and 4.2, respectively. Low thyroid and stomach uptake of  $^{99m}\text{Tc}$ -N4-Tyrosine was observed, suggesting its high stability *in vivo*.

**Table 4.1. Biodistribution of  $^{99m}\text{Tc}$ -N4-Tyrosine in normal Fischer 344 female rats.**

<b>%ID/g</b>	<b>30 MIN</b>	<b>120 MIN</b>	<b>240 MIN</b>
<b>blood</b>	0.88 ±0.040	0.20 ±0.018	0.17 ±0.009
<b>heart</b>	0.21 ±0.022	0.06 ±0.003	0.05 ±0.003
<b>lung</b>	0.50 ±0.023	0.19 ±0.011	0.14 ±0.006
<b>thyroid</b>	0.34 ±0.019	0.10 ±0.010	0.09 ±0.006
<b>pancreas</b>	0.17 ±0.017	0.07 ±0.012	0.05 ±0.002
<b>liver</b>	1.15 ±0.059	0.70 ±0.040	0.67 ±0.044
<b>spleen</b>	0.94 ±0.089	0.76 ±0.032	0.63 ±0.051
<b>kidney</b>	11.05 ±0.783	12.34 ±0.502	12.40 ±0.405
<b>stomach</b>	0.20 ±0.018	0.08 ±0.003	0.06 ±0.002
<b>intestine</b>	0.34 ±0.057	0.13 ±0.010	0.11 ±0.006
<b>muscle</b>	0.07 ±0.007	0.03 ±0.002	0.02 ±0.001
<b>bone&amp; joint</b>	0.24 ±0.021	0.15 ±0.008	0.12 ±0.008
<b>brain</b>	0.03 ±0.001	0.02 ±0.001	0.01 ±0.001

Each rat received  $^{99m}\text{Tc}$ -N4-Tyrosine (25  $\mu\text{Ci}$ , intravenously). Each value is percent of injected dose per gram weight (n= 3)/time interval. Each data represents mean of three measurements with standard deviation.

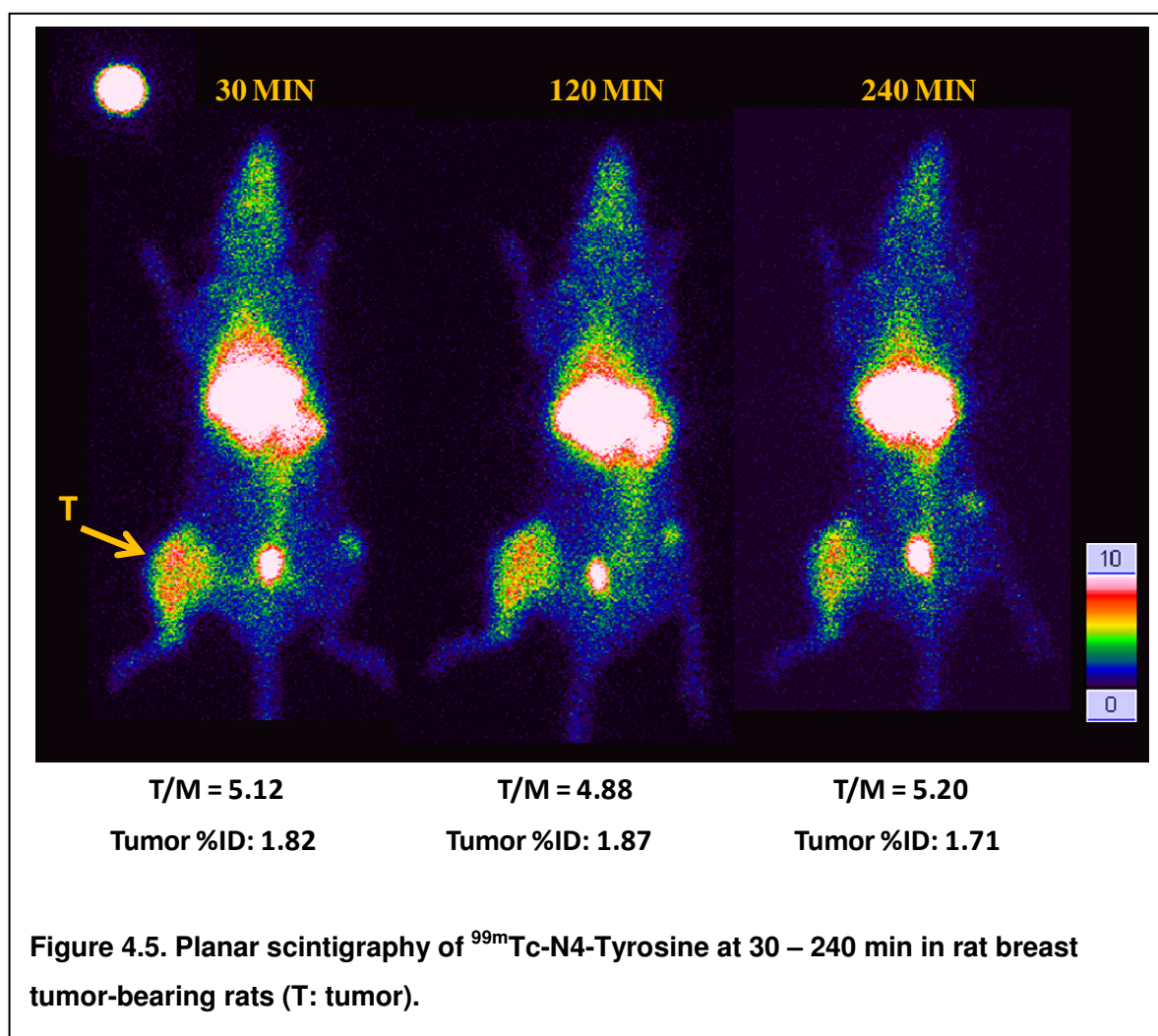
**Table 4.2. Biodistribution of  $^{18}\text{F}$ -FDG in normal Fischer 344 female rats.**

<b>%ID/g</b>	<b>30 MIN</b>	<b>60 MIN</b>	<b>120 MIN</b>
<b>blood</b>	0.40±0.042	0.13±0.006	0.06±0.002
<b>heart</b>	1.57±0.056	1.38±0.126	1.08±0.068
<b>lung</b>	0.55±0.056	0.42±0.024	0.46±0.027
<b>thyroid</b>	1.07±0.080	1.04±0.040	1.05±0.069
<b>pancreas</b>	0.26±0.028	0.21±0.006	0.20±0.016
<b>liver</b>	0.40±0.048	0.16±0.006	0.13±0.012
<b>spleen</b>	0.82±0.081	0.74±0.032	0.86±0.071
<b>kidney</b>	0.71±0.051	0.37±0.012	0.24±0.018
<b>stomach</b>	0.61±0.078	0.44±0.031	0.39±0.030
<b>intestine</b>	0.69±0.068	0.53±0.035	0.52±0.025
<b>muscle</b>	0.33±0.040	0.34±0.027	0.74±0.024
<b>bone&amp; joint</b>	0.33±0.036	0.44±0.065	0.50±0.034
<b>brain</b>	2.00±0.149	1.99±0.046	1.39±0.086

Each rat received  $^{18}\text{F}$ -FDG (25  $\mu\text{Ci}$ , intravenously). Each value is percent of injected dose per gram weight (n =3)/time interval. Each data represents mean of three measurements with standard deviation.

### Planar Scintigraphic Imaging Study

The selected planar scintigraphic images of  $^{99m}\text{Tc}$ -N4-Tyrosine at 30 min, 2h, and 4 h in breast tumor-bearing rats are shown in Fig. 4.5. Tumors could be clearly detected by  $^{99m}\text{Tc}$ -N4-Tyrosine at all time-points. The T/M ratios at 30 min, 2h, and 4 h were 5.12, 4.88, and 5.20, respectively. Tumor %ID at these three time-points were 1.82%, 1.87%, and 1.71%, respectively (Fig. 4.5).



### ***In Vivo* Uptake Blocking Study**

The liver, kidneys, tumor, and muscle %ID of  $^{99m}\text{Tc}$ -N4-Tyrosine, as well as the ratios of these organs to muscle before and after *in vivo* blocking by unlabeled L-Tyrosine were listed in Table 4.3 and 4.4. By using the blocking agent L-Tyrosine, only kidneys uptake of  $^{99m}\text{Tc}$ -N4-Tyrosine decreased at all time-points. The uptake (%ID) in liver, tumor and muscle even increased significantly. These results suggest that  $^{99m}\text{Tc}$ -N4-Tyrosine may not utilize the same transport system LAT as L-Tyrosine does *in vivo*.

**Table 4.3. Percentage of injected dose (%ID) of selected organs before and after *in vivo* blocking of  $^{99m}\text{Tc}$ -N4-Tyrosine by unlabeled L-Tyrosine in mammary tumor-bearing rats. Red font indicates the decreased %ID when compared to the corresponding control group. Blue shading indicates  $P < 0.05$  when compared to the corresponding control group (n=3/group/time interval).**

%ID	30 min			2 hr			4hr		
	Control	Block	Decrease	Control	Block	Decrease	Control	Block	Decrease
Liver	8.76±0.42	9.59±0.62	-9.47%	9.69±0.5	10.24±0.36	-5.68%	7.9±0.42	10.1±1.5	-27.85%
Kidney	26.8±3.3	19.7±0.8	26.49%	30.7±2.1	26.0±2.4	15.31%	29.8±1.7	28.6±3.7	4.03%
Tumor	0.78±0.04	1.43±0.15	-83.33%	0.34±0.03	0.72±0.03	-111.76%	0.20±0.02	0.47±0.02	-135.01%
Muscle	0.15±0.03	0.31±0.01	-106.67%	0.08±0.01	0.13±0.02	-62.50%	0.06±0.01	0.09±0.015	50.00%

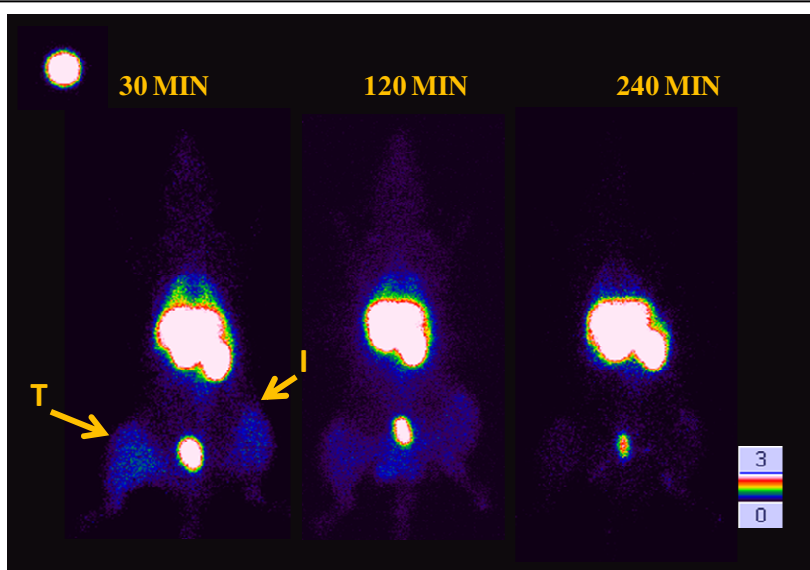
**Table 4.4. Selected organ to muscle ratios before and after *in vivo* blocking of <sup>99m</sup>Tc-N4-Tyrosine by unlabeled L-Tyrosine in mammary tumor-bearing rats. Red font indicates the decreased %ID when compared to the corresponding control group. Blue shading indicates P<0.05 when compared to the corresponding control group (n=3/group/time interval).**

Ratio	30 min			2 hr			4hr		
	Control	Block	Decrease	Control	Block	Decrease	Control	Block	Decrease
Liver/Muscle	57.6±3.8	30.7±2.4	46.70%	117.1±4.7	80.6±2.5	31.17%	126.1±4.2	114.1±4.5	9.52%
Kidney/Muscle	176.0±7.1	63.3±3.6	64.03%	371.4±11.6	204.6±6.8	44.91%	473.5±14.1	321.6±3.7	32.08%
Tumor/Muscle	5.12±0.34	4.57±0.12	10.74%	4.11±0.18	5.68±0.39	-38.20%	3.24±0.25	5.34±0.13	-64.81%



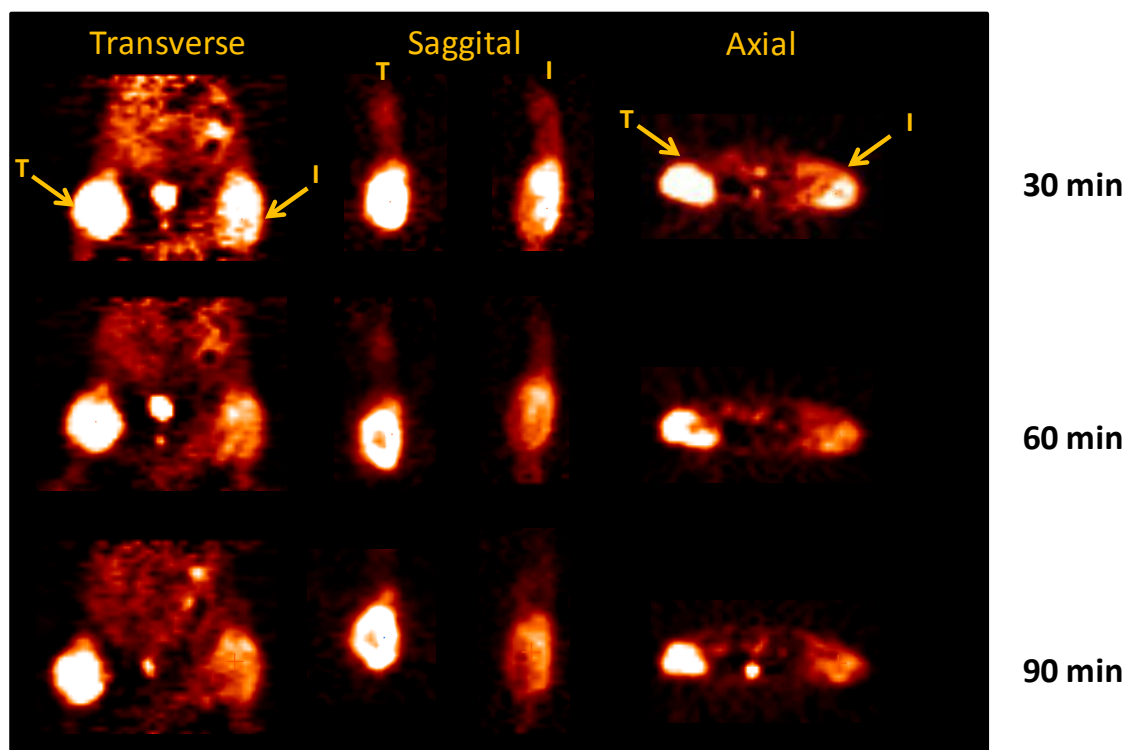
### Tumor and Inflammation Uptake Comparison *In Vivo*

The selected planar scintigraphic images of  $^{99m}\text{Tc}$ -N4-Tyrosine, as well as the micro-PET images of  $^{18}\text{F}$ -FDG in breast tumor and inflammation-bearing rats are shown in Fig. 4.6 and Fig. 4.7, respectively. The T/M of  $^{99m}\text{Tc}$ -N4-Tyrosine at each time interval was relatively higher than I/M. Although T/I at all time-points were above 1, which meant tumor had higher uptake than the inflammation site, the ratios were lower than those of  $^{18}\text{F}$ -FDG. Therefore, these results suggested that  $^{99m}\text{Tc}$ -N4-Tyrosine could not differentiate tumor from inflammation very well.



	30 min	2 hr	4 hr
T/M	5.12	4.11	3.24
I/M	4.26	3.62	2.45
T/I	1.20	1.14	1.32

**Figure 4.6. Planar scintigraphic images of  $^{99m}\text{Tc}$ -N4-Tyrosine at 30 – 240 min in rat breast tumor and inflammation-bearing rats (T: tumor, I: inflammation). The tumor-to-muscle ratios (T/Ms), inflammation-to-muscle ratios (I/Ms), and tumor-to-inflammation ratios (T/Is) are listed below the figure.**



	30 min	60 min	90 min
T/M	5.88	7.54	4.90
I/M	3.43	3.77	2.72
T/I	1.71	1.99	1.80

**Figure 4.7. microPET images of  $^{18}\text{F}$ -FDG at 30 – 90 min in rat breast tumor and inflammation-bearing rats (T: tumor, I: inflammation). The tumor-to-muscle ratios (T/Ms), inflammation-to-muscle ratios (I/Ms), and tumor-to-inflammation ratios (T/Is) are listed below the figure.**

## IV. Discussion

In the present study, we report the synthesis of  $^{99m}\text{Tc}$ -labeled tyrosine using N4 cyclam as a chelator and evaluate its potential in breast cancer diagnosis by using the breast tumor models *in vitro* and *in vivo*.

For chemical synthesis, the precursor N4-Tyrosine was successfully synthesized via a five-step procedure with an overall yield of 38%. Since the starting material N-*t*-Butoxycarbonyl-L-tyrosine methyl ester was commercially available, the synthetic yield of N4-Tyrosine was much higher than that of its  $\alpha$ -methyl derivative N4-AMT (14%). When the precursor N4-Tyrosine was labeled with  $^{99m}\text{Tc}$ , the radiochemical purity was more than 96%. Since  $^{99m}\text{Tc}$ -N4-Tyrosine is a kit-product and labeled without any further purification, the radiochemical yield was assumed to be identical to its radiochemical purity. As expected, the partition coefficient value (logP) of  $^{99m}\text{Tc}$ -N4-Tyrosine was lower than that of its  $\alpha$ -methyl derivative  $^{99m}\text{Tc}$ -N4-AMT ( $-2.83 \pm 0.082$  vs.  $-2.02 \pm 0.168$ ). As we know, the lower logP indicates the lower lipophilicity of the compound. The result verified our hypothesis that the lipophilicity of Tyrosine-based radiotracer could be increased by adding a methyl group on its  $\alpha$ -carbon.

In cellular uptake study,  $^{99m}\text{Tc}$ -N4-Tyrosine was taken up rapidly by rat mammary tumor cells, and the %Uptake of  $^{99m}\text{Tc}$ -N4-Tyrosine was significantly higher than that of the negative control  $^{99m}\text{Tc}$ -N4, suggesting high specificity of  $^{99m}\text{Tc}$ -N4-Tyrosine in tumor uptake. Besides,  $^{99m}\text{Tc}$ -N4-Tyrosine has even higher uptake than  $^{18}\text{F}$ -FDG in this *in vitro* breast cancer model. In competitive inhibition study using the same cell line,  $^{99m}\text{Tc}$ -N4-Tyrosine uptake could not be inhibited by

L-Tyrosine at any concentration. Its uptake even increased by adding unlabeled L-Tyrosine. Same results were observed in the *in vivo* uptake blocking studies using the unlabeled L-Tyrosine as the competitive inhibitor (Table 4.3 and 4.4). By using the blocking agent L-Tyrosine, only kidneys uptake of  $^{99m}\text{Tc}$ -N4-Tyrosine decreased at all time-points. The uptake (%ID) in liver, tumor and muscle even increased significantly. Taken the *in vitro* and *in vivo* findings together, we conclude that  $^{99m}\text{Tc}$ -N4-Tyrosine may not be transported by the same amino acid transporter LAT as L-tyrosine.

$^{99m}\text{Tc}$ -N4-Tyrosine had a very fast blood clearance in normal Fischer 344 rats (Fig. 4.4). Biodistribution study showed that  $^{99m}\text{Tc}$ -N4-Tyrosine had high uptake in kidneys of normal rats (Table 4.1), which was consistent with the imaging findings in the breast tumor-bearing rats (Fig. 4.5). This may due to the low lipophilicity of  $^{99m}\text{Tc}$ -N4-Tyrosine. In addition, it might be the characteristics of tyrosine because the similar results were also observed in our previously developed tyrosine-based radiotracer  $^{99m}\text{Tc}$ -EC-AMT and  $^{99m}\text{Tc}$ -EC-Tyrosine.

In planar imaging studies shown in Fig. 4.5, tumors could be clearly detected by  $^{99m}\text{Tc}$ -N4-Tyrosine at all time-points; however,  $^{99m}\text{Tc}$ -N4-Tyrosine appeared to be not ideal for differentiation of tumor from inflammation. Although T/Is were above 1 at all time-points, which meant tumor had higher uptake than the inflammatory tissue, the ratios were less than those of  $^{18}\text{F}$ -FDG. In this study, we used turpentine to induce inflammation chemically. In future, we may need to test  $^{99m}\text{Tc}$ -N4-Tyrosine in another animal model using the radiation to induce inflammation so it can more similarly mimic the patients undergoing radiation therapy.

In summary, N4-Tyrosine was synthesized and labeled with  $^{99m}\text{Tc}$  readily and efficiently with high radiochemical purity. Although *in vitro* and *in vivo* findings suggest that  $^{99m}\text{Tc}$ -N4-Tyrosine does not use LAT system to enter the tumor lesion, it has high tumor/muscle uptake ratios and can detect breast tumor clearly. Furthermore, it is not suitable to use  $^{99m}\text{Tc}$ -N4-Tyrosine to distinguish breast tumor from chemical-induced inflammation, however, we need to test its imaging potential in other inflammation models.

## CHAPTER 5 Development of $^{99m}\text{Tc}$ -N4-AMT for breast cancer imaging (adapted partially from[134])

### I. Introduction

$^{18}\text{F}$ -FDG, an  $^{18}\text{F}$ -labeled glucose analog, is the most common radiotracer for PET in cancer diagnosis[2]. However,  $^{18}\text{F}$ -FDG-PET has several limitations in practice, *e.g.*  $^{18}\text{F}$ -FDG cannot distinguish tumor from inflammatory or normal brain tissues. Therefore,  $^{18}\text{F}$ -labeled amino acid-based radiotracers have been reported as an alternative, which is based on the fact that tumor cells take up and consume more amino acids to maintain their sustained fast growth. Among those radiotracers,  $^{18}\text{F}$ -labeled AMT has shown high tumor uptake and great ability to differentiate tumor tissue from inflammatory sites in brain tumors and squamous cell carcinoma[130].  $^{18}\text{F}$ -AMT enters the tumor cells via LAT, which is the only system that can transport large neutral amino acids with aromatic rings[117]. LAT, especially its subtype LAT1, was reported to be highly expressed in many cancer cell lines and positively correlates with tumor growth[118, 135]. So far,  $^{18}\text{F}$ -AMT is the most suitable amino acid transporter-targeting radiotracer for tumor imaging, regardless of low synthesis yield and requirement of an on-site cyclotron to produce  $^{18}\text{F}$ .

Although PET has emerged as an advanced imaging tool for cancer diagnosis, only a limited number of facilities around the world can afford complete operation of PET and cyclotron for the local production of short-lived positron-emitting radionuclides such as  $^{11}\text{C}$  and  $^{18}\text{F}$ . Therefore, mature technologies, *i.e.* SPECT and its combination with CT, still play important and irreplaceable roles in nuclear

imaging area[15]. The most common radionuclide for SPECT is  $^{99m}\text{Tc}$  ( $t_{1/2}=6.02$  h), which is produced by an in-house generator and does not require the cyclotron[14]. Due to their similar chemistry, the diagnostic radioisotope  $^{99m}\text{Tc}$  and the therapeutic radioisotope  $^{188}\text{Re}$  could be labeled to the same ligand, which leads to the diagnostic/therapeutic matched pair. Unlike most of the cyclotron-produced radionuclides that utilize the covalent chemistry for labeling,  $^{99m}\text{Tc}$  requires a “chelator” to conjugate the radionuclide with the target ligand. The nitrogen, oxygen and sulfur combination have been shown to be stable chelators for  $^{99m}\text{Tc}$  such as  $\text{N}_4$  (e.g. DOTA, cyclam-14),  $\text{N}_3\text{S}$  (e.g. mercaptoacetyltriglycine),  $\text{N}_2\text{S}_2$  (e.g. ethylenedicycysteine diethyl ester),  $\text{NS}_3$ ,  $\text{S}_4$  (e.g. sulfur colloid), DTPA,  $\text{O}_2\text{S}_2$  (e.g. dimercaptosuccinic acid), and HYNIC[68, 101-105].

Here, we report the synthesis of precursor O-[3-(1,4,8,11-tetraazacyclotetradecan)-propyl]- $\alpha$ -methyl tyrosine ( $\text{N}_4$ -AMT) and its radiolabeling with  $^{99m}\text{Tc}$ . *In vitro* cellular uptake kinetics and planar scintigraphic imaging of  $^{99m}\text{Tc}$ - $\text{N}_4$ -AMT were also evaluated in breast cancer models.

## **II. Materials and methods**

### **Chemicals and Analysis**

All chemicals and sources used here were previously described in Chapter 2.

### **Synthesis of Precursor $\text{N}_4$ -AMT**

#### **a) $\alpha$ -Methyl tyrosine ethylester (Compound 2)**

Thionyl chloride (10 mL; 137.42 mmol) was added to a solution of  $\alpha$ -methyltyrosine **1** (10.00 g; 51.22 mmol) in anhydrous ethanol (60 mL) at 0 °C, and then heated at 78 °C for 4 h while stirring. After cooling, the volume of the reaction mixture was reduced to 20 mL, and then 10 mL of triethylamine was added into it. The mixture was poured into 100 mL of water and extracted with chloroform. The combined organic layers were dried over MgSO<sub>4</sub>. The desired compound was obtained as white solid. Yield: 9.00 g (40.32 mmol, 78.75 %). <sup>1</sup>H-NMR (CDCl<sub>3</sub>)  $\delta$  = 7.02 (d, 2H,  $J$  = 8.4 Hz), 6.70 (d, 2H,  $J$  = 8.4 Hz), 4.22 (dd, 2H,  $J$  = 7.2 Hz,  $J$  = 7.8 Hz), 3.14 (dd, 2H,  $J$  = 13.5 Hz,  $J$  = 13.5), 1.42 (s, 3H), 1.33 (t, 3H,  $J$  = 16.2 Hz) ppm. <sup>13</sup>C-NMR  $\delta$  = 175.47, 156.36, 130.66, 126.39, 114.87, 61.05, 58.65, 45.29, 24.08, 13.07 ppm, MS:  $m/z$  = 224.23 [M]<sup>+</sup>.

**b) *N*-t-Butoxycarbonyl- $\alpha$ -methyl tyrosine ethylester (Compound 3)**

Compound **2** (2.09 g; 9.36 mmol) was dissolved in 40 mL of anhydrous DMF under nitrogen, and treated with triethylamine (2.78 mL; 20 mmol) while stirring. Di-tert-butyl dicarbonate (3.27g; 15 mmol) was added to the reaction mixture and stirred over night at room temperature. The solvent was removed under reduced pressure to yield a residue, which was extracted with ethyl acetate and dried with anhydrous MgSO<sub>4</sub>. The extraction was filtered and evaporated to dryness to give yellow oil which was purified by loading on to a silica gel-packed column and eluted with hexane: ethyl acetate (5: 1.5 v/v). After evaporation of the solvent, yellow oil **3** was obtained. Yield: 2.00 g (6.18 mmol, 66.20 %). <sup>1</sup>H-NMR (CDCl<sub>3</sub>)  $\delta$  = 6.97 (d, 2H,  $J$  = 8.4 Hz), 6.75 (d, 2H,  $J$  = 8.7 Hz), 4.22 (dd, 2H,  $J$  = 2.7 Hz,  $J$  = 7.2 Hz), 3.32 (dd,



2H,  $J = 15.0$  Hz,  $J = 13.5$ ), 1.55 (s, 3H), 1.48 (s, 9H), 1.32 (t, 3H,  $J = 18.0$  Hz) ppm.  $^{13}\text{C}$ -NMR  $\delta = 174.16, 155.04, 154.51, 131.16, 128.50, 115.14, 77.25, 61.64, 60.54, 40.99, 28.39, 23.55, 14.77$  ppm, MS:  $m/z = 324.36$   $[\text{M}]^+$ .

**c) *N*-*t*-Butoxycarbonyl-*O*-[3-hydroxypropyl]- $\alpha$ -methyl tyrosine ethylester  
(Compound 4)**

Sodium metal (0.09 g; 14.02 mmol) was dissolved in 30 mL of anhydrous ethanol with stirring under nitrogen. Compound **3** (1.00 g; 3.09 mmol) was dissolved in 50 mL of anhydrous ethanol and treated with sodium ethoxide solution, and refluxed for 2.5 h at 70  $^{\circ}\text{C}$ . 3-Bromopropanol (0.56 mL; 6.18 mmol) was added into the reaction mixture, which was heated continuously over night. The ethanol was removed under reduced pressure and replaced with 40 mL of ethyl acetate. The solution was then washed with water and dried over  $\text{MgSO}_4$ . After removal of the solvent, the crude compound was purified by a silica gel-packed column and eluted with hexane/ ethylacetate (2/1), giving 0.83 g (2.17 mmol, 71 % yield) of the product as clear yellow oil.  $^1\text{H}$ -NMR ( $\text{CDCl}_3$ )  $\delta = 7.01$  (d, 2H,  $J = 6.3$  Hz), 6.81 (d, 2H,  $J = 6.6$  Hz), 4.20 (dd, 2H,  $J = 5.1$  Hz,  $J = 5.1$  Hz), 4.12 (t, 2H,  $J = 15.0$  Hz), 3.86 (t, 2H,  $J = 10.2$  Hz), 3.16 (dd,  $J = 13.5$  Hz,  $J = 12.9$  Hz), 2.06 (m, 2H), 1.54 (s, 3H), 1.47 (s, 9H), 1.31 (t, 3H,  $J = 12.3$  Hz) ppm.  $^{13}\text{C}$ -NMR  $\delta = 174.01, 171.91, 157.73, 154.35, 131.07, 128.65, 114.14, 79.39, 65.65, 61.54, 60.40, 60.24, 40.79, 32.01, 28.39, 23.58, 14.15$  ppm, MS:  $m/z = 381.033$   $[\text{M}]^+$ .

**d) *N*-*t*-Butoxycarbonyl-*O*-[3-*Br*-propyl]- $\alpha$ -methyl tyrosine ethylester**

**(Compound 5)**

A solution of **4** (5.44 g; 16.82 mmol) and 1,3- dibromopropane (136.74 g; 677.30 mmol) in 100 mL acetone was purged with nitrogen for 15 min. Potassium carbonate (22.62 g; 163.69 mmol) was added to the reaction mixture, the mixture was then refluxed for 12 h at 75 °C. After the removal of solvents and excessive reagents under reduced pressure, the residue was dissolved in chloroform, washed with water and dried over anhydrous magnesium sulfate. After filtration and solvent evaporation, yellow liquid was purified by a silica gel-packed flash column and eluted with hexane/ ethylacetate (2/1) to furnish compound **5** as pale yellow liquid. Yield: 4.80 g (7.52 mmol, 64.69 %). MS:  $m/z = 446.3$   $[M]^+$ .

**e) *N*<sup>1</sup>, *N*<sup>4</sup>-dioxylyl-1,4,8,11-tetraazabicyclotetradecane (*N*<sup>1</sup>,*N*<sup>4</sup>-cyclooxamide)**

**(Compound 6)**

N4 cyclam (15.00 g; 74.88 mmol) was dissolved in 150 mL of anhydrous ethanol, and then diethyl oxalate (10.94 g; 74.88 mmol) was added. The reaction mixture was refluxed 18 h at 75 °C. The solvent was evaporated and the crude product was recrystallized in acetone : ethanol to yield white crystals of *N*<sup>1</sup>,*N*<sup>4</sup>-dioxylyl-1,4,8,11-1,5,8,12-tetraazabicyclotetradecane (*N*<sup>1</sup>,*N*<sup>4</sup>-cyclooxamide) **6** . Yield: 13.64 g (17.31 mmol, 72.00 %). MS:  $m/z = 255.33$   $[M]^+$ .

**f)     *N*-t-Butoxycarbonyl-O-[3-( *N*<sup>1</sup>,*N*<sup>4</sup>-dioxylyl-1,4,8,11-tetraazabicyclotetradecane)-propyl]- $\alpha$ -methyl tyrosine ethylester (Compound 7)**

Compound **6** (1.00 g; 3.93 mmol) was dissolved in 20 mL of anhydrous DMF and treated with a solution of *N*-t-Butoxycarbonyl-O-[3-Br-propyl]- $\alpha$ -methyl tyrosine ethylester **5** (1.74 g; 3.93 mmol) in 40 mL of DMF under nitrogen atmosphere. The reaction mixture was heated to reflux for 18 h at 75 °C, and then allowed to cool down to room temperature. The solvent was removed *in vacuo*. The residue was dissolved in chloroform (30 mL), washed with water and 1M Na<sub>2</sub>CO<sub>3</sub>, (12 mL), and then separated for the organic layer. The organic layer was dried with anhydrous Magnesium sulfate, filtered and evaporated. The crude compound was purified by a silica gel-packed column and eluted with chloroform/ methanol (9/1). Yield: 1.00 g (1.63 mmol, 42.00 %). MS: *m/z* = 618.38 [M]<sup>+</sup>.

**g)     *O*-[3-(*N*<sup>1</sup>,*N*<sup>4</sup>-dioxylyl-1,4,8,11-tetraazabicyclotetradecane)-propyl]- $\alpha$ -methyltyrosine ethylester (Compound 8)**

Compound **7** (0.25 g; 0.40 mmol) was dissolved in dichloromethane (10 mL), and then trifluoroacetic acid (1.0 mL) was added to it. The solution was stirred over night at room temperature, and volatiles were removed *in vacuo*. The crude compound was purified by chromatography over silica gel (chloroform: methanol 9:1) as white solid. Yield: 0.20 g (0.39 mmol; 95.69 %). MS: *m/z* = 517.63 [M]<sup>+</sup>.

**h) *O*-[3-(1,4,8,11-tetraazabicyclohexadecane)-propyl]- $\alpha$ -methyl tyrosine (*N*<sub>4</sub>-AMT) (Compound 9)**

10N NaOH (2 mL) was added to a solution of compound **8** (0.20 g; 0.39 mmol), which was dissolved in 5 mL of water. The reaction mixture was stirred and refluxed over night at 90 °C. The solvent was evaporated under vacuum, giving white solid, which was dissolved in 5 mL of water and neutralized with 5N HCl solution to pH = 7. It was lyophilized and obtained as white solid. The solid was stirred in 25 mL anhydrous methanol. After filtration and solvent evaporation, white solid was obtained. Yield: 0.20 g (0.46 mmol: 99.0 %). MS:  $m/z = 436.327$  [M]<sup>+</sup>.

**Radiolabeling of N<sub>4</sub>-AMT with <sup>99m</sup>Tc**

N<sub>4</sub>-AMT (1 mg) was dissolved in 0.2 mL sterile water, followed by adding tin (II) chloride (0.1 mL, 1 mg/mL). Required amount of Na<sup>99m</sup>TcO<sub>4</sub> was added to N<sub>4</sub>-AMT solution. Radiochemical purity was determined by radio-HPLC (Waters, Milford, MA), eluted with acetonitrile: water (7:3) using a flow rate of 0.5 mL/min.

**Determination of the Partition Coefficient**

To determine the lipophilicity, 20  $\mu$ L of <sup>99m</sup>Tc-N<sub>4</sub>-AMT was added into an equal volume mixture of 1-octanol and sterile water in a centrifuge tube. The mixture was vortexed at room temperature for 1 min and then centrifuged at 5000 rpm for 5 min. From each phase, 0.1 mL of the aliquot was taken out and the radioactivity was measured by gamma counter (Cobra Quantum; Packard, MN). The measurement was repeated for three times, and care was taken to avoid cross contamination

between the phases. The partition coefficient value, expressed as logP, was calculated using the following equation:

$$\text{LogP} = \text{Log} (\text{radioactivity in 1-octanol layer} / \text{radioactivity in sterile water layer})$$

### ***In Vitro* Cellular Uptake Studies**

Rat breast tumor cell line 13762 (American Type Culture Collection, Rockville, MD) was selected and the same cell line was used to create the animal model for *in vivo* evaluation. Cells were maintained in Dulbecco's modified Eagle's medium and nutrient mixture F-12 Ham (DMEM/F12; GIBCO, Grand Island, NY) at 37 °C in a humidified atmosphere containing 5% CO<sub>2</sub>. Cells were plated onto 6-well tissue culture plates (2x10<sup>5</sup> cells/well) and incubated with <sup>99m</sup>Tc-N4-AMT (0.05 mg/well, 8 uCi/well), <sup>99m</sup>Tc-N4 (0.025 mg/well, 8 uCi/well) or <sup>18</sup>F-FDG (8 uCi/well) for 0-4 h. After incubation, cells were washed with ice-cold PBS twice and detached by treating them with 0.5 mL of trypsin for 5 min. Cells were then collected and the radioactivity was measured with gamma counter (Cobra Quantum; Packard, MN). Data were expressed in mean ±S.D. percent of cellular uptake (%Uptake) in triplicate.

### ***In Vitro* Competitive Inhibition Study**

To investigate the transport mechanisms of <sup>99m</sup>Tc-N4-AMT, the competitive inhibition study using L-tyrosine was conducted. The 13762 rat breast tumor cells were co-incubated with <sup>99m</sup>Tc-N4-AMT (8 µg/well, 8 µCi/well) and L-tyrosine for up to 1 h. A set of concentrations of L-tyrosine (10-1000x of the N4-AMT concentration)

were used. After incubation, cells were washed with ice-cold PBS twice and detached by treating them with 0.5 mL of trypsin for 5 min. Cells were then collected and the radioactivity was measured by gamma counter. Data were expressed in mean  $\pm$ S.D. percent of cellular uptake (%Uptake) in triplicate.

### **Blood Clearance**

All animal work was carried out in the Small Animal Imaging Facility (SAIF) at UTMDACC under a protocol approved by Institutional Animal Care and Use Committee (IACUC). For blood clearance analysis, three normal female Fischer 344 rats ( $150\pm 25$  g) (Harlan Sprague-Dawley, Indianapolis, IN) were intravenously injected with 30  $\mu$ Ci  $^{99m}\text{Tc}$ -N4-AMT. Blood samples were drawn through lateral tail vein at several time-points from 5 min to 24 h ( $n=3/\text{rat}$ ) by microliter pipettes (10  $\mu$ L). The blood samples were measured for radioactivity by gamma counter, and then were calculated as percentage of the injected dose per gram of blood (%ID/g).

### ***In vivo* Tissue Distribution Studies**

Tissue distribution studies of  $^{99m}\text{Tc}$ -N4-AMT (study I,  $n=9$ ) and  $^{18}\text{F}$ -FDG (study II,  $n=9$ ) were conducted by using normal female Fischer 344 rats ( $150\pm 25$  g,  $n=18$ ). For each compound, the rats were divided into three groups for three time intervals (0.5, 2, 4 h for  $^{99m}\text{Tc}$ -N4-AMT; 0.5, 1, 2 h for  $^{18}\text{F}$ -FDG;  $n=3/\text{time point}$ ). The injection activity was  $25\pm 0.5$   $\mu$ Ci/rat intravenously. At each time interval, the rats were sacrificed, and the selected tissues were excised, weighed and measured for radioactivity by gamma counter. Each sample was calculated as percentage of the

injected dose per gram of tissue wet weight (%ID/g). Counts from a diluted sample of the original injection were used as reference.

### **Planar Scintigraphic Imaging Study**

Female Fischer 344 rats were inoculated subcutaneously with 0.1 mL of breast tumor cells 13762 suspension in PBS ( $10^5$  cells/rat) into the right legs. Planar scintigraphic imaging of  $^{99m}\text{Tc}$ -N4-AMT was performed 12-14 days after inoculation when tumors reached approximately 1 cm in diameter. Planar scintigraphic images were obtained using M-CAM (Siemens Medical Solutions, Hoffman Estates, IL) equipped with a Low Energy High Resolution collimator. Anesthetized breast tumor-bearing rats were injected intravenously with  $^{99m}\text{Tc}$ -N4-AMT (0.3 mg/rat, 300  $\mu\text{Ci}$ /rat; n=3). The images were acquired up to 4 h post-administration of tracers. Computer outlined regions of interest (ROIs in counts per pixel) between tumor and muscle were used to calculate tumor/muscle (T/M) ratios. Percentage of the injected dose (%ID) of tumor was also calculated from the reference standard, which was 1/10 of the original injection activity.

### ***In Vivo* Uptake Blocking Study**

To ascertain whether  $^{99m}\text{Tc}$ -N4-AMT uptake is mediated specifically by LAT, *in vivo* blocking studies using the unlabeled L-Tyrosine as the competitive inhibitor was conducted. The same animal model used in the planar scintigraphic imaging study was employed. Unlabeled L-Tyrosine (50 mg/kg) dissolved in 0.3 mL saline (pH adjusted to 2-3) was administered intravenously to mammary tumor-bearing

rats 1 h prior to  $^{99m}\text{Tc}$ -N4-AMT injection. Planar scintigraphic images were acquired up to 4 h, and ROIs of liver, kidneys, tumor, and muscle were used to calculate the ratios of liver/muscle, kidney/muscle, and tumor/muscle, respectively. In addition, %IDs of liver, kidneys, tumor, and muscle were calculated from the reference standard, which was 1/10 of the original injection activity. The results were compared with those from the rats injected with  $^{99m}\text{Tc}$ -N4-AMT alone (control).

### **Tumor and Inflammation Uptake Comparison *In Vivo***

To investigate whether  $^{99m}\text{Tc}$ -N4-AMT can differentiate tumor from the inflammatory tissue, a rat model bearing both mammary tumor and turpentine oil-induced inflammation was created. 13762 rat mammary tumor cells ( $10^5$  cells/0.1 mL PBS/rat) were inoculated into the right calf muscles of the female Fischer 344 rats. After the tumors reached to 1 cm in diameter, turpentine oil (0.1 mL/rat) was injected into the left calf muscles of the rats to induce inflammation. The anesthetized rats (n=3) were injected intravenously with  $^{99m}\text{Tc}$ -N4-AMT 24 h after the turpentine injection. Planar scintigraphic images were acquired up to 4 h, and ROIs of tumor, inflammation, and muscle were used to calculate the tumor-to-muscle ratios (T/Ms), inflammation-to-muscle ratios (I/Ms), and tumor-to-inflammation ratios (T/Is), respectively. Same animal model was used to evaluate  $^{18}\text{F}$ -FDG. Micro-PET imaging of  $^{18}\text{F}$ -FDG was performed using R4 micro-PET scanner (Concorde Microsystems, TN). The rats were injected intravenously with  $^{18}\text{F}$ -FDG (500 uCi/rat, n=3), and dynamic PET scans were obtained for 90 min with a spatial resolution of 2.2 mm. PET images were reconstructed by using the



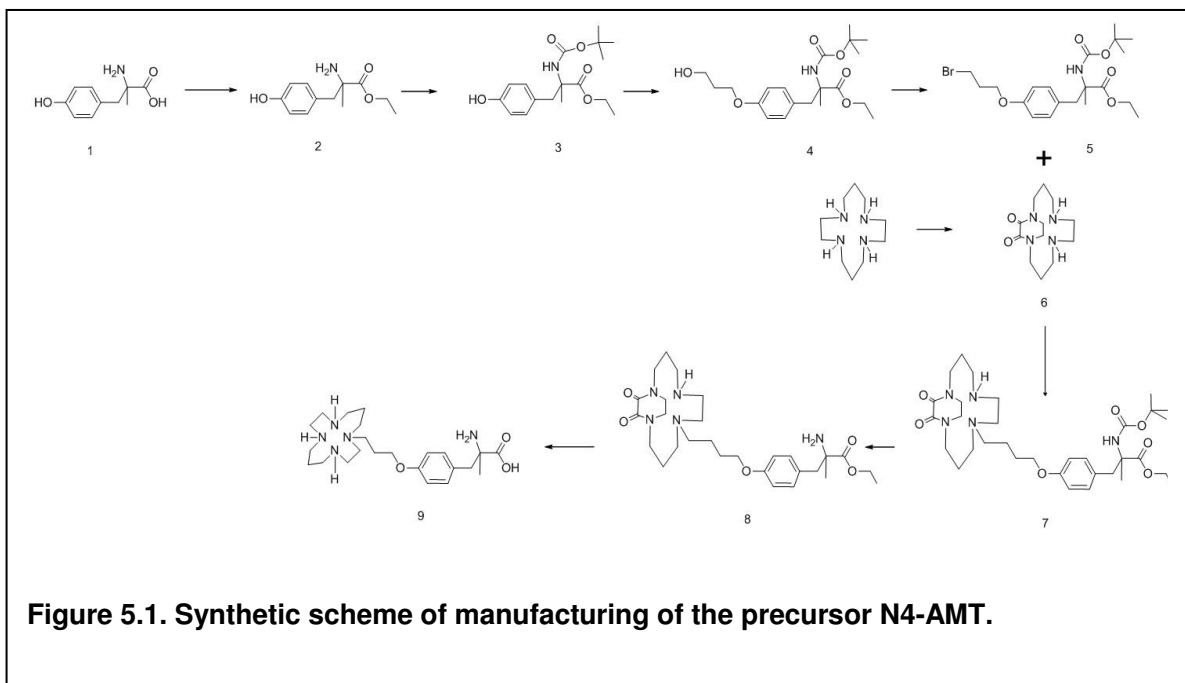
ordered subset expectation maximization (OSEM) algorithm. T/Ms, I/Ms and T/Is ratios were calculated based on the regional radioactivity concentrations ( $\mu\text{Ci}/\text{cm}^3$ ) that were estimated from the average pixels within ROIs drawn around the tumor, inflammation or muscle on transverse slices of the reconstructed image sets.

### III. Results

#### Chemistry and Radiochemistry

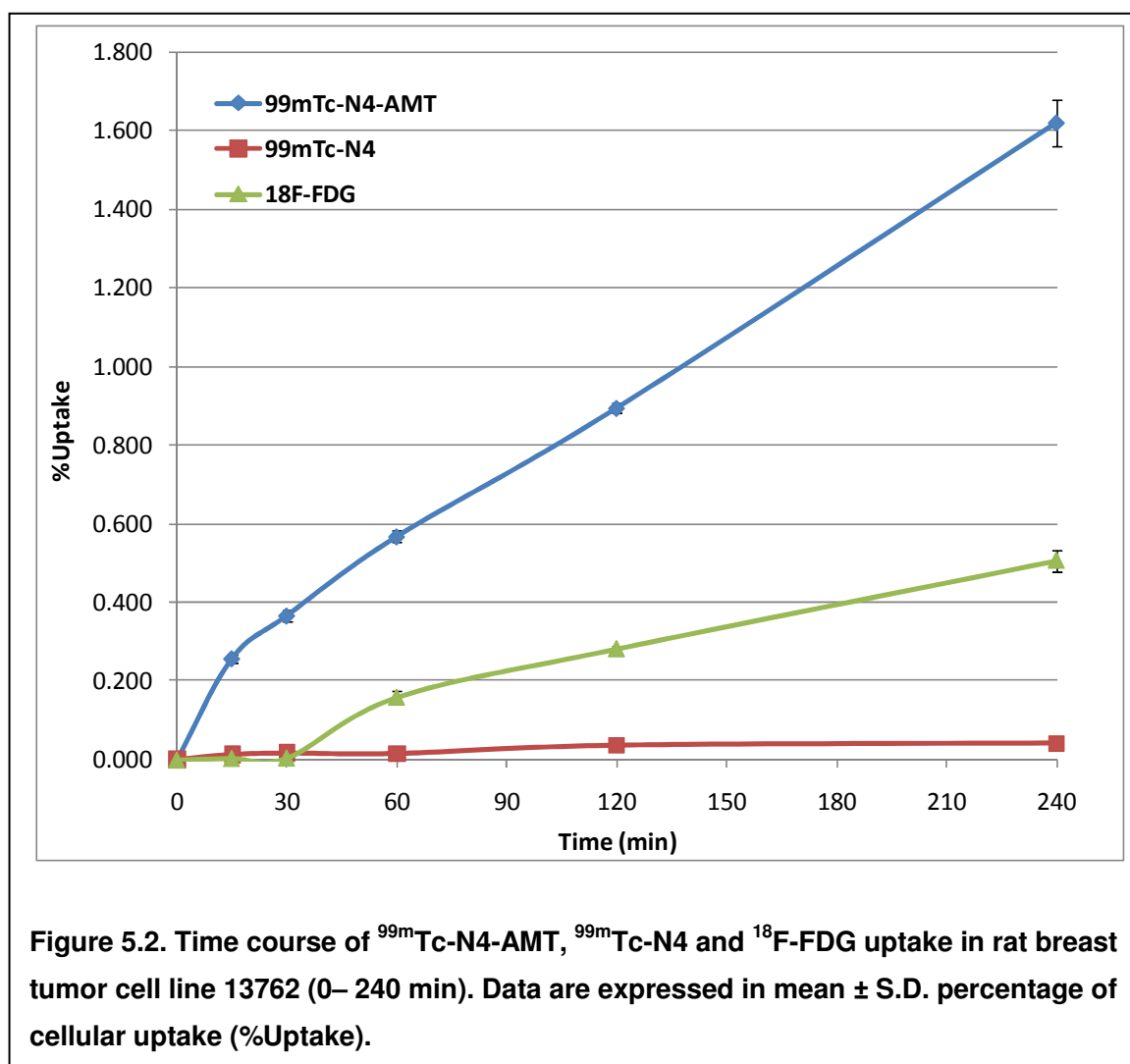
Precursor N4-AMT was synthesized via an eight-step procedure and the total synthesis yield was 14%. The synthetic scheme is shown in Fig.5.1. The structure and purity of N4-AMT was confirmed by  $^1\text{H}$ - and  $^{13}\text{C}$ - NMR, mass spectra, and HPLC. For N4-AMT, the  $^1\text{H}$ - and  $^{13}\text{C}$ -NMR results were  $^1\text{H}$  NMR ( $\text{D}_2\text{O}$ )  $\delta$  = 7.21 (d, 2H, J = 9.00 Hz), 7.00 (d, 2H, J = 9.00 Hz), 4.14 (t, 2H, J = 12.0 Hz), 3.10 (m, 5H), 2.94 (m, 2H), 2.84 (m, 13H), 1.95 (m, 6H), 1.33 (s, 3H) ppm.  $^{13}\text{C}$  NMR  $\delta$  = 180.69, 163.42, 163.16, 162.88, 162.60, , 157.06, 131.40, 129.19, 117.57, 115.26, 115.10, 112.93, 66.25, 60.73, 53.69, 51.46, 49.88, 49.26, 48.04, 47.84, 46.60, 45.42, 45.07, 43.94, 24.71, 24.32, 23.62, 22.55 ppm.

Precursor N4-AMT was labeled with  $^{99\text{m}}\text{Tc}$  successfully in a high radiochemical purity (>96%). For HPLC, the retention time of  $^{99\text{m}}\text{Tc}$ -N4-AMT was 6.899 min. The logP of  $^{99\text{m}}\text{Tc}$ -N4-AMT was  $-1.42 \pm 0.169$ .



### ***In Vitro* Cellular Uptake Studies**

The cellular uptake kinetics of  $^{99m}\text{Tc-N4-AMT}$ ,  $^{99m}\text{Tc-N4}$ , and  $^{18}\text{F-FDG}$  in rat breast tumor cells is shown in Fig. 5.2. There was a drastically increased uptake for  $^{99m}\text{Tc-N4-AMT}$  at 15-240 min, but not for  $^{99m}\text{Tc-N4}$  chelator itself, which suggested that  $^{99m}\text{Tc-N4-AMT}$  can enter and accumulate into tumor cells rapidly and specifically. In addition, the %Uptake of  $^{99m}\text{Tc-N4-AMT}$  was much higher than that of  $^{18}\text{F-FDG}$ .



### Competitive Inhibition Study of $^{99m}\text{Tc}$ -N4-AMT

After incubated with L-tyrosine at 10-1000 times as high as the concentrations of N4-AMT, 13762 cells showed a significant decrease in  $^{99m}\text{Tc}$ -N4-AMT uptake only at the 150- and 200-time concentrations (Fig. 5.3). These results indicate that  $^{99m}\text{Tc}$ -N4-AMT and L-tyrosine may be transported via the same transporter system LAT; however, LAT may not be the only transport route for  $^{99m}\text{Tc}$ -N4-AMT.

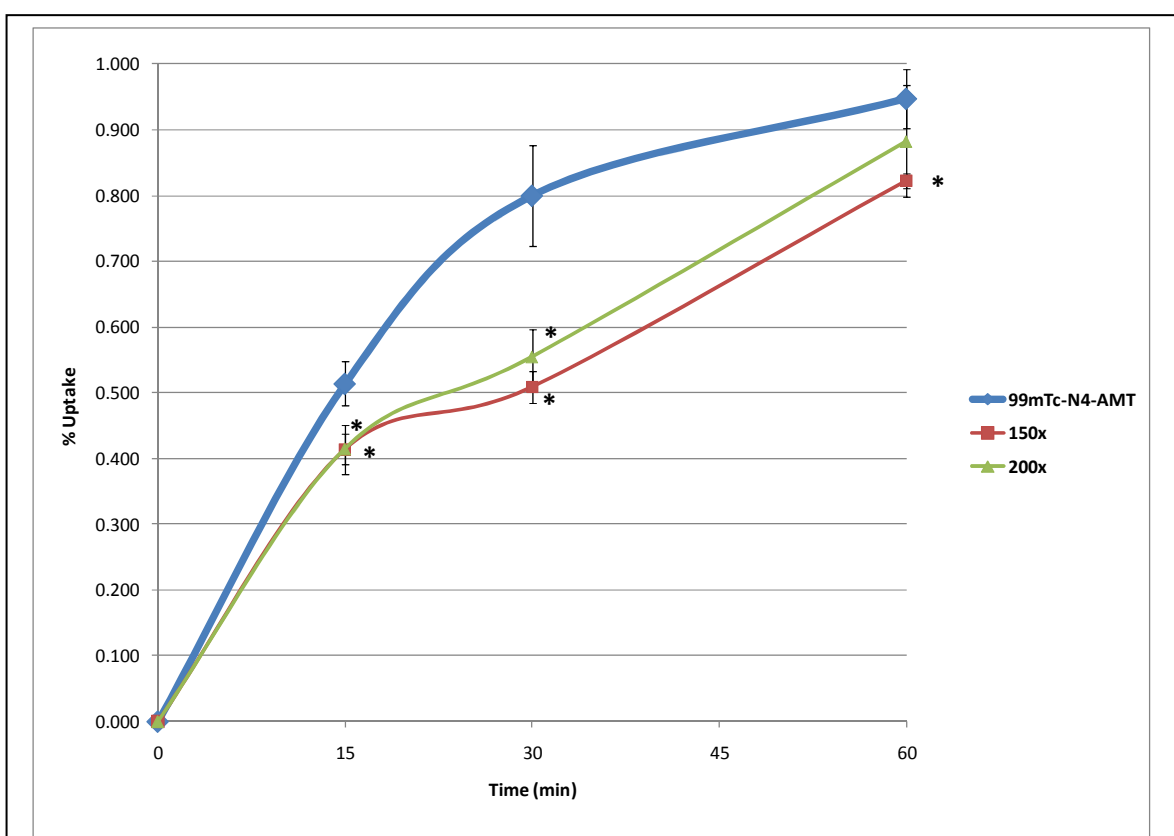
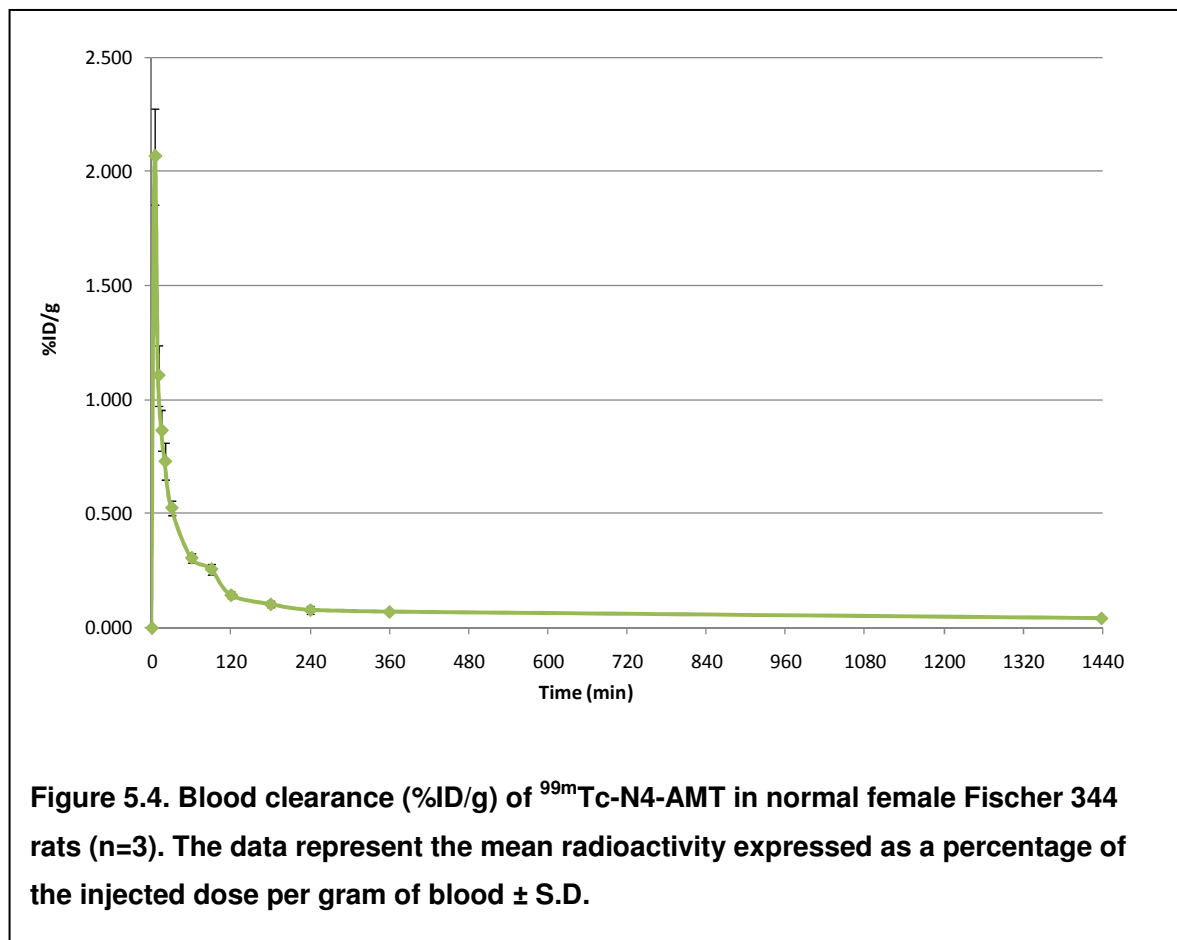


**Figure 5.3. Competitive inhibition uptake of  $^{99m}\text{Tc}$ -N4-AMT by L-tyrosine in rat breast tumor cell line 13762 up to 1 h. A set of concentrations of L-tyrosine [150X and 200X of N4-AMT concentration (8 mg/well)] were used. Data are expressed in mean  $\pm$  S.D. percentage of cellular uptake (%Uptake).**

## Blood Clearance

The blood clearance curve for  $^{99m}\text{Tc}$ -N4-AMT in normal Fischer 344 rats (n=3) is shown in Fig. 5.4. The plasma half-life of the distribution phase ( $t_{1/2 \alpha}$ ) was  $10.71 \pm 0.794$  min, while that of the elimination phase ( $t_{1/2 \beta}$ ) was  $99.32 \pm 5.182$  min.



### ***In Vivo* Tissue Distribution Studies**

The tissue distribution results of  $^{99m}\text{Tc}$ -N4-AMT and  $^{18}\text{F}$ -FDG in the normal Fischer 344 rats are shown in Tables 5.1 and 5.2, respectively. Low thyroid and stomach uptake of  $^{99m}\text{Tc}$ -N4-AMT was observed, suggesting its high *in vivo* stability.

**Table 5.1. Biodistribution of  $^{99m}\text{Tc}$ -N4-AMT in normal Fischer 344 female rats.**

<b>%ID/g</b>	<b>30 MIN</b>	<b>120 MIN</b>	<b>240 MIN</b>
<b>blood</b>	0.74 $\pm$ 0.024	0.28 $\pm$ 0.010	0.18 $\pm$ 0.008
<b>heart</b>	0.18 $\pm$ 0.013	0.08 $\pm$ 0.006	0.05 $\pm$ 0.003
<b>lung</b>	0.44 $\pm$ 0.029	0.22 $\pm$ 0.004	0.13 $\pm$ 0.008
<b>thyroid</b>	0.57 $\pm$ 0.040	0.31 $\pm$ 0.015	0.24 $\pm$ 0.012
<b>pancreas</b>	0.18 $\pm$ 0.006	0.09 $\pm$ 0.005	0.06 $\pm$ 0.002
<b>liver</b>	1.40 $\pm$ 0.077	0.83 $\pm$ 0.045	0.60 $\pm$ 0.023
<b>spleen</b>	0.24 $\pm$ 0.004	0.19 $\pm$ 0.002	0.18 $\pm$ 0.011
<b>kidney</b>	5.77 $\pm$ 0.355	5.32 $\pm$ 0.180	4.74 $\pm$ 0.332
<b>stomach</b>	0.50 $\pm$ 0.029	0.42 $\pm$ 0.031	0.43 $\pm$ 0.026
<b>intestine</b>	0.33 $\pm$ 0.019	0.18 $\pm$ 0.010	0.13 $\pm$ 0.006
<b>muscle</b>	0.09 $\pm$ 0.007	0.03 $\pm$ 0.002	0.02 $\pm$ 0.001
<b>bone &amp; joint</b>	0.27 $\pm$ 0.061	0.11 $\pm$ 0.006	0.06 $\pm$ 0.003
<b>brain</b>	0.03 $\pm$ 0.005	0.01 $\pm$ 0.001	0.01 $\pm$ 0.000

Each rat received  $^{99m}\text{Tc}$ -N4-AMT (25  $\mu\text{Ci}$ , intravenously). Each value is percent of injected dose per gram weight (n= 3)/time interval. Each data represents mean of three measurements with standard deviation.

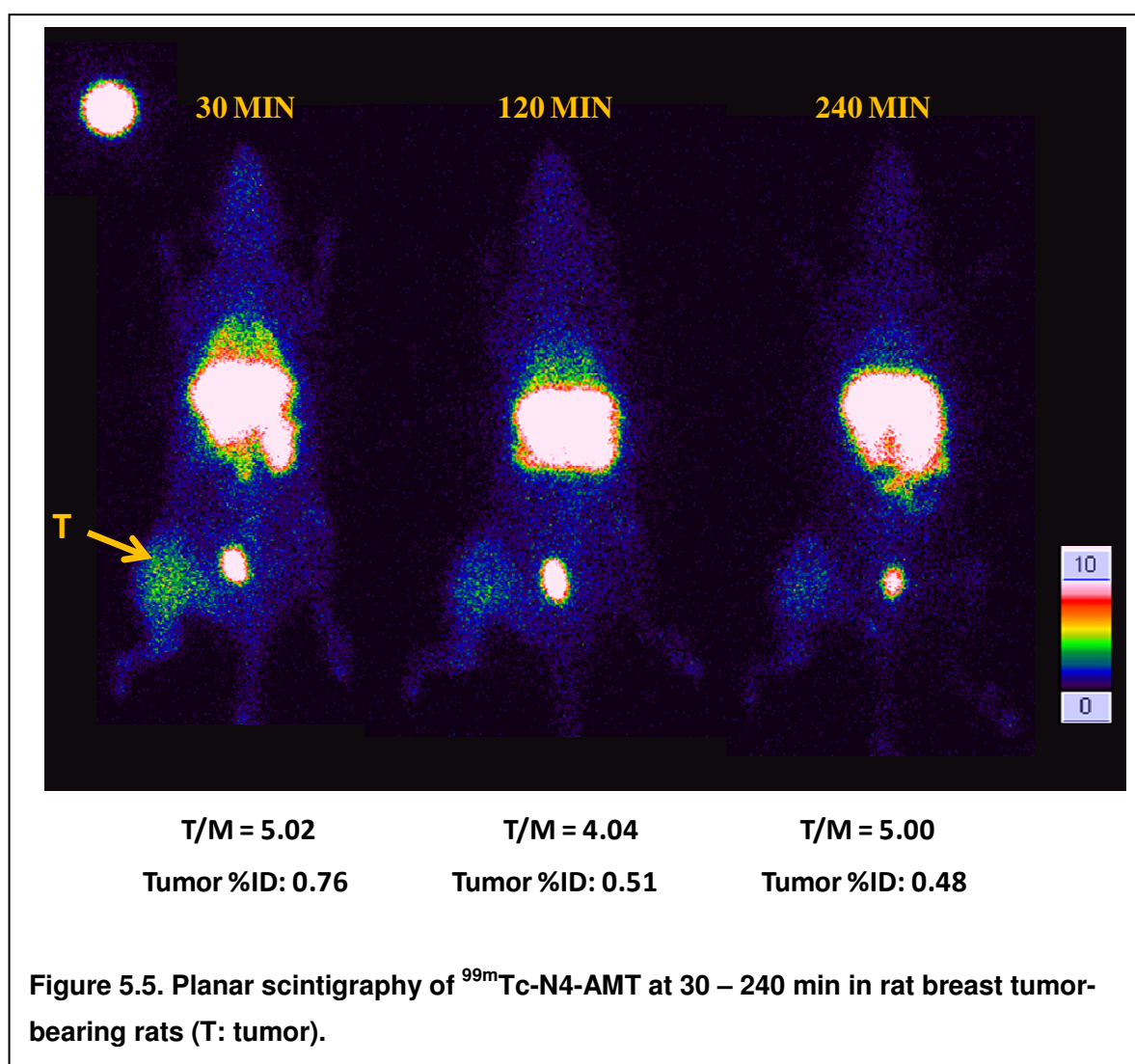
**Table 5.2. Biodistribution of  $^{18}\text{F}$ -FDG in normal Fischer 344 female rats.**

<b>%ID/g</b>	<b>30 MIN</b>	<b>60 MIN</b>	<b>120 MIN</b>
blood	0.40±0.042	0.13±0.006	0.06±0.002
heart	1.57±0.056	1.38±0.126	1.08±0.068
lung	0.55±0.056	0.42±0.024	0.46±0.027
thyroid	1.07±0.080	1.04±0.040	1.05±0.069
pancreas	0.26±0.028	0.21±0.006	0.20±0.016
liver	0.40±0.048	0.16±0.006	0.13±0.012
spleen	0.82±0.081	0.74±0.032	0.86±0.071
kidney	0.71±0.051	0.37±0.012	0.24±0.018
stomach	0.61±0.078	0.44±0.031	0.39±0.030
intestine	0.69±0.068	0.53±0.035	0.52±0.025
muscle	0.33±0.040	0.34±0.027	0.74±0.024
bone& joint	0.33±0.036	0.44±0.065	0.50±0.034
brain	2.00±0.149	1.99±0.046	1.39±0.086

Each rat received  $^{18}\text{F}$ -FDG (25  $\mu\text{Ci}$ , intravenously). Each value is percent of injected dose per gram weight (n =3)/time interval. Each data represents mean of three measurements with standard deviation.

## Planar Scintigraphic Imaging Study

The representative planar scintigraphic images of  $^{99m}\text{Tc}$ -N4-AMT at 30 min, 2h, and 4 h in breast tumor-bearing rats are shown in Fig. 5.5. Tumors were clearly detected by  $^{99m}\text{Tc}$ -N4-AMT at all time-points. The T/M ratios at 30 min, 2h, and 4 h were 5.02, 4.04, and 5.00, respectively. Tumor %IDs at these three time-points were 0.76%, 0.51%, and 0.48%, respectively (Fig. 5.5).





## ***In Vivo* Uptake Blocking Study**

The liver, kidneys, tumor, and muscle %IDs of  $^{99m}\text{Tc}$ -N4-AMT, as well as the ratios of these organs to muscle before and after *in vivo* blocking by unlabeled L-Tyrosine were listed in Table 5.3 and 5.4. By using the blocking agent L-Tyrosine,  $^{99m}\text{Tc}$ -N4-AMT uptake in liver, kidney, and tumor decreased significantly at all time-points. Muscle uptake also decreased at the 30 min time-point, which may due to the blood flow effect. These results suggest that  $^{99m}\text{Tc}$ -N4-AMT utilizes the same transport system LAT as L-Tyrosine does *in vivo*.

**Table 5.3. Percentage of injected dose (%ID) of selected organs before and after *in vivo* blocking of  $^{99m}\text{Tc}$ -N4-AMT by unlabeled L-Tyrosine in mammary tumor-bearing rats. Red font indicates the decreased %ID when compared to the corresponding control group. Blue shading indicates  $P < 0.05$  when compared to the corresponding control group (n=3/group/time interval).**

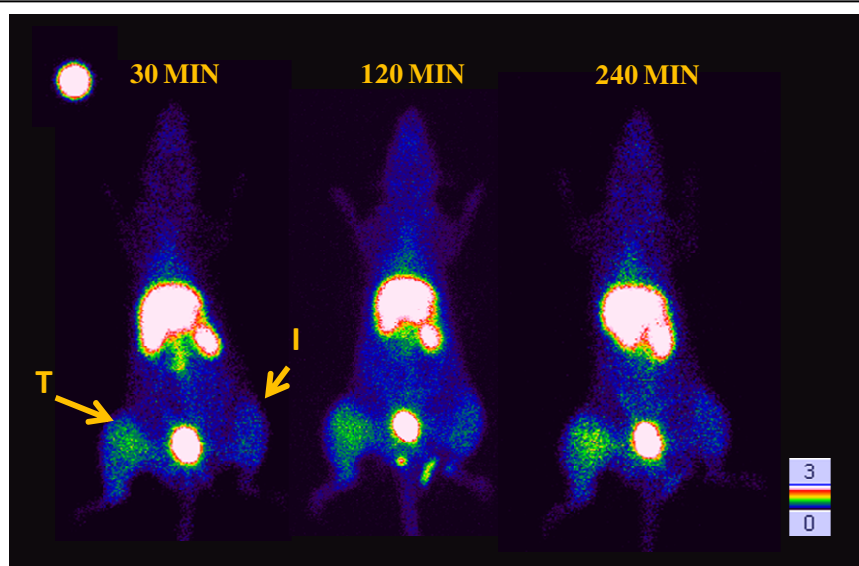
%ID	30 min			2 hr			4hr		
	Control	Block	Decrease	Control	Block	Decrease	Control	Block	Decrease
Liver	7.63±0.47	6.31±0.18	17.30%	5.12±0.24	4.40±0.33	14.06%	4.49±0.32	3.39±0.09	24.50%
Kidney	5.81±0.35	4.62±0.45	20.48%	4.26±0.25	3.32±0.14	22.07%	4.35±0.33	3.05±0.16	29.89%
Tumor	2.71±0.22	1.63±0.05	39.85%	0.84±0.05	0.43±0.04	48.81%	0.55±0.04	0.37±0.02	32.73%
Muscle	0.58±0.11	0.42±0.04	27.59%	0.11±0.02	0.11±0.04	0.00%	0.077±0.005	0.082±0.012	-6.49%

**Table 5.4. Selected organ to muscle ratios before and after *in vivo* blocking of <sup>99m</sup>Tc-N4-AMT by unlabeled L-Tyrosine in mammary tumor-bearing rats. Red font indicates the decreased %ID when compared to the corresponding control group. Blue shading indicates P<0.05 when compared to the corresponding control group (n=3/group/time interval).**

Ratio	30 min			2 hr			4hr		
	Control	Block	Decrease	Control	Block	Decrease	Control	Block	Decrease
Liver/Muscle	13.1±0.5	15.1±0.4	-15.27%	45.6±1.5	41.1±2.1	9.87%	58.0±2.3	41.1±2.2	29.14%
Kidney/Muscle	9.96±0.49	11.0±0.53	-10.24%	38.0±1.3	31.1±2.4	18.16%	56.1±1.3	37.0±0.3	34.05%
Tumor/Muscle	4.65±0.28	3.89±0.1	16.34%	7.48±0.34	4.03±0.16	46.12%	7.12±0.35	4.55±0.27	36.10%

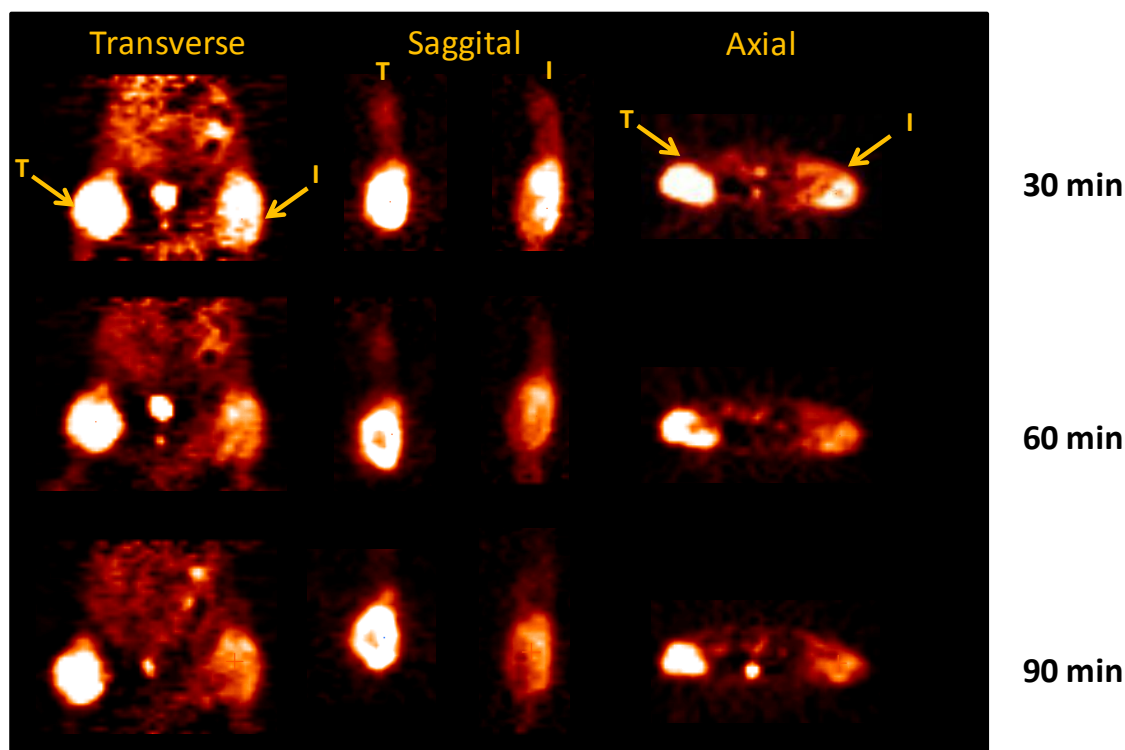
### Tumor and Inflammation Uptake Comparison *In Vivo*

The representative planar scintigraphic images of  $^{99m}\text{Tc}$ -N4-AMT, as well as the micro-PET images of  $^{18}\text{F}$ -FDG in breast tumor and inflammation-bearing rats are shown in Fig. 5.6 and Fig. 5.7, respectively. The T/M of  $^{99m}\text{Tc}$ -N4-AMT at each time-point was much higher than I/M. Although T/I at all time-points were above 1, which indicated that tumor had higher uptake than the inflammation site, the ratios were similar to those of  $^{18}\text{F}$ -FDG. Therefore, these results suggested that  $^{99m}\text{Tc}$ -N4-AMT was not superior to  $^{18}\text{F}$ -FDG in differentiating tumor from inflammation.



	30 min	2 hr	4 hr
T/M	4.49	5.59	5.15
I/M	2.95	3.47	2.71
T/I	1.52	1.61	1.90

**Figure 5.6.** Planar scintigraphic images of  $^{99m}\text{Tc}$ -N4-AMT at 30 – 240 min in rat breast tumor and inflammation-bearing rats (T: tumor, I: inflammation). The tumor-to-muscle ratios (T/Ms), inflammation-to-muscle ratios (I/Ms), and tumor-to-inflammation ratios (T/Is) are listed below the figure.



	30 min	60 min	90 min
T/M	5.88	7.54	4.90
I/M	3.43	3.77	2.72
T/I	1.71	1.99	1.80

**Figure 5.7. microPET images of  $^{18}\text{F}$ -FDG at 30 – 90 min in rat breast tumor and inflammation-bearing rats (T: tumor, I: inflammation). The tumor-to-muscle ratios (T/Ms), inflammation-to-muscle ratios (I/Ms), and tumor-to-inflammation ratios (T/Is) are listed below the figure.**

## IV. Discussion

The present study investigated the imaging capability of  $^{99m}\text{Tc}$ -N<sub>4</sub>-AMT in breast tumor models *in vitro* and *in vivo*. For chemical synthesis, the precursor N<sub>4</sub>-AMT was synthesized via an eight-step procedure (Fig. 5.1). Commercially available  $\alpha$ -methyl tyrosine **1** was converted into corresponding acid chloride, then to ethyl ester by reacting with thionyl chloride in ethanol. The amine in  $\alpha$ -methyl tyrosine ethyl ester **2** was protected as its Boc-derivative N-t-butoxycarbonyl- $\alpha$ -methyl tyrosine ethylester **3** with triethylamine and di-t-butyldicarbonate in DMF. The chain at the -OH group was extended when compound **3** was treated with 1, 3-dibromopropane and obtained as N-t-butoxycarbonyl-O-[3-bromopropyl]- $\alpha$ -methyl tyrosine ethylester **4**. Acylation of 1,4,8,11-tetraazacyclo-tetradecane (N<sub>4</sub> cyclam) with diethyloxalate led to N<sup>1</sup>,N<sup>4</sup>-dioxalyl 1,4,8,11-tetraazacyclotetradecane (N<sup>1</sup>,N<sup>4</sup>-cyclamoxamide) **5**. Under SN<sup>2</sup> condition **4** and **5** were efficiently converted to alkylated compound N-t-butoxycarbonyl-O-[3-(N<sup>1</sup>,N<sup>4</sup>-dioxalyl-1,4,8,11-tetraazacyclotetradecane)-propyl]- $\alpha$ -methyl tyrosine ethylester **6**. Exposure of **6** to trifluoroacetic acid in CH<sub>2</sub>Cl<sub>2</sub> caused qualitative de-t-butoxycarboxylation to yield O-[3-(N<sup>1</sup>, N<sup>4</sup>-dioxalyl 1,4,8,11-tetraazacyclotetradecane)-propyl]- $\alpha$ -methyl tyrosine ethylester **7**. 10 N NaOH in water at 75 °C promoted the hydrolysis of ester to acid and a simultaneous deoxalation of **7** to yield the final compound O-[3-(1,4,8,11-tetraazacyclotetradecan)-propyl]- $\alpha$ -methyl tyrosine (N<sub>4</sub>-AMT) **8**. The total synthesis yield was 14%, which can be adapted to industrial manufacturing. The structure and purity of the compounds at each step were validated by <sup>1</sup>H- and <sup>13</sup>C- NMR, mass spectra, and HPLC. Precursor N<sub>4</sub>-AMT could be labeled with  $^{99m}\text{Tc}$  successfully in

a high radiochemical purity (>96%). Given that  $^{99m}\text{Tc}$ -N4-AMT is a kit-product and labeled without any further purification, the radiochemical yield was assumed to be identical to its radiochemical purity.

In cellular uptake study,  $^{99m}\text{Tc}$ -N4-AMT was taken up rapidly by rat mammary tumor cells, and the %Uptake of  $^{99m}\text{Tc}$ -N4-AMT was significantly higher than that of the chelator  $^{99m}\text{Tc}$ -N4, suggesting its high specificity in tumor uptake. Besides,  $^{99m}\text{Tc}$ -N4-AMT has much more uptake than  $^{18}\text{F}$ -FDG in this *in vitro* breast cancer model. In competitive inhibition study,  $^{99m}\text{Tc}$ -N4-AMT uptake could be significantly inhibited by L-tyrosine only at the 150- and 200-time concentrations, which indicates that  $^{99m}\text{Tc}$ -N4-AMT and L-tyrosine may be transported via the same transporter system LAT; however, LAT may not be the only transport route for  $^{99m}\text{Tc}$ -N4-AMT. To further investigate other transport routes, different types of amino acid transporter inhibitors need to be tested in order to block the  $^{99m}\text{Tc}$ -N4-AMT uptake in this breast cancer cell line in future.

For *in vivo* evaluation,  $^{99m}\text{Tc}$ -N4-AMT had a relatively fast blood clearance in normal Fischer 344 rats (Fig. 5.4). Biodistribution study showed that  $^{99m}\text{Tc}$ -N4-AMT had a favorable distribution pattern in normal rats (Table 5.1). The two major organs for  $^{99m}\text{Tc}$ -N4-AMT metabolism are kidneys and liver. In planar imaging studies shown in Fig. 5.5, tumors were clearly detected by  $^{99m}\text{Tc}$ -N4-AMT at all time-points. Although its T/Ms were relatively high, the tumor %IDs were lower than that of other  $^{99m}\text{Tc}$ -labeled tyrosine derivatives we developed previously. To ascertain whether  $^{99m}\text{Tc}$ -N4-AMT uptake is mediated specifically by LAT, we then conducted the *in vivo* uptake blocking studies using the unlabeled L-Tyrosine as the competitive

inhibitor (Table 5.3 and 5.4). Upon blocking,  $^{99m}\text{Tc}$ -N4-AMT uptake in liver, kidney, and tumor decreased significantly at all time-points. Although muscle uptake also decreased at the 30 min time-point, the decreasing rate was not statistically significant and it may be due to the blood flow effect. These results suggest that  $^{99m}\text{Tc}$ -N4-AMT may utilize the same transport system LAT as L-Tyrosine does *in vivo*. To test whether  $^{99m}\text{Tc}$ -N4-AMT can distinguish tumor from inflammatory tissues, we have established a rat model bearing both mammary tumor and turpentine oil-induced inflammation. Although T/Is at all time-points were above 1, which indicated that tumor had higher uptake than the inflammation site, the ratios were similar to those of  $^{18}\text{F}$ -FDG. Nevertheless, since the uptake in inflammatory tissue was caused by blood flow effect, T/I ratios of  $^{99m}\text{Tc}$ -N4-AMT increased by time. Therefore,  $^{99m}\text{Tc}$ -N4-AMT may be able to distinguish tumor from inflammation in a later time-point by taking the advantage of using the long half-life radioisotope  $^{99m}\text{Tc}$ . In addition, we may need to test  $^{99m}\text{Tc}$ -N4-AMT in another animal model using radiation to induce inflammation in future so it can more similarly mimic the patients undergoing radiation therapy.

In conclusion, efficient synthesis of N4-AMT was achieved. *In vitro* cellular uptake and *in vivo* imaging findings collectively suggest that  $^{99m}\text{Tc}$ -N4-AMT is a potential radiotracer for breast cancer imaging. In compliance with the chelating capability of N4, N4-AMT could be labeled with positron emitting radionuclides such as Gallium-68 or with short-ranged beta emitters for internal radiotherapeutic purposes hereafter.

## CHAPTER 6 Overview: comparison of $^{99m}\text{Tc}$ -labeled Tyrosine-based radiotracers in breast cancer imaging

In this dissertation, four  $^{99m}\text{Tc}$ -labeled tyrosine derivatives have been synthesized and evaluated *in vitro* and *in vivo* for their imaging potential in breast cancer models (Fig. 6.1). The detailed methods and results of the synthesis and evaluation of each radiotracer have already been stated in Chapter 2-5. The studies designed for each specific aim were listed in Table 6.1. Here, we will compare these four radiotracers and score them as 1 to 4. Score 1 indicates the best compound and score 4 is the worst compound for each study. Therefore, the compound with the least score will be the best radiotracer for imaging breast cancer modeled here overall.

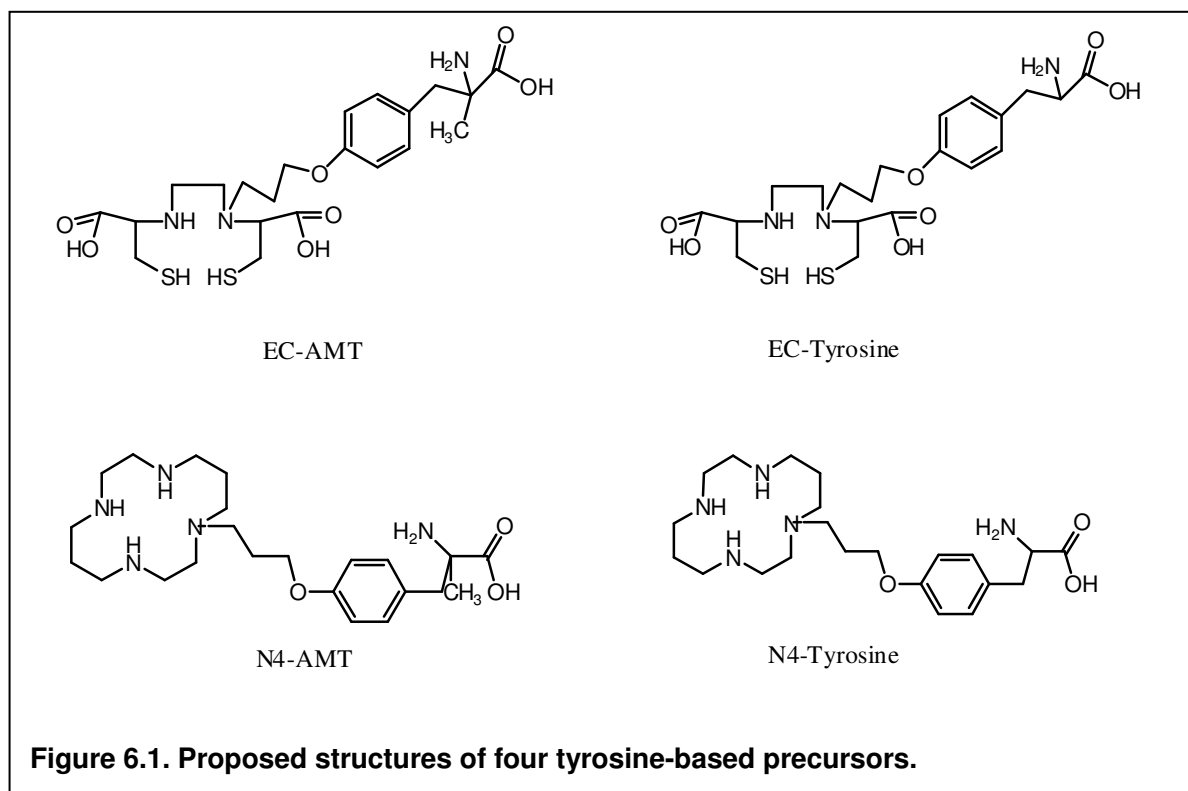




**Table 6.1. The studies designed to synthesize and evaluate four radiotracers.**

	EC-AMT	EC-Tyrosine	N4-AMT	N4-Tyrosine
SA1	Precursor Synthesis			
	<sup>99m</sup> Tc Labeling			
	Partition Coefficient			
SA2	Uptake Kinetics			
	Competitive Inhibition using L-Tyrosine			
SA3	Blood Clearance			
	Biodistribution			
	Planar Imaging (breast cancer model)			
	Planar Imaging ( <i>in vivo</i> blocking)			
	Planar Imaging (breast cancer vs. inflammation model)			

## I. Specific Aim 1

Table 6.2 summarized the chemical synthesis of four precursors. Since N-*t*-Butoxycarbonyl-L-tyrosine methyl ester, the starting material of the protected Br-tyrosine compound was commercially available; the required synthetic steps of EC-Tyrosine and N4-Tyrosine were fewer than those of their  $\alpha$ -methyl derivatives, hence, the overall synthetic yields were much higher than EC-AMT and N4-AMT, respectively. As shown in Table 6.2, the best compound with fewest synthesis steps and highest synthetic yield was EC-Tyrosine. Nevertheless, the other three compounds also had acceptable synthetic yield.

When label the precursors with  $^{99m}\text{Tc}$ , the radiochemical purity of four compounds was all above 95%. Since they are kit-products and labeled without any further purification, the radiochemical yield is assumed to be identical to their radiochemical purity. However, EC seemed to have better chelation ability with  $^{99m}\text{Tc}$  than N4 because EC-AMT and EC-Tyrosine can be labeled with  $^{99m}\text{Tc}$  using lesser physical amount than their N4 counterpart.

**Table 6.2. Summary of the chemical synthesis of four precursors.**

	Synthesis Steps	Overall Yield
EC-AMT	5	23%
EC-Tyrosine	3	80%
N4-AMT	8	14%
N4-Tyrosine	5	38%

The partition coefficient values (logPs) of four radiotracers were listed in Table 6.3. Since all four compounds are small molecule, the compound with higher lipophilicity is preferred because they will have better chance to be slowly washed out from body than the compound with lower lipophilicity. Based on the results,  $^{99m}\text{Tc}$ -EC-AMT had highest lipophilicity and therefore was the best compound among these four radiotracers. As expected, the logPs of tyrosine-based radiotracers were lower than those of their  $\alpha$ -methyl derivatives. As we know, the lower logP indicates the lower lipophilicity of the compound. The result verified our hypothesis that the lipophilicity of tyrosine-based radiotracer could be increased by adding a methyl group on its  $\alpha$ -carbon. In addition, we found that EC-chelated radiotracers had higher lipophilicity than their N4 counterpart. When we compared lipophilicity of chelator EC and N4 using ChemBioDraw Ultra 12.0 software (CambridgeSoft Corporation, Cambridge, MA), the same result was presented. The logP of precursor EC was -1.05 whereas that of N4 was -1.3. Although it contains

two hydrophilic carboxylic groups, the higher logP of EC may be due to its two lipophilic thiol groups.

**Table 6.3. The partition coefficient value (logP) of four radiotracers at pH=5-6 (n=6).**

	<sup>99m</sup> Tc-EC-AMT	<sup>99m</sup> Tc-EC-Tyrosine	<sup>99m</sup> Tc-N4-AMT	<sup>99m</sup> Tc-N4-Tyrosine
LogP	-1.14±0.072	-2.02±0.168	-1.42±0.169	-2.83±0.082

Table 6.4 summarizes the conclusion for Specific Aim 1. From the chemical point of view, EC-chelated compounds tied for the first place, which suggests that both EC-chelated compounds have more favorable chemical characteristics than N4-chelated compounds.

**Table 6.4. Conclusion of Specific Aim 1. Score 1 indicates the best compound, and score 4 indicates the worst compound.**

		EC-AMT	EC-Tyrosine	N4-AMT	N4-Tyrosine
SA1	Precursor Synthesis	3	1	4	2
	<sup>99m</sup> Tc Labeling	1	1	2	2
	Partition Coefficient	1	3	2	4
Conclusions		1	1	2	2

## II. Specific Aim 2

Specific Aim 2 was to investigate the uptake kinetics and transport mechanisms of  $^{99m}\text{Tc}$ -labeled tyrosine/AMT-based radiotracer in rat mammary tumor cell line 13762. This is a well-documented cell line for established *in vivo* rat mammary tumor model, as well as for the rat model carrying both tumor and inflammation employed in differential diagnostic studies. In addition, since we were evaluating the compounds using planar scintigraphic imaging, rat model would provide better imaging quality than mouse model in terms of resolution.

Fig. 6.2 demonstrates the cellular uptake kinetics of all four  $^{99m}\text{Tc}$ -labeled tyrosine-based compounds in comparison with that of  $^{18}\text{F}$ -FDG. All four radiotracers were taken up rapidly by rat mammary tumor cells and had much higher %Uptake than that of  $^{18}\text{F}$ -FDG, suggesting their higher imaging potentials than  $^{18}\text{F}$ -FDG *in vitro*.

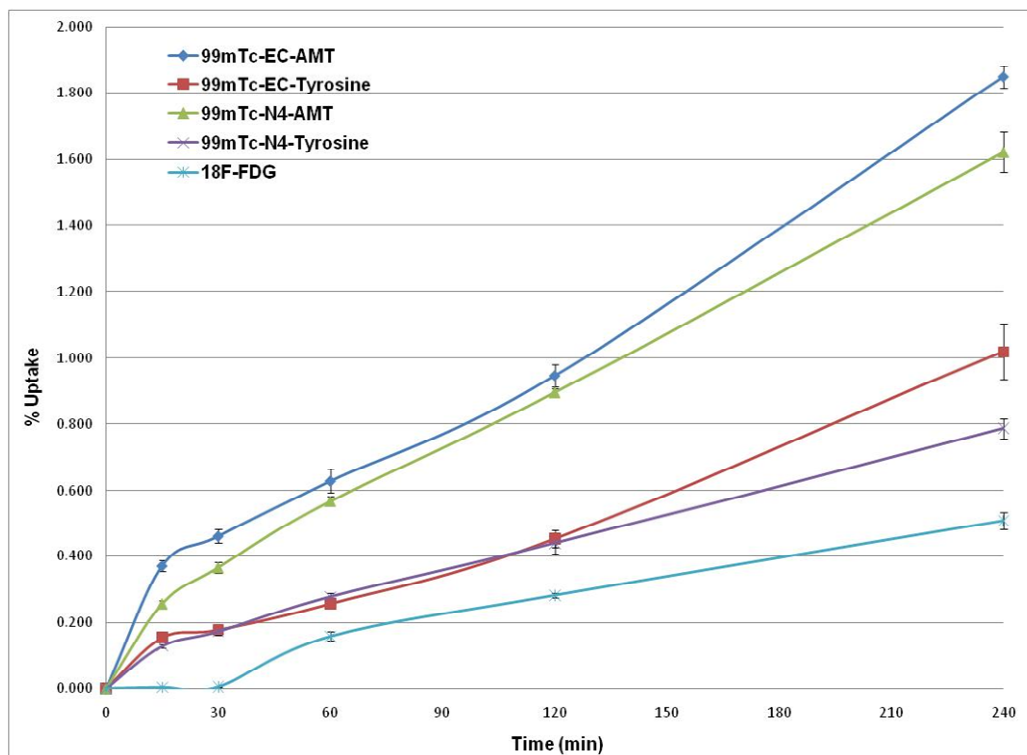


**Figure 6.2. Time course of  $^{99m}\text{Tc}$ -labeled four radiotracers and  $^{18}\text{F}$ -FDG uptake in rat breast tumor cell line 13762 (0– 240 min). Data are expressed in mean  $\pm$  S.D. percentage of cellular uptake (%Uptake).**

In competitive inhibition study using the same cell line, the uptake of both  $^{99m}\text{Tc}$ -EC-AMT and  $^{99m}\text{Tc}$ -EC-Tyrosine could be blocked by L-Tyrosine from 10-time concentration, whereas that of  $^{99m}\text{Tc}$ -N4-AMT could only be blocked at 150- and 200-time concentrations of precursor. For  $^{99m}\text{Tc}$ -N4-Tyrosine, the uptake could not be inhibited at any concentration and the uptake even increased by adding unlabeled L-Tyrosine. Taken together, these findings suggest that  $^{99m}\text{Tc}$ -EC-labeled compounds most likely share the same transport mechanism as L-Tyrosine, which is predominantly transported via LAT system. For  $^{99m}\text{Tc}$ -N4-labeled compounds, they most likely do not use LAT as a major transport system.

Table 6.5 summarizes the conclusion for Specific Aim 2. When evaluating these four compounds in breast cancer cell line,  $^{99m}\text{Tc}$ -EC-AMT shows the most favorable characteristics *in vitro*.

**Table 6.5. Conclusion of Specific Aim 2. Score 1 indicates the best compound, and score 4 indicates the worst compound.**

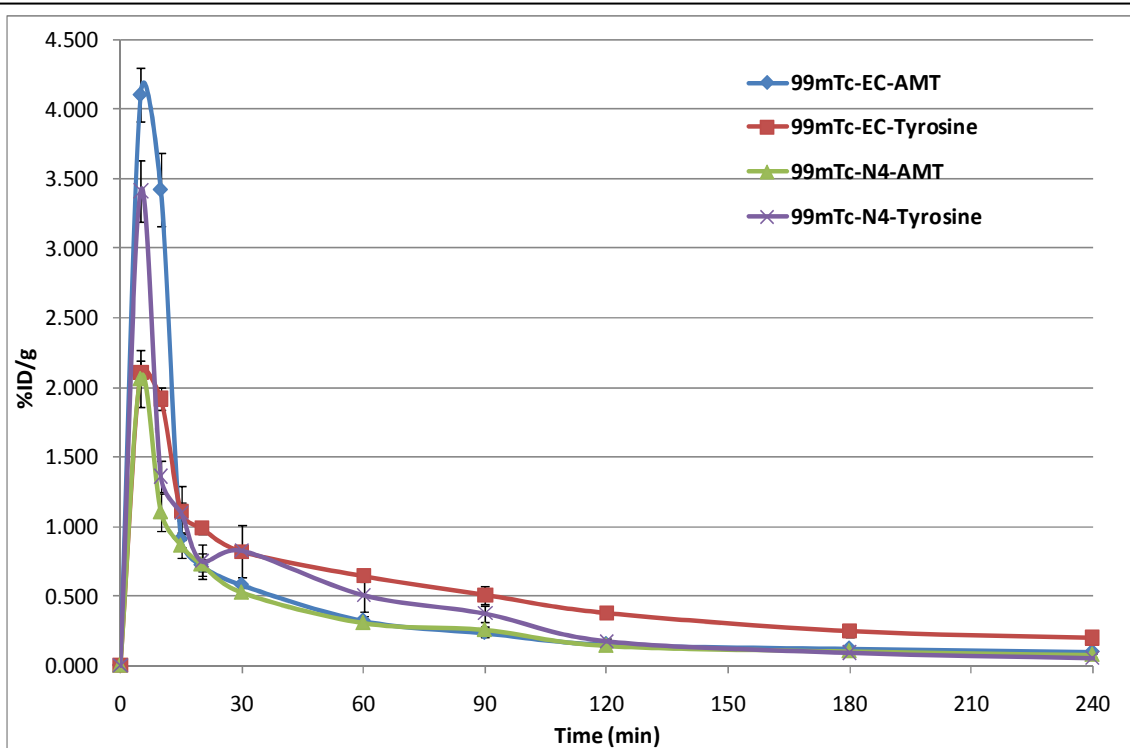
		EC-AMT	EC-Tyrosine	N4-AMT	N4-Tyrosine
SA2	Uptake Kinetics	1	3	2	4
	Competitive Inhibition using L-Tyrosine	1	1	2	3
Conclusions		1	2	2	3

### III. Specific Aim 3

Specific Aim 3 was to assess the kinetics of  $^{99m}\text{Tc}$ -labeled tyrosine/AMT-based radiotracer accumulation in tumor and inflammation tissues in mammary tumor-bearing rat model. The rat tumor model was created using the same rat mammary tumor cell line as in the *in vitro* evaluation.

All four radiotracers had relatively rapid blood clearance in normal Fischer 344 rats (Fig. 6.3). Among them,  $^{99m}\text{Tc}$ -N4-Tyrosine had the fastest clearance for both distribution phase ( $T_{1/2} \alpha = 9.31 \pm 0.759$  min) and excretion phase ( $T_{1/2} \beta = 90.14 \pm 1.901$  min), whereas  $^{99m}\text{Tc}$ -EC-Tyrosine had the slowest but still acceptable clearance for both distribution phase ( $T_{1/2} \alpha = 13.68 \pm 1.067$  min) and excretion phase ( $T_{1/2} \beta = 117.51 \pm 5.727$  min).





Time (min)	$^{99m}\text{Tc-EC-AMT}$	$^{99m}\text{Tc-EC-Tyrosine}$	$^{99m}\text{Tc-N4-AMT}$	$^{99m}\text{Tc-N4-Tyrosine}$
$T_{1/2} \alpha$	$9.41 \pm 0.202$	$13.68 \pm 1.067$	$10.71 \pm 0.794$	$9.31 \pm 0.759$
$T_{1/2} \beta$	$98.75 \pm 5.377$	$117.51 \pm 5.727$	$99.32 \pm 5.182$	$90.14 \pm 1.901$

**Figure 6.3. Blood clearance (%ID/g) of four  $^{99m}\text{Tc}$ -labeled radiotracers in normal female Fischer 344 rats up to 240 min (n=3). The data represent the mean radioactivity expressed as a percentage of the injected dose per gram of blood  $\pm$  S.D.**

For biodistribution study, all four radiotracers had high *in vivo* stability in normal Fischer 344 rats. High kidney uptakes of all compounds were observed up to 4 hr, indicating that the kidneys are the major organ for metabolism and excretion of these compounds. The high kidney uptake, nevertheless, could be blocked by intravenously administration of unlabeled L-Tyrosine, which suggested that the four radiotracers may utilize the same metabolism and excretion route as L-Tyrosine does in rat kidneys.

In planar imaging studies, mammary tumors were clearly detected by all radiotracers up to 4 hr.  $^{99m}\text{Tc}$ -EC-AMT had the highest T/M ratios, and due to the washout of non-specific uptake, the T/M ratios increased by time. Therefore,  $^{99m}\text{Tc}$ -EC-AMT is the best compound for imaging mammary tumor in this rat model. The T/M ratios of the other three compounds also ranged from 4 to 5, and were promising for tumor imaging, however,  $^{99m}\text{Tc}$ -N4-AMT may have the least potential because its low tumor %ID.

To ascertain whether the radiotracers uptakes are mediated specifically by amino acid transporter system LAT, we conducted the *in vivo* uptake blocking studies using the unlabeled L-Tyrosine as the competitive inhibitor. Except for  $^{99m}\text{Tc}$ -N4-Tyrosine, all other three compounds were confirmed to transport via the same LAT system as unlabeled L-Tyrosine does. These findings were consistent with the *in vitro* competitive inhibition results. Since the lipophilicity of  $^{99m}\text{Tc}$ -N4-Tyrosine was much lower in comparison with the other three compounds, it was possible that N4-Tyrosine was under some conformational changes when be labeled with  $^{99m}\text{Tc}$ . Thus,  $^{99m}\text{Tc}$ -N4-Tyrosine could not be recognized as an amino

acid and then to be transported via LAT system. In order to test this hypothesis, we need to synthesize the cold reference standard Re-N4-Tyrosine and study its crystalline structure to confirm the binding site of rhenium in the future.

To test whether the radiotracers could differentiate breast tumor from inflammation, we performed tumor and inflammation uptake comparison study *in vivo*. All radiotracers other than  $^{99m}\text{Tc}$ -EC-AMT had tumor-to-inflammation (T/I) ratio above 1, which indicated that tumor had higher radiotracer uptake than inflammatory site. However, when compared with the clinical gold standard  $^{18}\text{F}$ -FDG, only  $^{99m}\text{Tc}$ -EC-Tyrosine had better T/Is up to 4 hr. Therefore, we conclude that  $^{99m}\text{Tc}$ -EC-Tyrosine is the most suitable compound for in differentiating tumor from inflammatory sites.

Table 6.6 summarizes the conclusion for Specific Aim 3. When evaluating these four compounds *in vivo*,  $^{99m}\text{Tc}$ -EC-AMT shows the most favorable characteristics overall. However,  $^{99m}\text{Tc}$ -EC-Tyrosine will be the most suitable candidate for differential diagnosis of tumor from inflammation.

**Table 6.6. Conclusion of Specific Aim 3. Score 1 indicates the best compound, and score 4 indicates the worst compound.**

		EC-AMT	EC-Tyrosine	N4-AMT	N4-Tyrosine
SA3	Blood Clearance	2	4	3	1
	Biodistribution	2	3	1	3
	Planar Imaging (breast cancer model)	1	2	4	2
	Planar Imaging (in vivo blocking)	1	2	1	3
	Planar Imaging (breast cancer vs. inflammation model)	4	1	2	3
Conclusions		1	3	2	3

#### **IV. Conclusions and Future Directions**

In conclusion, four tyrosine and AMT-based precursors have been successfully synthesized and radiolabeled with  $^{99m}\text{Tc}$ . Table 6.7 summarizes the final conclusions of the whole project. Base on the score system, we conclude that  $^{99m}\text{Tc}$ -EC-AMT is the most suitable radiotracer for breast cancer imaging overall, however,  $^{99m}\text{Tc}$ -EC-Tyrosine will be a more preferential choice for differential diagnosis of tumor from inflammation.

In the future, we will use  $^{99m}\text{Tc}$ -EC-Tyrosine to evaluate the treatment response of anti-cancer drugs or radiation therapy since it showed impressive capability to distinguish the actual tumors from treatment-induced inflammation. In addition, we will label these four precursors with gallium-68 and investigate their imaging potentials in breast cancer imaging using PET or PET/CT. Furthermore, we would like to label precursor EC-AMT with therapeutic radioisotope rhenium-188 or yttrium-90 for cancer treatment given its high tumor accumulation (tumor %ID) and T/M ratios.

**Table 6.7. Final conclusions of the dissertation. Score 1 indicates the best compound, and score 4 indicates the worst compound.**

		EC-AMT	EC-Tyrosine	N4-AMT	N4-Tyrosine
SA1	Precursor Synthesis	3	1	4	2
	<sup>99m</sup> Tc Labeling	1	1	2	2
	Partition Coefficient	1	3	2	4
SA2	Uptake Kinetics	1	3	2	4
	Competitive Inhibition using L-Tyrosine	1	1	2	3
SA3	Blood Clearance	2	4	3	1
	Biodistribution	2	3	1	3
	Planar Imaging (breast cancer model)	1	2	4	2
	Planar Imaging (in vivo blocking)	1	2	1	3
	Planar Imaging (breast cancer vs. inflammation model)	4	1	2	3
Conclusions		1	2	3	4

## BIBLIOGRAPHY

1. American Cancer Society. 2010. Breast Cancer Facts & Figures 2009-2010. American Cancer Society.
2. Buerkle, A., and W. A. Weber. 2008. Imaging of tumor glucose utilization with positron emission tomography. *Cancer Metastasis Rev* 27:545-554.
3. Jonson, S. D., and M. J. Welch. 1998. PET imaging of breast cancer with fluorine-18 radiolabeled estrogens and progestins. *Q J Nucl Med* 42:8-17.
4. Wijns, W., and P. G. Camici. 1997. The value of quantitative myocardial perfusion imaging with positron emission tomography in coronary artery disease. *Herz* 22:87-95.
5. DeNardo, S. J. 2005. Radioimmunodetection and therapy of breast cancer. *Semin Nucl Med* 35:143-151.
6. Buck, A. K., H. Schirrmeister, T. Mattfeldt, and S. N. Reske. 2004. Biological characterisation of breast cancer by means of PET. *Eur J Nucl Med Mol Imaging* 31 Suppl 1:S80-87.
7. Lim, H. S., W. Yoon, T. W. Chung, J. K. Kim, J. G. Park, H. K. Kang, H. S. Bom, and J. H. Yoon. 2007. FDG PET/CT for the detection and evaluation of breast diseases: usefulness and limitations. *Radiographics* 27 Suppl 1:S197-213.
8. Misra, S., N. L. Solomon, F. L. Moffat, and L. G. Koniaris. 2010. Screening criteria for breast cancer. *Adv Surg* 44:87-100.
9. Aukema, T. S., E. J. Rutgers, W. V. Vogel, H. J. Teertstra, H. S. Oldenburg, M. T. Vrancken Peeters, J. Wesseling, N. S. Russell, and R. A. Valdes Olmos. 2010.

The role of FDG PET/CT in patients with locoregional breast cancer recurrence: a comparison to conventional imaging techniques. *Eur J Surg Oncol* 36:387-392.

10. Mahner, S., S. Schirrmacher, W. Brenner, L. Jenicke, C. R. Habermann, N. Avril, and J. Dose-Schwarz. 2008. Comparison between positron emission tomography using 2-[fluorine-18]fluoro-2-deoxy-D-glucose, conventional imaging and computed tomography for staging of breast cancer. *Ann Oncol* 19:1249-1254.

11. Schirrmeister, H. 2007. Detection of bone metastases in breast cancer by positron emission tomography. *Radiol Clin North Am* 45:669-676, vi.

12. Tseng, J., L. K. Dunnwald, E. K. Schubert, J. M. Link, S. Minoshima, M. Muzi, and D. A. Mankoff. 2004. <sup>18</sup>F-FDG kinetics in locally advanced breast cancer: correlation with tumor blood flow and changes in response to neoadjuvant chemotherapy. *J Nucl Med* 45:1829-1837.

13. Benard, F., and E. Turcotte. 2005. Imaging in breast cancer: Single-photon computed tomography and positron-emission tomography. *Breast Cancer Res* 7:153-162.

14. Schechter, N. R., D. J. Yang, A. Azhdarinia, and M. Chanda. 2007. Technologies for translational imaging using generators in oncology. *Recent Pat Anticancer Drug Discov* 2:251-258.

15. Mariani, G., L. Bruselli, and A. Duatti. 2008. Is PET always an advantage versus planar and SPECT imaging? *Eur J Nucl Med Mol Imaging* 35:1560-1565.

16. Filippi, L., A. Pulcini, S. Remediani, E. Masci, A. Redler, F. Scopinaro, and G. De Vincentis. 2006. Usefulness of scintimammography with tc-99m MIBI in clinical practice. *Clin Nucl Med* 31:761-763.

17. Aktolun, C., H. Bayhan, and M. Kir. 1992. Clinical experience with Tc-99m MIBI imaging in patients with malignant tumors. Preliminary results and comparison with Tl-201. *Clin Nucl Med* 17:171-176.
18. Scopinaro, F., O. Schillaci, M. Scarpini, P. L. Mingazzini, L. Di Macio, M. Banci, R. Danieli, M. Zerilli, M. R. Limiti, and A. Centi Colella. 1994. Technetium-99m sestamibi: an indicator of breast cancer invasiveness. *Eur J Nucl Med* 21:984-987.
19. Liberman, M., F. Sampalis, D. S. Mulder, and J. S. Sampalis. 2003. Breast cancer diagnosis by scintimammography: a meta-analysis and review of the literature. *Breast Cancer Res Treat* 80:115-126.
20. Kim, I. J., Y. T. Bae, S. J. Kim, Y. K. Kim, D. S. Kim, and J. S. Lee. 2006. Determination and prediction of P-glycoprotein and multidrug-resistance-related protein expression in breast cancer with double-phase technetium-99m sestamibi scintimammography. Visual and quantitative analyses. *Oncology* 70:403-410.
21. Cayre, A., F. Cachin, J. Maublant, D. Mestas, V. Feillel, J. P. Ferriere, F. Kwiaktowski, S. Chevillard, F. Finat-Duclos, P. Verrelle, and F. Penault-Llorca. 2002. Single static view 99mTc-sestamibi scintimammography predicts response to neoadjuvant chemotherapy and is related to MDR expression. *Int J Oncol* 20:1049-1055.
22. Taillefer, R. 2005. Clinical applications of 99mTc-sestamibi scintimammography. *Semin Nucl Med* 35:100-115.
23. Hruska, C. B., J. C. Boughey, S. W. Phillips, D. J. Rhodes, D. L. Wahner-Roedler, D. H. Whaley, A. C. Degnim, and M. K. O'Connor. 2008. Scientific Impact



Recognition Award: Molecular breast imaging: a review of the Mayo Clinic experience. *Am J Surg* 196:470-476.

24. Ferrara, A. 2010. Nuclear imaging in breast cancer. *Radiol Technol* 81:233-246.

25. SHIKANO N, K. N., ISHIKAWA N 2002 Molecular biology of L-type amino acid transporters. *Acta Scientiarum Valetudinariae Universitatis Praefecturae Ibarakiensis* VOL.7;NO.;PAGE.21-32(2002)

26. Johnstone, R. M., and P. G. Scholefield. 1965. Amino acid transport in tumor cells. *Adv Cancer Res* 9:143-226.

27. Souba, W. W., and A. J. Pacitti. 1992. How amino acids get into cells: mechanisms, models, menus, and mediators. *JPEN J Parenter Enteral Nutr* 16:569-578.

28. Christensen, H. N. 1990. Role of amino acid transport and countertransport in nutrition and metabolism. *Physiol Rev* 70:43-77.

29. Busch, H., J. R. Davis, G. R. Honig, D. C. Anderson, P. V. Nair, and W. L. Nyhan. 1959. The uptake of a variety of amino acids into nuclear proteins of tumors and other tissues. *Cancer Res* 19:1030-1039.

30. Isselbacher, K. J. 1972. Sugar and amino acid transport by cells in culture--differences between normal and malignant cells. *N Engl J Med* 286:929-933.

31. Ganapathy, V., M. Thangaraju, and P. D. Prasad. 2009. Nutrient transporters in cancer: relevance to Warburg hypothesis and beyond. *Pharmacol Ther* 121:29-40.

32. Jager, P. L., W. Vaalburg, J. Pruim, E. G. de Vries, K. J. Langen, and D. A. Piers. 2001. Radiolabeled amino acids: basic aspects and clinical applications in oncology. *J Nucl Med* 42:432-445.
33. Langen, K. J., and S. Broer. 2004. Molecular transport mechanisms of radiolabeled amino acids for PET and SPECT. *J Nucl Med* 45:1435-1436.
34. McGivan, J. D., and M. Pastor-Anglada. 1994. Regulatory and molecular aspects of mammalian amino acid transport. *Biochem J* 299 ( Pt 2):321-334.
35. Mackenzie, B., and J. D. Erickson. 2004. Sodium-coupled neutral amino acid (System N/A) transporters of the SLC38 gene family. *Pflug Arch Eur J Phy* 447:784-795.
36. Kondoh, N., N. Imazeki, M. Arai, A. Hada, K. Hatsuse, H. Matsuo, O. Matsubara, S. Ohkura, and M. Yamamoto. 2007. Activation of a system A amino acid transporter, ATA1/SLC38A1, in human hepatocellular carcinoma and preneoplastic liver tissues. *Int J Oncol* 31:81-87.
37. Kaira, K., N. Oriuchi, H. Imai, K. Shimizu, N. Yanagitani, N. Sunaga, T. Hisada, T. Ishizuka, Y. Kanai, H. Endou, T. Nakajima, and M. Mori. 2008. Prognostic significance of L-type amino acid transporter 1 (LAT1) and 4F2 heavy chain (CD98) expression in early stage squamous cell carcinoma of the lung. *Cancer Sci*.
38. Yanagida, O., Y. Kanai, A. Chairoungdua, D. K. Kim, H. Segawa, T. Nii, S. H. Cha, H. Matsuo, J. Fukushima, Y. Fukasawa, Y. Tani, Y. Taketani, H. Uchino, J. Y. Kim, J. Inatomi, I. Okayasu, K. Miyamoto, E. Takeda, T. Goya, and H. Endou. 2001.

Human L-type amino acid transporter 1 (LAT1): characterization of function and expression in tumor cell lines. *Biochim Biophys Acta* 1514:291-302.

39. Kaira, K., N. Oriuchi, H. Imai, K. Shimizu, N. Yanagitani, N. Sunaga, T. Hisada, O. Kawashima, H. Iijima, T. Ishizuka, Y. Kanai, H. Endou, T. Nakajima, and M. Mori. 2008. Expression of L-type amino acid transporter 1 (LAT1) in neuroendocrine tumors of the lung. *Pathol Res Pract* 204:553-561.

40. Nawashiro, H., N. Otani, N. Shinomiya, S. Fukui, H. Ooigawa, K. Shima, H. Matsuo, Y. Kanai, and H. Endou. 2006. L-type amino acid transporter 1 as a potential molecular target in human astrocytic tumors. *Int J Cancer* 119:484-492.

41. Uchino, H., Y. Kanai, D. K. Kim, M. F. Wempe, A. Chairoungdua, E. Morimoto, M. W. Anders, and H. Endou. 2002. Transport of amino acid-related compounds mediated by L-type amino acid transporter 1 (LAT1): insights into the mechanisms of substrate recognition. *Mol Pharmacol* 61:729-737.

42. Kim, C. S., S. H. Cho, H. S. Chun, S. Y. Lee, H. Endou, Y. Kanai, and K. Kim do. 2008. BCH, an inhibitor of system L amino acid transporters, induces apoptosis in cancer cells. *Biol Pharm Bull* 31:1096-1100.

43. McConathy, J., and M. M. Goodman. 2008. Non-natural amino acids for tumor imaging using positron emission tomography and single photon emission computed tomography. *Cancer Metastasis Rev* 27:555-573.

44. Pruim, J., A. T. Willemsen, W. M. Molenaar, A. van Waarde, A. M. Paans, M. A. Heesters, K. G. Go, G. M. Visser, E. J. Franssen, and W. Vaalburg. 1995. Brain tumors: L-[1-C-11]tyrosine PET for visualization and quantification of protein synthesis rate. *Radiology* 197:221-226.

45. Kole, A. C., O. E. Nieweg, J. Pruim, A. M. Paans, J. T. Plukker, H. J. Hoekstra, H. Schraffordt Koops, and W. Vaalburg. 1997. Standardized uptake value and quantification of metabolism for breast cancer imaging with FDG and L-[1-11C]tyrosine PET. *J Nucl Med* 38:692-696.
46. de Boer, J. R., J. Pruim, B. F. van der Laan, T. H. Que, A. T. Willemsen, F. W. Albers, and W. Vaalburg. 2003. L-1-11C-tyrosine PET in patients with laryngeal carcinomas: comparison of standardized uptake value and protein synthesis rate. *J Nucl Med* 44:341-346.
47. Plaat, B., A. Kole, M. Mastik, H. Hoekstra, W. Molenaar, and W. Vaalburg. 1999. Protein synthesis rate measured with L-[1-11C]tyrosine positron emission tomography correlates with mitotic activity and MIB-1 antibody-detected proliferation in human soft tissue sarcomas. *Eur J Nucl Med* 26:328-332.
48. Halldin, C., K. O. Schoeps, S. Stone-Elander, and F. A. Wiesel. 1987. The Bucherer-Strecker synthesis of D- and L-(1-11C)tyrosine and the in vivo study of L-(1-11C)tyrosine in human brain using positron emission tomography. *Eur J Nucl Med* 13:288-291.
49. Bjurling, P., G. Antoni, Y. Watanabe, and B. Langstrom. 1990. Enzymatic-Synthesis of Carboxy-C-11-Labeled L-Tyrosine, L-Dopa, L-Tryptophan and 5-Hydroxy-L-Tryptophan. *Acta Chemica Scandinavica* 44:178-182.
50. Luurtsema, G., J. Medema, P. H. Elsinga, G. M. Visser, and W. Vaalburg. 1994. Robotic Synthesis of L-[1-C-11]Tyrosine. *Applied Radiation and Isotopes* 45:821-828.

51. Braams, J. W., J. Pruim, P. G. Nikkels, J. L. Roodenburg, W. Vaalburg, and A. Vermey. 1996. Nodal spread of squamous cell carcinoma of the oral cavity detected with PET-tyrosine, MRI and CT. *J Nucl Med* 37:897-901.
52. Daemen, B. J., R. Zwertbroek, P. H. Elsinga, A. M. Paans, H. Doorenbos, and W. Vaalburg. 1991. PET studies with L-[1-11C]tyrosine, L-[methyl-11C]methionine and 18F-fluorodeoxyglucose in prolactinomas in relation to bromocryptine treatment. *Eur J Nucl Med* 18:453-460.
53. Kole, A. C., B. E. Plaat, H. J. Hoekstra, W. Vaalburg, and W. M. Molenaar. 1999. FDG and L-[1-11C]-tyrosine imaging of soft-tissue tumors before and after therapy. *J Nucl Med* 40:381-386.
54. de Boer, J. R., J. Pruim, F. W. Albers, F. Burlage, W. Vaalburg, and B. F. van der Laan. 2004. Prediction of survival and therapy outcome with 11C-tyrosine PET in patients with laryngeal carcinoma. *J Nucl Med* 45:2052-2057.
55. Kole, A. C., H. J. Hoekstra, D. T. Sleijfer, O. E. Nieweg, H. Schraffordt Koops, and W. Vaalburg. 1998. L-[1-carbon-11]tyrosine imaging of metastatic testicular nonseminoma germ-cell tumors. *J Nucl Med* 39:1027-1029.
56. Langen, K. J., D. Pauleit, and H. H. Coenen. 2002. 3-[(123)I]iodo-alpha-methyl-L-tyrosine: uptake mechanisms and clinical applications. *Nucl Med Biol* 29:625-631.
57. Kawai, K., Y. Fujibayashi, H. Saji, Y. Yonekura, J. Konishi, A. Kubodera, and A. Yokoyama. 1991. A strategy for the study of cerebral amino acid transport using iodine-123-labeled amino acid radiopharmaceutical: 3-iodo-alpha-methyl-L-tyrosine. *J Nucl Med* 32:819-824.

58. Jager, P. L., E. J. Franssen, W. Kool, B. G. Szabo, H. J. Hoekstra, H. J. Groen, E. G. de Vries, G. W. van Imhoff, W. Vaalburg, and D. A. Piers. 1998. Feasibility of tumor imaging using L-3-[iodine-123]-iodo-alpha-methyl-tyrosine in extracranial tumors. *J Nucl Med* 39:1736-1743.
59. Schmidt, D., K. J. Langen, H. Herzog, J. Wirths, M. Holschbach, J. C. Kiwit, K. Ziemons, H. H. Coenen, and H. Muller-Gartner. 1997. Whole-body kinetics and dosimetry of L-3--123I-iodo-alpha-methyltyrosine. *Eur J Nucl Med* 24:1162-1166.
60. Grosu, A. L., W. Weber, H. J. Feldmann, B. Wuttke, P. Bartenstein, M. W. Gross, C. Lumenta, M. Schwaiger, and M. Molls. 2000. First experience with I-123-alpha-methyl-tyrosine spect in the 3-D radiation treatment planning of brain gliomas. *Int J Radiat Oncol Biol Phys* 47:517-526.
61. Grosu, A. L., W. A. Weber, M. Franz, S. Stark, M. Piert, R. Thamm, H. Gumprecht, M. Schwaiger, M. Molls, and C. Nieder. 2005. Reirradiation of recurrent high-grade gliomas using amino acid PET (SPECT)/CT/MRI image fusion to determine gross tumor volume for stereotactic fractionated radiotherapy. *Int J Radiat Oncol Biol Phys* 63:511-519.
62. Kuwert, T., B. Woesler, C. Morgenroth, H. Lerch, M. Schafers, S. Palkovic, P. Matheja, W. Brandau, H. Wassmann, and O. Schober. 1998. Diagnosis of recurrent glioma with SPECT and iodine-123-alpha-methyl tyrosine. *J Nucl Med* 39:23-27.
63. Jager, P. L., H. J. Groen, A. van der Leest, J. W. van Putten, R. M. Pieterman, E. G. de Vries, and D. A. Piers. 2001. L-3-[123I]iodo-alpha-methyl-tyrosine SPECT in non-small cell lung cancer: preliminary observations. *J Nucl Med* 42:579-585.

64. Flamen, P., N. Bernheim, P. Deron, V. Caveliers, K. Chavatte, P. R. Franken, and A. Bossuyt. 1998. Iodine-123 alpha-methyl-I-tyrosine single-photon emission tomography for the visualization of head and neck squamous cell carcinomas. *Eur J Nucl Med* 25:177-181.
65. Boni, R., H. Steinert, R. Huch Boni, G. K. Von Schulthess, J. Meyer, R. Dummer, G. Burg, and G. Westera. 1997. Radioiodine-labelled alpha-methyl-tyrosine in malignant melanoma: cell culture studies and results in patients. *Br J Dermatol* 137:96-100.
66. Jager, P. L., B. E. Plaat, E. G. de Vries, W. M. Molenaar, W. Vaalburg, D. A. Piers, and H. J. Hoekstra. 2000. Imaging of soft-tissue tumors using L-3-[iodine-123]iodo-alpha-methyl-tyrosine single photon emission computed tomography: comparison with proliferative and mitotic activity, cellularity, and vascularity. *Clin Cancer Res* 6:2252-2259.
67. Plotkin, M., R. Wurm, D. Kuczer, P. Wust, R. Michel, T. Denecke, J. Ruf, L. Schlenger, A. Bischoff, R. Felix, and H. Amthauer. 2006. Diagnostic value of 123I-IMT SPECT in the follow-up of head and neck cancer. *Onkologie* 29:147-152.
68. Plotkin, M., R. Wurm, J. Eisenacher, K. Szerewicz, R. Michel, L. Schlenger, M. Pech, T. Denecke, D. Kuczer, A. Bischoff, R. Felix, and H. Amthauer. 2006. Combined SPECT/CT imaging using 123I-IMT in the detection of recurrent or persistent head and neck cancer. *Eur Radiol* 16:503-511.
69. Lahoutte, T., V. Caveliers, L. Dierickx, M. Vekeman, H. Everaert, J. Mertens, and A. Bossuyt. 2001. In vitro characterization of the influx of 3-[125I]iodo-L-alpha-

methyltyrosine and 2-[125I]iodo-L-tyrosine into U266 human myeloma cells: evidence for system T transport. *Nucl Med Biol* 28:129-134.

70. Nakajima, S., N. Shikano, T. Kotani, M. Ogura, R. Nishii, M. Yoshimoto, N. Yamaguchi, Y. Iwamura, N. Kubota, N. Ishikawa, and K. Kawai. 2007. Pharmacokinetics of 3-[125I]iodo-alpha-methyl-L-tyrosine, a tumor imaging agent, after probenecid loading in mice implanted with colon cancer DLD-1 cells. *Nucl Med Biol* 34:1003-1008.

71. Shikano, N., Y. Kanai, K. Kawai, J. Inatomi, D. K. Kim, N. Ishikawa, and H. Endou. 2003. Isoform selectivity of 3-125I-iodo-alpha-methyl-L-tyrosine membrane transport in human L-type amino acid transporters. *J Nucl Med* 44:244-246.

72. Coenen, H. H., P. Kling, and G. Stocklin. 1989. Cerebral metabolism of L-[2-18F]fluorotyrosine, a new PET tracer of protein synthesis. *J Nucl Med* 30:1367-1372.

73. Wienhard, K., K. Herholz, H. H. Coenen, J. Rudolf, P. Kling, G. Stocklin, and W. D. Heiss. 1991. Increased amino acid transport into brain tumors measured by PET of L-(2-18F)fluorotyrosine. *J Nucl Med* 32:1338-1346.

74. Hustinx, R., C. Lemaire, G. Jerusalem, P. Moreau, D. Cataldo, B. Duysinx, J. Aerts, M. F. Fassotte, J. Foidart, and A. Luxen. 2003. Whole-body tumor imaging using PET and 2-18F-fluoro-L-tyrosine: preliminary evaluation and comparison with 18F-FDG. *J Nucl Med* 44:533-539.

75. Inoue, T., T. Shibasaki, N. Oriuchi, K. Aoyagi, K. Tomiyoshi, S. Amano, M. Mikuni, I. Ida, J. Aoki, and K. Endo. 1999. 18F alpha-methyl tyrosine PET studies in patients with brain tumors. *J Nucl Med* 40:399-405.



76. Urakami, T., K. Sakai, T. Asai, D. Fukumoto, H. Tsukada, and N. Oku. 2009. Evaluation of O-[(18)F]fluoromethyl-d-tyrosine as a radiotracer for tumor imaging with positron emission tomography. *Nucl Med Biol* 36:295-303.
77. Tomiyoshi, K., K. Amed, S. Muhammad, T. Higuchi, T. Inoue, K. Endo, and D. Yang. 1997. Synthesis of isomers of 18F-labelled amino acid radiopharmaceutical: position 2- and 3-L-18F-alpha-methyltyrosine using a separation and purification system. *Nucl Med Commun* 18:169-175.
78. Watanabe, H., T. Inoue, T. Shinozaki, T. Yanagawa, A. R. Ahmed, K. Tomiyoshi, N. Oriuchi, M. Tokunaga, J. Aoki, K. Endo, and K. Takagishi. 2000. PET imaging of musculoskeletal tumours with fluorine-18 alpha-methyltyrosine: comparison with fluorine-18 fluorodeoxyglucose PET. *Eur J Nucl Med* 27:1509-1517.
79. Miyakubo, M., N. Oriuchi, Y. Tsushima, T. Higuchi, K. Koyama, K. Arai, B. Paudyal, Y. Iida, H. Hanaoka, T. Ishikita, Y. Nakasone, A. Negishi, K. Mogi, and K. Endo. 2007. Diagnosis of maxillofacial tumor with L-3-[18f]-fluoro-alpha-methyltyrosine (FMT) PET: a comparative study with FDG-PET. *Ann Nucl Med* 21:129-135.
80. Miyashita, G., T. Higuchi, N. Oriuchi, Y. Arisaka, H. Hanaoka, H. Tominaga, S. Morita, M. Miyakubo, T. Ishikita, Y. Nakasone, A. Negishi, S. Yokoo, and K. Endo. (1)F-FAMT uptake correlates with tumor proliferative activity in oral squamous cell carcinoma: comparative study with (1)F-FDG PET and immunohistochemistry. *Ann Nucl Med* 24:579-584.
81. Kaira, K., N. Oriuchi, Y. Otani, K. Shimizu, S. Tanaka, H. Imai, N. Yanagitani, N. Sunaga, T. Hisada, T. Ishizuka, K. Dobashi, Y. Kanai, H. Endou, T. Nakajima, K.

Endo, and M. Mori. 2007. Fluorine-18-alpha-methyltyrosine positron emission tomography for diagnosis and staging of lung cancer: a clinicopathologic study. Clin Cancer Res 13:6369-6378.

82. Kaira, K., N. Oriuchi, K. Shimizu, H. Imai, H. Tominaga, N. Yanagitani, N. Sunaga, T. Hisada, T. Ishizuka, Y. Kanai, T. Oyama, M. Mori, and K. Endo. Comparison of L-type amino acid transporter 1 expression and L-[3-18F]-alpha-methyl tyrosine uptake in outcome of non-small cell lung cancer. Nucl Med Biol 37:911-916.

83. Kaira, K., N. Oriuchi, K. Shimizu, T. Ishikita, T. Higuchi, H. Imai, N. Yanagitani, N. Sunaga, T. Hisada, T. Ishizuka, Y. Kanai, H. Endou, T. Nakajima, K. Endo, and M. Mori. 2009. Correlation of angiogenesis with 18F-FMT and 18F-FDG uptake in non-small cell lung cancer. Cancer Sci 100:753-758.

84. Langen, K. J., K. Hamacher, M. Weckesser, F. Floeth, G. Stoffels, D. Bauer, H. H. Coenen, and D. Pauleit. 2006. O-(2-[18F]fluoroethyl)-L-tyrosine: uptake mechanisms and clinical applications. Nucl Med Biol 33:287-294.

85. Wester, H. J., M. Herz, W. Weber, P. Heiss, R. Senekowitsch-Schmidtke, M. Schwaiger, and G. Stocklin. 1999. Synthesis and radiopharmacology of O-(2-[18F]fluoroethyl)-L-tyrosine for tumor imaging. J Nucl Med 40:205-212.

86. Hamacher, K., and H. H. Coenen. 2002. Efficient routine production of the 18F-labelled amino acid O-2-18F fluoroethyl-L-tyrosine. Appl Radiat Isot 57:853-856.

87. Krasikova, R. N., O. F. Kuznetsova, O. S. Fedorova, V. I. Maleev, T. F. Saveleva, and Y. N. Belokon. 2008. No carrier added synthesis of O-(2'-[18F]fluoroethyl)-L-tyrosine via a novel type of chiral enantiomerically pure

precursor, Nill complex of a (S)-tyrosine Schiff base. *Bioorg Med Chem* 16:4994-5003.

88. Weber, W. A., H. J. Wester, A. L. Grosu, M. Herz, B. Dzewas, H. J. Feldmann, M. Molls, G. Stocklin, and M. Schwaiger. 2000. O-(2-[<sup>18</sup>F]fluoroethyl)-L-tyrosine and L-[methyl-<sup>11</sup>C]methionine uptake in brain tumours: initial results of a comparative study. *Eur J Nucl Med* 27:542-549.

89. Stober, B., U. Tanase, M. Herz, C. Seidl, M. Schwaiger, and R. Senekowitsch-Schmidtke. 2006. Differentiation of tumour and inflammation: characterisation of [methyl-<sup>3</sup>H]methionine (MET) and O-(2-[<sup>18</sup>F]fluoroethyl)-L-tyrosine (FET) uptake in human tumour and inflammatory cells. *Eur J Nucl Med Mol Imaging* 33:932-939.

90. Rau, F. C., W. A. Weber, H. J. Wester, M. Herz, I. Becker, A. Kruger, M. Schwaiger, and R. Senekowitsch-Schmidtke. 2002. O-(2-[(<sup>18</sup>F)Fluoroethyl)- L-tyrosine (FET): a tracer for differentiation of tumour from inflammation in murine lymph nodes. *Eur J Nucl Med Mol Imaging* 29:1039-1046.

91. Popperl, G., C. Gotz, W. Rachinger, F. J. Gildehaus, J. C. Tonn, and K. Tatsch. 2004. Value of O-(2-[<sup>18</sup>F]fluoroethyl)- L-tyrosine PET for the diagnosis of recurrent glioma. *Eur J Nucl Med Mol Imaging* 31:1464-1470.

92. Plotkin, M., C. Blechschmidt, G. Auf, F. Nyuyki, L. Geworski, T. Denecke, W. Brenner, and F. Stockhammer. Comparison of F-18 FET-PET with F-18 FDG-PET for biopsy planning of non-contrast-enhancing gliomas. *Eur Radiol* 20:2496-2502.

93. Rachinger, W., C. Goetz, G. Popperl, F. J. Gildehaus, F. W. Kreth, M. Holtmannspotter, J. Herms, W. Koch, K. Tatsch, and J. C. Tonn. 2005. Positron

emission tomography with O-(2-[18F]fluoroethyl)-L-tyrosine versus magnetic resonance imaging in the diagnosis of recurrent gliomas. *Neurosurgery* 57:505-511; discussion 505-511.

94. Floeth, F. W., D. Pauleit, H. J. Wittsack, K. J. Langen, G. Reifenberger, K. Hamacher, M. Messing-Junger, K. Zilles, F. Weber, W. Stummer, H. J. Steiger, G. Woebker, H. W. Muller, H. Coenen, and M. Sabel. 2005. Multimodal metabolic imaging of cerebral gliomas: positron emission tomography with [18F]fluoroethyl-L-tyrosine and magnetic resonance spectroscopy. *J Neurosurg* 102:318-327.

95. Mehrkens, J. H., G. Popperl, W. Rachinger, J. Herms, K. Seelos, K. Tatsch, J. C. Tonn, and F. W. Kreth. 2008. The positive predictive value of O-(2-[18F]fluoroethyl)-L-tyrosine (FET) PET in the diagnosis of a glioma recurrence after multimodal treatment. *J Neurooncol* 88:27-35.

96. Hutterer, M., M. Nowosielski, D. Putzer, D. Waitz, G. Tinkhauser, H. Kostron, A. Muigg, I. J. Virgolini, W. Staffen, E. Trink, T. Gotwald, A. H. Jacobs, and G. Stockhammer. O-(2-18F-Fluoroethyl)-L-Tyrosine PET Predicts Failure of Antiangiogenic Treatment in Patients with Recurrent High-Grade Glioma. *J Nucl Med* 52:856-864.

97. Floeth, F. W., D. Pauleit, M. Sabel, G. Stoffels, G. Reifenberger, M. J. Riemenschneider, P. Jansen, H. H. Coenen, H. J. Steiger, and K. J. Langen. 2007. Prognostic value of O-(2-18F-fluoroethyl)-L-tyrosine PET and MRI in low-grade glioma. *J Nucl Med* 48:519-527.

98. Thiele, F., J. Ehmer, M. D. Piroth, M. J. Eble, H. H. Coenen, H. J. Kaiser, W. M. Schaefer, U. Buell, and C. Boy. 2009. The quantification of dynamic FET PET

imaging and correlation with the clinical outcome in patients with glioblastoma. *Phys Med Biol* 54:5525-5539.

99. Pauleit, D., G. Stoffels, W. Schaden, K. Hamacher, D. Bauer, L. Tellmann, H. Herzog, S. Broer, H. H. Coenen, and K. J. Langen. 2005. PET with O-(2-<sup>18</sup>F-Fluoroethyl)-L-Tyrosine in peripheral tumors: first clinical results. *J Nucl Med* 46:411-416.

100. Balogova, S., S. Perie, K. Kerrou, D. Grahek, F. Montravers, B. Angelard, B. Susini, P. El Chater, J. L. St Guily, and J. N. Talbot. 2008. Prospective comparison of FDG and FET PET/CT in patients with head and neck squamous cell carcinoma. *Mol Imaging Biol* 10:364-373.

101. Pauleit, D., A. Zimmermann, G. Stoffels, D. Bauer, J. Risse, M. O. Fluss, K. Hamacher, H. H. Coenen, and K. J. Langen. 2006. <sup>18</sup>F-FET PET compared with <sup>18</sup>F-FDG PET and CT in patients with head and neck cancer. *J Nucl Med* 47:256-261.

102. Paul E. Christian, K. M. W.-R. 2007. Nuclear Medicine and PET/CT Technology and Techniques

103. Jurisson, S., C. Cutler, and S. V. Smith. 2008. Radiometal complexes: characterization and relevant in vitro studies. *Q J Nucl Med Mol Imaging* 52:222-234.

104. Liu, S. 2004. The role of coordination chemistry in the development of target-specific radiopharmaceuticals. *Chem Soc Rev* 33:445-461.

105. Anderson, C. J., C. S. John, Y. J. Li, R. D. Hancock, T. J. McCarthy, A. E. Martell, and M. J. Welch. 1995. N,N'-ethylene-di-L-cysteine (EC) complexes of

Ga(III) and In(III): molecular modeling, thermodynamic stability and in vivo studies. Nucl Med Biol 22:165-173.

106. Yang, D., M. Yukihiro, D. F. Yu, M. Ito, C. S. Oh, S. Kohanim, A. Azhdarinia, C. G. Kim, J. Bryant, E. E. Kim, and D. Podoloff. 2004. Assessment of therapeutic tumor response using <sup>99m</sup>Tc-ethylenedicysteine-glucosamine. Cancer Biother Radiopharm 19:443-456.

107. Marzilli, L. G. 1994. Linking Deprotonation and Denticity of Chelate Ligands. Rhenium(V) Oxo Analogs of Technetium-99m Radiopharmaceuticals Containing N<sub>2</sub>S<sub>2</sub> Chelate Ligands. Inorganic Chemistry 33:4850-4860.

108. Ketrin, A. R., D. E. Troutner, T. J. Hoffman, D. K. Stanton, W. A. Volkert, and R. A. Holmes. 1984. Biodistribution of lipophilic <sup>99m</sup>Tc complexes of cyclam derivatives. Int J Nucl Med Biol 11:113-119.

109. Troutner, D. E., J. Simon, A. R. Ketrin, W. Volkert, and R. A. Holmes. 1980. Complexing of Tc-99m with cyclam: concise communication. J Nucl Med 21:443-448.

110. Van Nerom, C. G., G. M. Bormans, M. J. De Roo, and A. M. Verbruggen. 1993. First experience in healthy volunteers with technetium-99m L,L-ethylenedicysteine, a new renal imaging agent. Eur J Nucl Med 20:738-746.

111. Strauss, L. G. 1997. Positron Emission Tomography: Current Role for Diagnosis and Therapy Monitoring in Oncology. Oncologist 2:381-388.

112. Chang, J. M., H. J. Lee, J. M. Goo, H. Y. Lee, J. J. Lee, J. K. Chung, and J. G. Im. 2006. False positive and false negative FDG-PET scans in various thoracic diseases. Korean J Radiol 7:57-69.

113. Rosenbaum, S. J., T. Lind, G. Antoch, and A. Bockisch. 2006. False-positive FDG PET uptake--the role of PET/CT. *Eur Radiol* 16:1054-1065.
114. Tsukada, H., K. Sato, D. Fukumoto, and T. Kakiuchi. 2006. Evaluation of D-isomers of O-18F-fluoromethyl, O-18F-fluoroethyl and O-18F-fluoropropyl tyrosine as tumour imaging agents in mice. *Eur J Nucl Med Mol Imaging* 33:1017-1024.
115. Tsukada, H., K. Sato, D. Fukumoto, S. Nishiyama, N. Harada, and T. Kakiuchi. 2006. Evaluation of D-isomers of O-11C-methyl tyrosine and O-18F-fluoromethyl tyrosine as tumor-imaging agents in tumor-bearing mice: comparison with L- and D-11C-methionine. *J Nucl Med* 47:679-688.
116. Ishiwata, K., H. Tsukada, K. Kubota, T. Nariai, N. Harada, K. Kawamura, Y. Kimura, K. Oda, R. Iwata, and K. Ishii. 2005. Preclinical and clinical evaluation of O-[11C]methyl-L-tyrosine for tumor imaging by positron emission tomography. *Nucl Med Biol* 32:253-262.
117. del Amo, E. M., A. Urtti, and M. Yliperttula. 2008. Pharmacokinetic role of L-type amino acid transporters LAT1 and LAT2. *Eur J Pharm Sci* 35:161-174.
118. Sakata, T., G. Ferdous, T. Tsuruta, T. Satoh, S. Baba, T. Muto, A. Ueno, Y. Kanai, H. Endou, and I. Okayasu. 2009. L-type amino-acid transporter 1 as a novel biomarker for high-grade malignancy in prostate cancer. *Pathol Int* 59:7-18.
119. Ishiwata, K., W. Vaalburg, P. H. Elsinga, A. M. Paans, and M. G. Woldring. 1988. Metabolic studies with L-[1-14C]tyrosine for the investigation of a kinetic model to measure protein synthesis rates with PET. *J Nucl Med* 29:524-529.
120. Kawai, K., Y. Fujibayashi, Y. Yonekura, J. Konishi, H. Saji, A. Kubodera, and A. Yokoyama. 1992. An artificial amino acid radiopharmaceutical for single photon

emission computed tomographic study of pancreatic amino acid transports 123I-3-iodo-alpha-methyl-L-tyrosine. *Ann Nucl Med* 6:169-175.

121. Langen, K. J., M. Jarosch, H. Muhlensiepen, K. Hamacher, S. Broer, P. Jansen, K. Zilles, and H. H. Coenen. 2003. Comparison of fluorotyrosines and methionine uptake in F98 rat gliomas. *Nucl Med Biol* 30:501-508.

122. Taylor, A. T., M. Lipowska, L. Hansen, E. Malveaux, and L. G. Marzilli. 2004. <sup>99m</sup>Tc-MAEC complexes: new renal radiopharmaceuticals combining characteristics of (99m)Tc-MAG3 and (99m)Tc-EC. *J Nucl Med* 45:885-891.

123. Shikano, N., K. Kawai, S. Nakajima, R. Nishii, L. G. Flores, 2nd, A. Kubodera, N. Kubota, N. Ishikawa, and H. Saji. 2004. Renal accumulation and excretion of radioiodinated 3-iodo-alpha-methyl-L-tyrosine. *Ann Nucl Med* 18:263-270.

124. Kong, F. L., Y. Zhang, M. S. Ali, C. Oh, R. Mendez, S. Kohanim, N. Tsao, M. Chanda, W. C. Huang, and D. J. Yang. Synthesis of (99m)Tc-EC-AMT as an imaging probe for amino acid transporter systems in breast cancer. *Nucl Med Commun* 31:699-707.

125. Delbeke, D., R. E. Coleman, M. J. Guiberteau, M. L. Brown, H. D. Royal, B. A. Siegel, D. W. Townsend, L. L. Berland, J. A. Parker, K. Hubner, M. G. Stabin, G. Zubal, M. Kachelriess, V. Cronin, and S. Holbrook. 2006. Procedure guideline for tumor imaging with 18F-FDG PET/CT 1.0. *J Nucl Med* 47:885-895.

126. Langen, K. J., H. Muhlensiepen, M. Holschbach, H. Hautzel, P. Jansen, and H. H. Coenen. 2000. Transport mechanisms of 3-[123I]iodo-alpha-methyl-L-tyrosine in a human glioma cell line: comparison with [3H]methyl-L-methionine. *J Nucl Med* 41:1250-1255.



127. Miyagawa, T., T. Oku, H. Uehara, R. Desai, B. Beattie, J. Tjuvajev, and R. Blasberg. 1998. "Facilitated" amino acid transport is upregulated in brain tumors. *J Cereb Blood Flow Metab* 18:500-509.
128. Lindstrom, L. H., O. Gefvert, G. Hagberg, T. Lundberg, M. Bergstrom, P. Hartvig, and B. Langstrom. 1999. Increased dopamine synthesis rate in medial prefrontal cortex and striatum in schizophrenia indicated by L-(beta-11C) DOPA and PET. *Biol Psychiatry* 46:681-688.
129. Kersemans, K., M. Bauwens, and J. Mertens. 2008. Method for stabilizing non carrier added 2-[(18F)fluoromethyl-L-phenylalanine, a new tumour tracer, during radiosynthesis and radiopharmaceutical formulation. *Nucl Med Biol* 35:425-432.
130. Yamaura, G., T. Yoshioka, H. Fukuda, K. Yamaguchi, M. Suzuki, S. Furumoto, R. Iwata, and C. Ishioka. 2006. O-[18F]fluoromethyl-L-tyrosine is a potential tracer for monitoring tumour response to chemotherapy using PET: an initial comparative in vivo study with deoxyglucose and thymidine. *Eur J Nucl Med Mol Imaging* 33:1134-1139.
131. Yang, D. J., K. Ozaki, C. S. Oh, A. Azhdarinia, T. Yang, M. Ito, A. Greenwell, J. Bryant, S. Kohanim, V. K. Wong, and E. E. Kim. 2005. (99m)Tc-EC-guanine: synthesis, biodistribution, and tumor imaging in animals. *Pharm Res* 22:1471-1479.
132. Iznaga-Escobar, N. 1998. 188Re-direct labeling of monoclonal antibodies for radioimmunotherapy of solid tumors: biodistribution, normal organ dosimetry, and toxicology. *Nucl Med Biol* 25:441-447.

133. Moore, K. E., P. F. Wright, and J. K. Bert. 1967. Toxicologic studies with alpha-methyltyrosine, an inhibitor of tyrosine hydroxylase. *J Pharmacol Exp Ther* 155:506-515.
134. Kong, F. L., M. S. Ali, Y. Zhang, C. S. Oh, D. F. Yu, M. Chanda, and D. J. Yang. Synthesis and Evaluation of Amino Acid-Based Radiotracer Tc-N4-AMT for Breast Cancer Imaging. *J Biomed Biotechnol* 2011:276907.
135. Yagita, H., T. Masuko, and Y. Hashimoto. 1986. Inhibition of tumor cell growth in vitro by murine monoclonal antibodies that recognize a proliferation-associated cell surface antigen system in rats and humans. *Cancer Res* 46:1478-1484.

## VITA

FanLin Kong was born in Shanghai, China on September 11, 1982, the daughter of QingWen Kong and Qi Zuo. She moved to Japan with her family in July 1997. In March 2005, she received the degree of Bachelor of Science in Bioorganic Chemistry from Utsunomiya University in Tochigi, Japan. In August 2006, she entered the University of Texas Health Science Center at Houston, Graduate School of Biomedical Sciences where she conducted her research in nuclear medicine and molecular imaging under the supervision of Dr. David J Yang in the Department of Experimental Diagnostic Imaging at the University of Texas, M.D. Anderson Cancer Center. During her predoctoral career, she received R.W. Butcher Award and several student travel awards from the graduate school. In addition, she was the 1st place winner of the abstract competition of Trainee Research Day 2010 at M.D. Anderson Cancer Center. Furthermore, she served as the student representative of her graduate school at the Committee on the Status of Women at the University of Texas Health Science Center at Houston. She also served as an international student representative in The Student Intercouncil at the University of Texas Health Science Center at Houston. She completed her Ph.D. in October 2011 and intends to pursue a career as a scientist in cancer diagnosis and treatment.

**Permanent Address:** 20B East Shady Ln,  
Houston, Texas 77063